ASSEMBLY OF THE Mot PROTEIN COMPLEX INTO THE *Escherichia coli* FLAGELLAR MOTOR

A Dissertation

by

EDAN ROBERT HOSKING

Submitted to the Office of Graduate Studies of
Texas A&M University
in partial fulfillment of the requirements for the degree of

DOCTOR OF PHILOSOPHY

May 2007

Major Subject: Microbiology

ASSEMBLY OF THE Mot PROTEIN COMPLEX INTO THE *Escherichia coli* FLAGELLAR MOTOR

A Dissertation

by

EDAN ROBERT HOSKING

Submitted to the Office of Graduate Studies of
Texas A&M University
in partial fulfillment of the requirements for the degree of

DOCTOR OF PHILOSOPHY

Approved by:

Chair of Committee, Michael Manson
Committee Members, Ryland Young
Susan Golden
Arthur Johnson
Head of Department, Vincent Cassone

May 2007

Major Subject: Microbiology

ABSTRACT

Assembly of the Mot Protein Complex into the *Escherichia coli* Flagellar Motor. (May 2007)

Edan Robert Hosking, B.S., Central Michigan University

Chair of Advisory Committee: Dr. Michael D. Manson

The MotA and MotB proteins of *E. coli* form a $MotA_4MotB_2$ complex. Proton flow through a transmembrane channel in the complex powers flagellar rotation. Protonation of Asp-32 of MotB within the channel is proposed to cause a conformational change in the large cytoplasmic loop of MotA, which pushes against FliG in the rotor. MotB is believed to anchor the complex to the cell wall via a conserved sequence that is found in many proteins that bind peptidoglycan. The research presented in this dissertation focused primarily on the formation and activation of the MotAB proton channel. A proposed amphipathic α-helical region, extending from residue 52 through 65 of the periplasmic domain of MotB, was discovered to block proton flow through the channel in its inactive state prior to incorporation into a flagellar motor. The plug is thought to lie parallel to the periplasmic face of the cell membrane and to be removed from the membrane by a conformational change triggered by contact with the motor. Negatively charged residues near the cytoplasmic C-terminus of MotA and positively charged residues at the cytoplasmic N-terminus of MotB were identified as being important for motility. A mutational analysis and subsequent suppressor analysis suggest that these residues may align MotA and MotB to form the $MotA_4MotB_2$ complex in the

proper position relative to FliG and the rotor. The underlying mechanism for producing MotA and MotB in a 2:1 ratio was also investigated and found to be primarily due to translational coupling of *motA* and *motB*. The stop codon of *motA* and the start codon of *motB* overlap, allowing the ribosome that has just completed translation of *motA* to reinitiate and translate *motB*. The efficiency of reinitiation is about 66%; presumably degradation of excess MotB not in the $MotA_4MotB_2$ complex produces the final 2:1 ratio. Research was also conducted to determine whether MotB binds directly to the peptidoglycan layer of the cell wall. Although inconclusive, the preliminary results appear to support this notion. The overall work provides insights into several aspects of the assembly and subsequent activation of the stator component of the bacterial flagellar motor.

ACKNOWLEDGEMENTS

I would like to thank my mentor and friend, Dr. Michael Manson, for allowing me to learn and grow as a scientist and for having the faith that I could, and would succeed; the members of my committee, Drs. Ry Young, Art Johnson, and Susan Golden, who have given to me their invaluable time and input into my research; the many friends and colleagues, those who have come and have gone and to those who I leave behind, especially all of my "Mike Manson friends". You were willing to take my mind off research with good conversation or whatever else, when necessary, but were always a resource for great ideas to get over the hurdles.

Most importantly, I wish to thank my parents for all their kind words and support. To my wife Marcy, a simple thank you just doesn't seem enough, but thank you, thank you, thank you for all of your understanding, patience and support throughout these years as you were always there for me. Finally, to my beautiful daughter Jordan, you have served as a true inspiration to me every day as I watch you investigate, discover and understand the world that surrounds you, for these are the characteristics of a scientist and I leave you with this final thought……Never stop!

TABLE OF CONTENTS

CHAPTER Page

CHAPTER Page

LIST OF FIGURES

FIGURE Page

FIGURE Page

LIST OF TABLES

CHAPTER I

INTRODUCTION

Anatomy of the flagellar motor

The Gram-negative bacterium *Escherichia coli* swims by rotating 5-7 left-handed helical flagellar filaments, which are positioned randomly around the cell. Each flagellum is powered by its own rotary motor. The flagella rotate counterclockwise (CCW) or clockwise (CW) at equal velocity. The filament is assembled from a single protein, called flagellin, and contains 11 protofilaments.[1,2] Differences in the lengths of these protofilaments, caused by unequal packing of the flagellin subunits, result in the left-handed helicity of the filament.[3,4] The filament can take on different helical pitches depending on the pH, ionic strength, and physical stress, all of which affect the stability of the long and short protofilaments.[5-7] The packing of the subunits within the filament was revealed through the crystal structure, which showed the differences in the packing orientations.[8]

Attached to the filament is the hook, which serves as a flexible coupler between the filament and the rod. The distal end of the rod passes through the L and P rings, the former situated in the outer membrane and the latter associated with the peptidoglycan layer of the cell.[9] The L and P rings act as a bushing for the rod to pass through, and rotate within, the outer layers of the Gram-negative cell envelope.[10-12]

This dissertation follows the style of the *Journal of Molecular Biology*.

The MS ring is located at the proximal end of the rod, with the M portion in the cell membrane and the S portion just outside (Supramembrane).[9] The C ring is on the cytoplasmic face of the MS ring[13,14] (**Fig. 1.1**). Together, the rings and rod comprise the basal body. Electron micrographs of the flagellar motor have revealed these structures in great detail[14,15,16,17] (**Fig. 1.2**).

The flagellum can be divided into two functionally distinct entities: the rotor, which turns with respect to the cell wall, and the stator, which remains fixed. Rotor elements include the MS and C rings with the attached rod, hook, and filament. Stator elements include the P and L rings and possibly the MotA/MotB complex. Single-particle reconstructions of the basal body appear to contain all components of the flagellar motor except the MotA/B complexes (**Fig. 1.2**), which lie within the cell membrane at the periphery of the motor.[18] MotAB complexes have been observed as studs surrounding the motor in freeze-fracture images of the cell membrane[18,19] (**Fig. 1.3**), and these studs are absent in cells lacking MotA and MotB.[18] From the freeze-fracture images of *E. coli*, it was estimated that 11 ± 1 complexes exist around the motor.[18] Fluorescence-bleaching experiments using MotB-GFP (green fluorescent protein),[20] and very careful, incremental resurrection experiments, where motAB was expressed and the gene products were incorporated into a pre-existing flagellar motor resulting in a stepwise increase in the rotational rate of the flagellum,[21] have also suggested that there are about 11 MotAB complexes per motor.

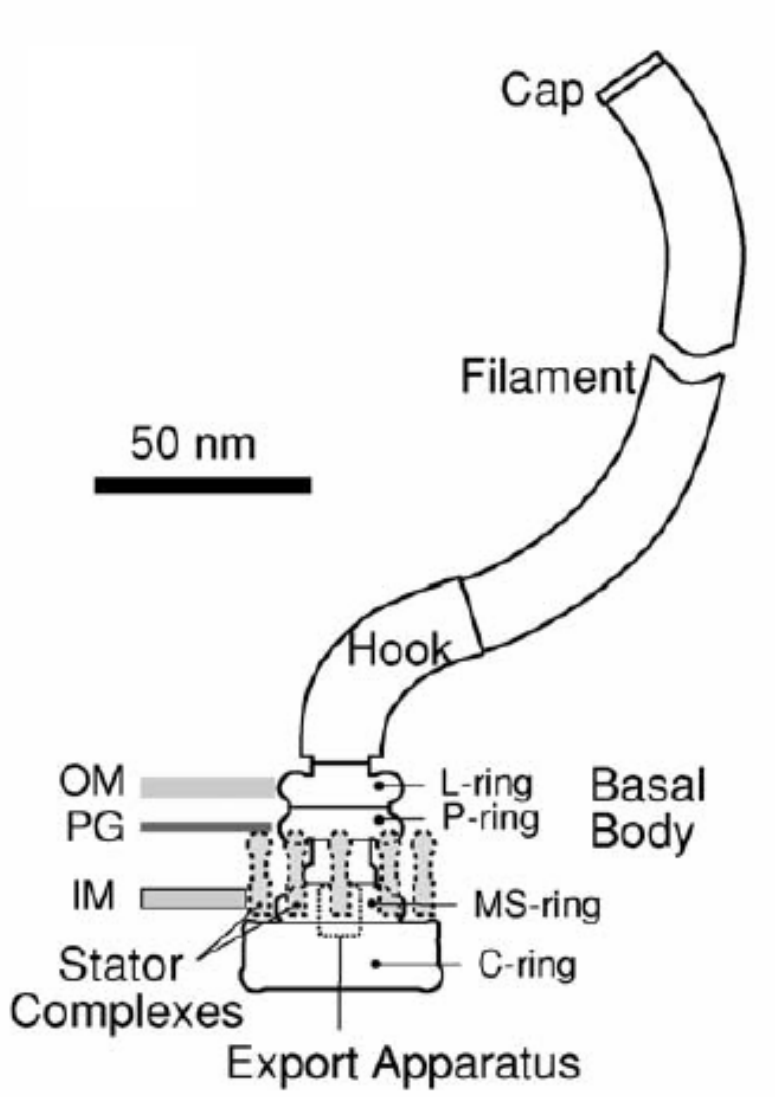

Figure 1.1. Schematic of the flagellar motor. (Reprinted with permission from David Blair[15]).

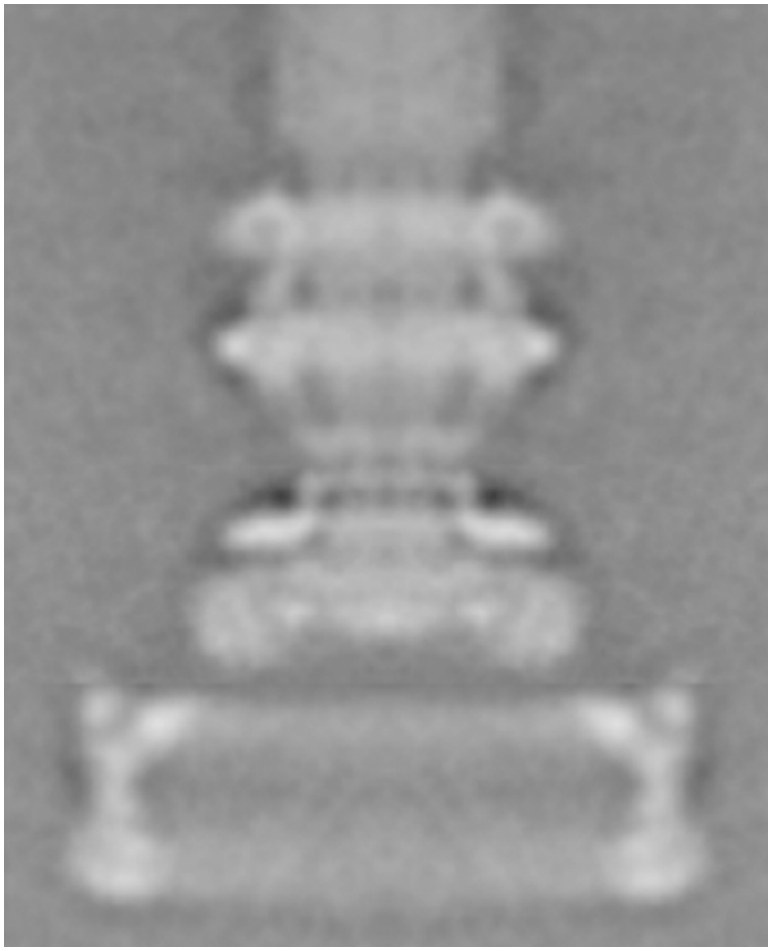

Figure 1.2. Cross-section of an electron micrographic reconstruction of the flagellar basal body from *Salmonella*. The image was created by averaging micrographs of single particles. (From David DeRosier[14],with permission).

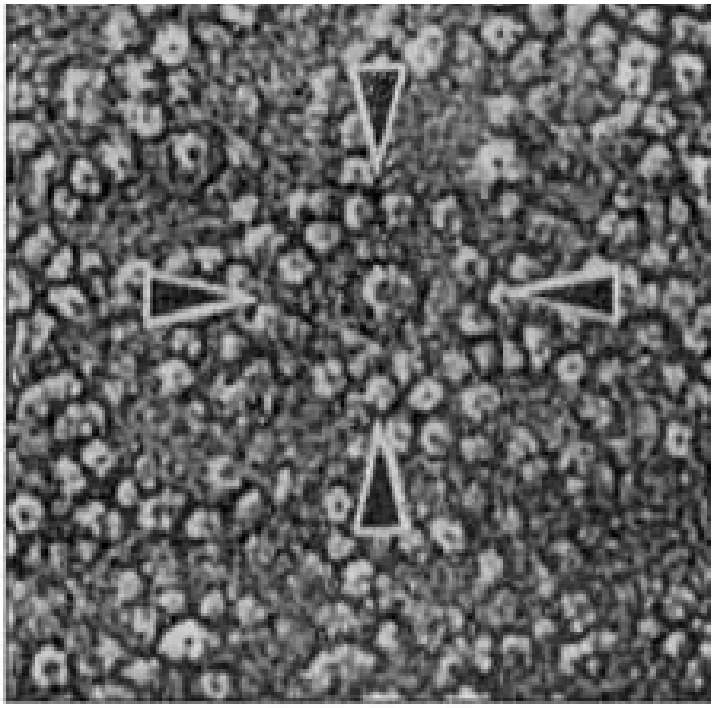

Figure 1.3. Electron micrograph from *Salmonella* of a circular array of particles believed to be MotA and MotB complexes embedded in the membrane. The central protrusion is the basal body rod most proximal to the membrane (Reprinted with permission from David Blair[15]).

Control of flagellar genes

Flagellar genes are classified based on whether they are expressed during the early, middle, or late phase of flagellar assembly (**Table 1.1**), approximately at the time they are needed.[22,23] The two early genes, *flhD* and *flhC*, encode the master regulatory proteins of flagellar synthesis, which form an $FlhD_2FlhC_2$ tetramer that activates transcription of the middle genes.[24] Their expression also indirectly regulates the late genes, since no flagellar genes are expressed until the $FlhD_2FlhC_2$ tetramer is available.[24]

Because synthesis of the flagellar motor requires extensive resources, expression of *flhD* and *flhC* is under tight control. Moderate overexpression of FlhD and FlhC results in twice the number of flagella (12-16) and approximately a double-length filament, circumstances that impede motility (Gus Wright, unpublished data). Expression of $FlhD_2FlhC_2$ is linked to the cell cycle[25-27] and is also regulated by temperature,[28-30] acetyl phosphate,[31] salt or other solutes,[32,33] and cAMP/CRP.[30,34] The *flhDC* operon is stimulated by $FlhD_2FlhC_2$ when σ^{28} (FliA) is present, and *flhDC* transcription from this operon is inhibited when σ^{28} is at low levels.[35] The proteins encoded by the thirty middle genes are necessary to assemble the basal body-hook structure and also control the transcription of late genes. The late genes encode flagellin and the three HAPs (hook-associated proteins), which are needed to assemble the filament, and the motility (*mot*) and chemotaxis (*che*) genes, which encode proteins that power and control the flagellar motor.

Transcription of the late genes is not significant until assembly of the basal body-hook structure is complete. If a basal body-hook protein is defective, expression of the

Table 1.1. Operons and genes involved in assembly of the flagellar motor[a].

Early Genes	Middle Genes	Late Genes
*flh*DC	*flg*AMN	*flg*MN
	*flg*BCDEFGHIJKL	*fgi*KL
	*flh*BAE	*fli*C
	*fli*AZY	*fli*DST
	*fli*DST	*mot*AB*che*AW[b]
	*fli*E	*tar tap che*RBYZ[b]
	*fli*FGHIJK	*aer*
	*fli*LMNOPQR	*trg*
		tsr

[a] The three groups, termed early, middle, and late, of flagellar operons expressed during each phase of assembly.
[b] Chemotaxis genes are included as late genes.

late genes is reduced. FliA (σ^{28}), a middle gene product, is responsible for the transition between expression of the middle and late genes.[36] The anti-sigma factor FlgM, also a middle-gene product, inhibits σ^{28} when levels of FlgM are high. Upon completion of the basal body-hook structure, FlgM is exported from the cell and σ^{28} is able to turn on transcription of the late genes[37-40] (**Table 1.1**).

Several genes are transcribed from both the middle and late promoters, including those that encode the HAP proteins, export chaperones, and FlgM. This phenomenon ensures that pools of these proteins are present when needed for assembly. One protein in particular, FliD (the HAPII filament-capping protein), may exist in excess to help repair filaments that break. Filaments that lack the cap export flagellin into the medium, rather than assembling it.[41] FlgM, whose importance as a middle gene is outlined above, may also be present at a low, constant level to regulate the length of the growing filaments. Shorter filaments should export FlgM more quickly than longer ones, so, as FlgM gets depleted when shorter filaments are present, FliD and flagellin production would increase. This would especially be true when a filament breaks and more flagellin and FliD are necessary for repair.[40]

Assembly of the flagellar motor

Mutations that block assembly of the motor at particular steps have allowed for a basic understanding of the assembly of the flagellar motor.[42-47] The motor assembles starting with structures within the cell membrane and cytoplasm and builds outwards (**Fig. 1.4**).

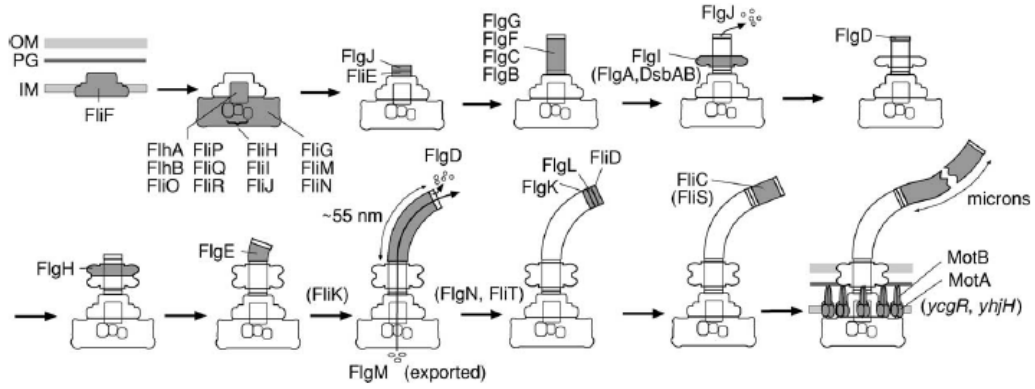

Figure 1.4. Order of the assembly of the flagellar motor. The component(s) added at each step are shaded. (Reprinted with permission from David Blair[15]).

The first structure to be made is the MS ring. This ring and the most-proximal portion of the rod are formed by FliF. Overexpression of FliF causes numerous MS ring/rod structures to form in the membrane.[48] The MS ring serves as the base for the assembly of the rest of the motor. The C-ring is added to the cytoplasmic face of the MS ring. The C ring contains the proteins FliG, FliM and FliN,[49-50] which make up the switch-motor complex. The rod begins its assembly on the periplasmic side of the MS ring. The export apparatus, which exports most of the external proteins of the flagellum, assembles within the C ring at the entrance to the central conduit that extends through the middle of the rod.[2,47,51-53] The flagellar export apparatus is related to the type III secretion apparatus that Gram-negative pathogenic bacteria use to inject toxins into their host cells.[54-56] If the export apparatus is defective, assembly of the motor ceases with the MS and C rings and the innermost (FliF) portion of the rod. Deletion of *fliG*, *fliM*, or *fliN* also stalls flagellar assembly, presumably because the export apparatus cannot assemble properly within an incomplete C ring.[46,57]

The rod consists of six different proteins (FliF, FliE, FlgB, FlgC, FlgF, and FlgG).[58] The latter four proteins constitute the bulk of the rod subunits.[58] FliF is joined to the rest of the rod by FliE.[59] FlgJ forms a cap on the end of the growing rod, under which the subunits of the rod are assembled. The C-terminal half of FlgJ has homology with the active center of some muramidase enzymes from gram-positive bacteria.[60] Purified FlgJ was found to function as a muramidase and this function was retained when the C-terminal half was purified.[60] Specific mutations within the active center of the enzyme resulted in less activity.[60] It is therefore believed that FlgJ is a muramidase whose role is

to hydrolyze peptidoglycan to form a hole in the peptidoglycan layer of the cell so that the rod can proceed through it.[60,61]

Once the rod is complete, the P and L rings, comprised of FlgI and the lipoprotein FlgH, respectively, assemble around it.[12,62] Unlike most flagellar proteins, which are exported through the rod by the type III export apparatus, FlgI and FlgH are exported by the Sec system.[63,64] FlgA acts as a periplasmic chaperone for FlgI,[65] and DsbA acts to catalyze the formation of a crucial disulfide bond in FlgI,[66] so that all three proteins are required for P ring formation.

The hook assembles onto the distal end of the rod. FlgE, the hook subunit, polymerizes under the hook-capping protein FlgD.[67] The hook grows to a fairly constant length of 55 $\pm$ 6 nm,[68] at which time the FlgD cap dissociates and is replaced by FlgK, onto which are assembled FlgL and FliD.[69] FlgK, FliD, and FlgL are also known as HAP1-3, respectively. Assembly of FlgK and FlgL is assisted by the chaperone FlgN, whereas FliT acts as an assembly chaperone for FliD.[70-72] FlgK and FlgL join the hook and the filament, and FliD serves as the filament cap that is required for polymerization of flagellin.[73,74]

At some point during assembly, MotA and MotB distribute themselves around the MS ring. This process is independent of rotor assembly, since deletion of either one or both proteins still allows for the formation of the flagellum, albeit a non-functional one. MotA and/or MotB can be expressed after completion of flagellar assembly to restore motility,[75,76] but the location at which they initially insert into the membrane is not known.

The flagellar export apparatus has been extensively studied. It contains six membrane proteins (FlhA, FlhB, FliO, FliP, FliQ, and FliR) that are believed to be housed under the MS ring and inside the C ring.[77] The membrane topologies and possible functions of each of these six proteins has been inferred from their amino acid sequences. The exact arrangement of the six proteins within the export apparatus, as well as their stoichiometries, is unknown. FlhA, an export apparatus subunit, is believed to interact with the MS ring protein FliF.[78] A deletion mutation in *fliF* that result in a non-motile phenotype was able to be suppressed by mutations in or near the transmembrane domains of *flhA*.[78] This mutant in *fliF* does not allow for assembly of the flagellar motor to proceed past incorporation of the C-ring. The suppressors found in *flhA* were able to restore motility by restoring export and subsequent assembly of flagellar motor structures and the suppressing mutations in *flhA* had no effect on an otherwise wild-type cell.[78] These results suggest an interaction between the MS ring (FliF) and FlhA of the export apparatus.[78] In *Clostridium botulinum*, FliR and FlhB exist as a single, fused protein,[47,79] which implies that these proteins exist in equal amounts and are located near each other within the export apparatus.

The energy for export of flagellar components is provided by the soluble ATPase FliI,[80] which shows similarity to the β subunit of the F_O subunit of ATP synthase.[81] The ATPase activity decreases when FliI is bound to another soluble protein, FliH, at a ratio of 1:2, respectively.[82-84] A third soluble protein, FliJ, interacts with FliH and FliI.[56,85] There are common structural features between FliJ and the *Salmonella* flagellar proteins FliS, FlgN, and FliT, which are putative chaperones for the filament-type substrates FliC,

FlgK and FlgL, and FliD, as well as other members of the type III chaperone family in Yersinia.[85] Mutants of FliJ have been found that fail to export rod and hook proteins into the periplasm.[85] This suggests that FliJ may serve as a general chaperone that delivers substrate proteins to the export apparatus.[56,85]

During assembly of the flagellar motor, a switch occurs that changes the specificity of the export apparatus from recognition of components that form the rod and hook to recognition of late components such as hook-associated proteins (HAPS), flagellin, and FlgM. This switch minimizes competition during export, an important consideration since flagellin is made in very high amounts but is not needed until late in flagellar assembly.[47,77,86]

The last substrate of the early phase of export is the hook protein FlgE, and the switch appears to control the length of the hook. After the switch, the hook stops growing. The switch occurs when a specific bond is cleaved in FlhB.[87] FliK also plays a role in control of hook length.[42,68,88-90] FliK is a middle gene product that is exported much more efficiently in cells that lack hooks compared to when they are present.[91] Cells deleted for *fliK* have exceptionally long hooks, called polyhooks, with no filaments.[88,89] Mutations in *fliK* are suppressible by mutations in *flhB*, indicating that FlhB and FliK interact. This interaction may trigger the switch from early to late substrates.[92,93] The concentration of FliK increases as the hook is formed, but whether it is directly responsible for the cleavage of FlhB is unknown.

Flagellar rotation and switching proteins

Of the approximately two dozen proteins that make up the flagellum, only five appear to be involved in causing rotation (MotA, MotB, FliG, FliM, and FliN). Mutations in any of these can prevent rotation while still allowing for proper flagellar assembly.[94] MotA and MotB are membrane-bound proteins which together form the stator component.[18,95-97] They also form a channel that conducts protons across the membrane.[98,99] FliG, FliM, and FliN form the switch complex, which is necessary for rotation, switching of rotation from clockwise (CW) to counter-clockwise (CCW), and flagellar assembly.[57,100]

Most of the C-ring is formed by FliM and FliN.[14,101] The main role of FliM seems to be in switching between CW and CCW,[102] and it is the target to which the output of the chemotaxis signaling pathway, phosphorylated CheY (CheY-P), binds.[103] CheY-P binds near the N-terminus of FliM[104-106] and perhaps also contacts the C-terminus.[106] The role of FliN seems to be primarily structural or in flagellar assembly,[81] since it plays a minimal role in switching and rotation.[107,108]

FliG is directly involved in flagellar rotation through its C-terminal domain,[107-109] which interacts through charged residues with oppositely charged residues in MotA.[109] The N-terminus of FliG, known as the assembly domain, interacts with FliF of the MS ring.[110] The exact location of FliG is unknown, but electron micrographs of basal bodies with and without FliG indicate that it is attached to the bottom of the MS ring.[17]

The motor is estimated to contain 34 ($\pm$6) FliM and 111 ($\pm$13) FliN subunits, as determined by enhanced chemiluminscence (ECL) immunoassays and densitometry.[101]

Work with *T. maritima* has found that FliN forms a stable tetramer and that the stoichiometry of FliM to FliN is 1:4.[111] FliG has been estimated to have as many as 44 subunits[101] and as few as 25.[112] Two estimates of FliF both gave values of about 26,[64,113] and a FliF-FliG chimera allowed assembly of relatively normal and functional flagella.[17,114] Based on this finding, one would expect that FliG and FliF exist in a 1:1 ratio. It has been proposed that there is 1:1 ratio of FliG relative to FliM.[104,115,116] However, careful measurements by Thomas et al. (2006),[117] made by single-particle analysis, indicate that there are from 24 to 28 FliG subunits and 32 to 36 FliM subunits in the basal body of *Salmonella enterica*, with no particular correlation between the two numbers. The large discrepancy in the FliG measurements makes the average value of 34 seem reasonable, and a recent model for the interaction of FliM and FliG is consistent with the existence of an average of 26 FliG subunits and 34 FliM subunits.[118] Given the fact that perfect matches of proteins within the C and MS rings do not exist, it has been proposed that multiple symmetries exist within a rotor and that sites of protein mismatch on the rotor may form the sites of interaction with MotA in torque generation.[16]

Many mutations affecting the switch complex change the bias between CW and CCW rotation,[100] and so do specific mutations within the stator proteins MotA and MotB.[119,120] Switching of the direction of rotation is highly sensitive to the concentration of CheY-P and has a Hill coefficient of around 10, indicating high cooperativity of binding of CheY-P to FliM.[121] Based on the effect of certain mutations[100] and the strong cooperativity,[121] it could be that conformational changes within the switch complex, or

some repositioning relative to the rotor-stator interface, results in the change in rotational direction.[122]

Physiology of the flagellar motor

An experiment in which cells are attached to cover slips by one flagellar filament, termed a tethered-cell assay, showed that a single flagellar motor rotates a cell relatively slowly (at 1-20 Hz) at a high viscous load.[123] The observed rotation was very smooth, and it was therefore proposed that rotation involves relatively small steps.[10] When the tethered cell assay was performed with artificially energized cells,[124-126] it was found that: 1) for a given protonmotive force (Δp) rotational speed varies inversely with the viscosity of the medium, which implies that there is constant torque; 2) at up to 150 mV, torque is proportional to Δp; 3) torque does not significantly vary at temperatures between 5^{o}C and 40^{o}C; and 4) torque is the same in H_2O and D_2O.

Rotation of flagellar filaments[127] or small spheres attached to sheared filaments[128] was used to examine the behavior of individual flagella at lower viscous loads.[129-131] When rotation is monitored by light microscopy,[127,128,132] rates of 300 Hz or faster were obtained at very light loads, and the speed depended both on temperature and whether the observations were made on cells exposed to H_2O or D_2O.[127,128,133] This suggests that the speed of the motor depends on the rate of proton dissociation when the external load is light. The idea is bolstered by studies of the Na^+ motor of *Vibrio alginolyticus*. In the presence of Na^+, rotation rates of up to 1,700 Hz have been measured.[132] When lithium ions were substituted, the speed of rotation was the same

under heavy load but four fold slower at light load, perhaps due to slower dissociation of Li^+, relative to Na^+, caused by a higher affinity for Li^+ than Na^+ with a sodium-binding site within the channel that is responsible for transfer of Na^+ through the channel.[134]

Even though the top speed of flagellar rotation appears limited by proton dissociation, rotational speed does not vary much at external pH values between 4.7 and 8.8.[133] This result is interesting, since the relative contributions of $\Delta\Psi$ and ΔpH to Δp vary linearly across this range of pH.[135] However, the motors of *Bacillus subtilis* and *Streptococcus* show a dependence on external pH.[126,136]

To understand the mechanism of rotation more completely, one needs to look at the torque/speed relationship. Torque is proportional to the number of complexes per motor when the flagellum operates at high load.[128,129,137] This was found by attaching polystyrene beads to a flagellar filament of a cell (Δ*motA*) that was fixed to a glass slide. Upon induction of MotA, speed increased in a stepwise manner, as had been seen previously,[76] and that the torque produced with N number of torque generating units was simply N times the torque produced by a motor with a single torque generating unit.[137] Using optical tweezers, it was found that when the flagella rotated forward, were stalled, or were artificially rotated backwards, the torque produced in all three instances were identical.[138] It was concluded that the torque/speed relationship indicates a power-stroke mechanism, in which chemical energy drives rotation, as opposed to a "thermal ratchet" mechanism, which uses chemical energy to bias movements that are thermally driven.[131]

Based on their location around the periphery of the motor, it was first suggested,[139] and later confirmed by "resurrection" experiments using tethered cells, that

MotA and MotB can be incorporated into an otherwise complete motor.[75,76] Rotation was slow at first but accelerated rapidly in a series of steps until normal rotational speed was achieved. A total of eight steps were seen, leading to the idea that there were eight MotA and MotB complexes, each representing an independent torque-generating unit.[76] However, recent work has suggested that up to twelve torque generators service a single motor.[21] Under light loads, using a small bead attached to a sheared flagellum, it was found that nearly full rotational speed was obtained after insertion of a single torque-generating unit.[137]

It was subsequently shown that MotA and MotB form a channel through which protons flow to provide the energy for flagellar rotation.[98,140] This was achieved by measuring the proton flux into membrane vesicles containing wild-type MotA or mutant MotA's that resulted in relatively smaller swarm diameters.[98] Proton permeability into the vesicles was lower with the MotA mutants than with wild-type MotA.[98] In sodium motors, independent torque generators have also been observed by slowing rotation through the use of a sodium-channel blocker, and the numbers of torque generators have been estimated to be between five and nine.[141]

It is presumed that motor rotation happens through a series of small steps.[10] These steps are difficult to see, since the flexible hook and filament act as an elastic damper that smoothes discrete steps. Analysis of fluctuations in the rotational speed of tethered cells, based on the assumption that the time between steps follows a Poisson distribution, led to an estimate of 400 steps per revolution.[142] When cells with only one, or a few, torque generators were analyzed, it was found that each torque-generating unit

steps independently and that the units do not function in any particular order or at a specific interval.[142,143] About 26 steps per revolution in *E. coli* are observed in a motor driven by a sodium current through a single, hybrid stator complex that is made up of a *V. alginolyticus* PomAB sodium channel fused to an *E. coli* MotB periplasmic domain.[144] This number is in agreement with the most recent estimates of the number of FliG subunits per motor.

MotA and MotB

MotA contains 295 residues and is predicted to have four transmembrane helices (TM1-TM4), two short periplasmic loops joining TM1-TM2 and TM3-TM4, and two relatively large cytoplasmic domains, one between TM2 and TM3 and another following TM4[95,145] (**Fig. 1.5**). No crystal structure has been obtained. Two charged residues, Arg-90 and Glu-98, in the cytoplasmic loop between TM2 and TM3, when mutated to residues of opposite charge, or to neutral charge, resulted in a non-motile phenotype.[109] The C-terminal motility domain of FliG in the rotor also contains conserved charged residues that when mutated collectively effects motility.[146] However, certain combinations of MotA charge mutations with FliG charge mutations show suppression in a manner that suggests the two MotA charge mutations interact with charged residues in FliG and this interaction is essential for torque generation.[109,146] A third charged residue in MotA, Glu-150, appears to be somewhat important for torque generation as well.[147] Two of these charged residues in PomA, the MotA ortholog in *Vibrio*, were also found to be important for rotation.[148] Two conserved Pro residues at positions 173 and

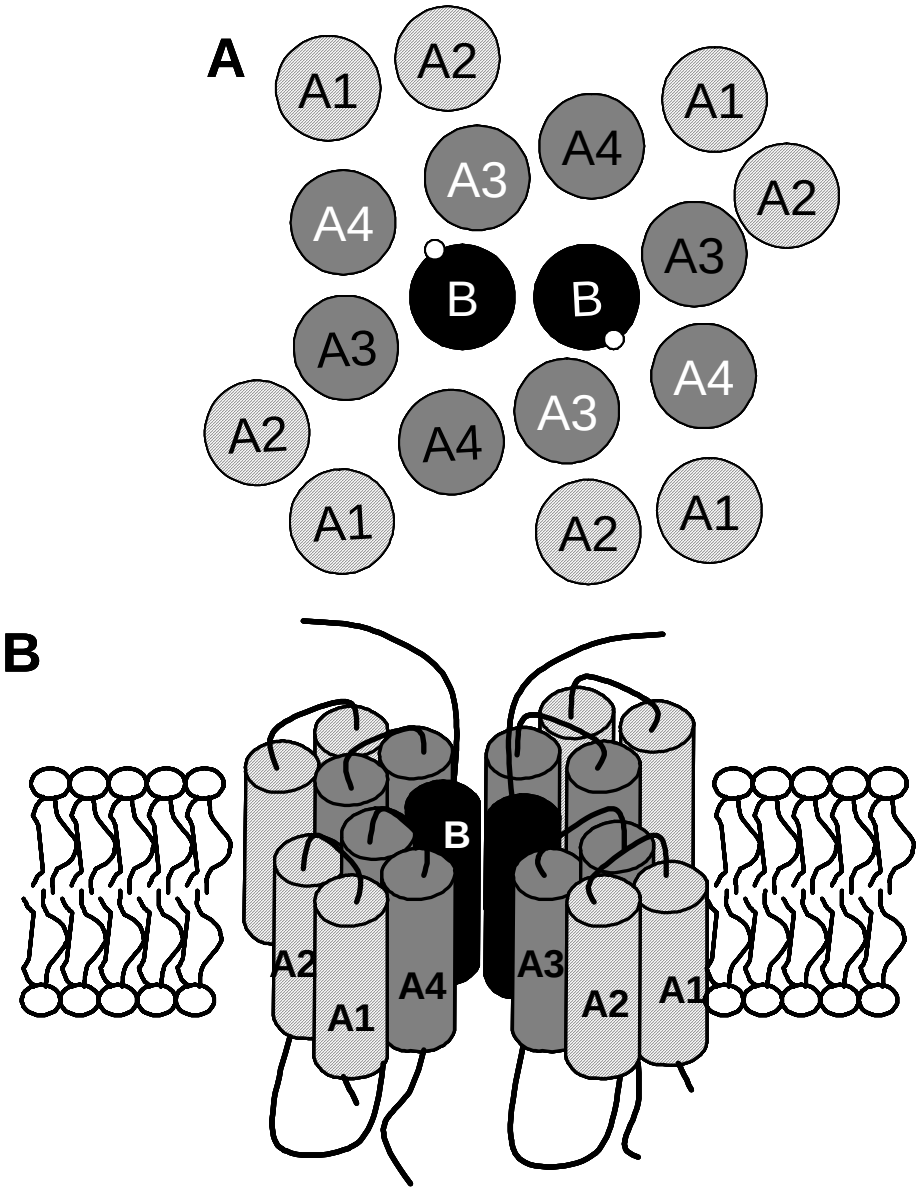

Figure 1.5. Model for the arrangement of the $MotA_4MotB_2$ complex. (A) Periplasmic view. (B) Side view. Cross-linking experiments have shown that MotA and MotB exist in a ratio of 2:1, respectively, with MotB existing as a dimer. This model was developed based on experiments in which transmembrane segments 3 and 4 were found to cross-link to each other as well as to the transmembrane domain of MotB, this model was developed. The placement of MotA TM1 and TM2 is unknown. (Adapted from Braun[164]).

222, which lie just beneath the cytoplasmic membrane at the base of TM3 and TM4 respectively, are also important for motility, perhaps because they are involved in conformational changes within the cytoplasmic loop of MotA.[149] Missense mutations affecting the TM regions or periplasmic loops of MotA can be suppressed by mutations in the periplasmic domain of MotB in an allele-specific manner,[150] suggesting that a precise alignment of the MotAB complex relative to FliG is critical.

MotB contains 308 residues and consists of a short N-terminal cytoplasmic domain, a single membrane-spanning helix, and a large periplasmic domain.[96,97,151] The periplasmic domain contains a sequence corresponding to a consensus peptidoglycan-binding motif that is thought to anchor the stator to the cell wall.[99,152] This sequence shares homology with known peptidoglycan-binding proteins, such as OmpA[153-157] and Pal.[157,158] Specifically, the region from Asn-210 to Gly-228 is very similar in sequence to known peptidoglycan-binding proteins.[159] The last 40 residues of MotB are dispensable for motility.[120] Mutations have been found that seem to misalign the MotAB complex with the rotor, and that some of these mutations are suppressed by changes in MotA or FliG.[119,160]

MotB by itself forms a symmetric dimer in the membrane as was found through Cys substitutions throughout the transmembrane domain that resulted in higher yields of MotB dimer at intervals of 3-4 residues. Such that the Cys substitutions that gave a higher yield of MotB dimer were clustered on one particular face of the TM.[161] This arrangement places a critical Asp-32 residue on the opposite side of the transmembrane domain.[161] Dimerization does not require MotA and occurs within a pre-existing

complex and is not due to two MotB's simply colliding in the membrane.[161] MotA may also form a dimer as the MotA homolog, PomA, in the sodium motor of *V. alginolyticus* has been found to do.[162,163] The stoichiometric ratio of MotA to MotB in the cell is 2:1. It is proposed that a functional MotAB complex contains two MotA dimers and one MotB dimer.[161,164] A similar organization was described for the homologous PomAB complex of the *V. alginolyticus* sodium-driven polar flagellum.[162,163] Braun et al.[164] performed targeted disulfide cross-linking in which double Cys mutants were created by placing single Cys substitutions into the MotA transmembrane domains 3 and 4, as well as the single MotB transmembrane domain and looking at the cross-linking patterns that occurred between MotA TM3/TM4, MotA TM3/MotB TM, and MotA TM4/MotB TM.[164] After analysis of which double Cys mutants formed dimers, either MotA homodimers or MotA/MotB heterodimers, and the dimer yields obtained, it was concluded that the proton channel consists of TM3 and TM4 of one MotA and the single TM of MotB.[164] The analysis of their results does not allow for a proton channel to be formed by two MotA's and the transmembrane domain of MotB.[164] This arrangement may allow two ion channels to form per complex[161,164] (**Fig. 1.5**). The location of TM1 and TM2 of MotA, presumably on the periphery of the complex, has not yet been identified. These results are consistent with a tryptophan-scanning analysis that found that TM3 and TM4 are constrained by nearby structures, whereas TM1 and TM2 are not.[165]

Replacement of residues within the TM of MotB found that the only critical residue for flagellar rotation was Asp-32.[166] Replacement with any residue other than

glutamate resulted in a non-motile phenotype, and even the D32E mutant was only partially motile. Rounds of protonation and deprotonation of Asp-32 are proposed to drive conformational changes in the cytoplasmic region of MotA that interacts with FliG to generate flagellar rotation.[109,166,167] Asp-32 lies close to the N-terminal, cytoplasmic end of the MotB TM helix and faces into the proton channel.[161,164] Although there may be two functional proton channels per complex, each with its own Asp-32 residue, it is unknown whether both function at the same time. This issue may not be resolved until the orientation of the MotAB complex relative to the flagellar motor is determined.

It has been estimated that there is a flow of 65 protons per torque generator per revolution.[75] It was also concluded that the kinetic properties of the motor are best explained for if the motor uses two protons at a timetogether.[131] Simulations performed on an electrostatic model of the motor found that the measured torque could be achieved if there were 22 active channels per motor.[168] Either 22 MotAB complexes with only one active channel or 11 complexes with two active channels could account for this number. Various recent measurements of an average of 11 Mot complexes per motor are in agreement with the second possibility.[18,20,21]

Although they appear different at first glance, the overall structure of the torque generating channels of the sodium-driven motor and the proton-driven motor must be similar. Rotation of either motor can be induced by the presence of the stator from the other.[169,170] Chimeras made between the stator units of proton-driven and sodium-driven motors can function for sodium-driven motility, so that the determination of ion specificity cannot reside totally in the transmembrane domains.[169,171] In *V. alginolyticus*,

the periplasmic domain of PomB is required for motility, probably because of its interaction with the outer membrane proteins MotX and MotY.[172] Although the exact role of MotX and MotY are unknown, it appears to be specific to *Vibrio*, since a chimera of MotB-PomB confers motility in *E. coli* and is sodium driven[172] in the absence of MotX and MotY.

MotB is relatively unstable in the absence of MotA, but MotA is stable in the absence of MotB.[173] MotA and MotB can be co-overexpressed up to 50 fold and accumulate to high levels in the cytoplasmic membrane with no obvious deleterious effect on the cells.[174] This result suggests that the excess MotAB complexes are inactive as proton channels.[173] However, when the first 60 residues of MotB, including the membrane-spanning helix, are fused to a 50-residue sequence encoded by an open reading frame in the TetA gene, cell growth is inhibited when the fusion protein is co-overexpressed with MotA, presumably because of a proton leak.[98,99,166] A substitution at the critical Asp-32 residue by Asn eliminates the growth defect associated with the $MotB_{60}$-TetA fusion by blocking proton flow through the channel.[166] Of 14 MotB-PhoA fusions identified previously,[97] only the most N-terminal, in which the fusion joint was after residue 67 of MotB, caused a severe growth defect.

Limited proteolysis studies of MotA, with and without MotB, in inside out membrane vesicles found that the conformation of MotA changes based on the pattern of digestion seen when the digests were performed with wild-type MotAB as compared to $MotAB_{D32N}$.[167] The sites of cleavage in MotA were determined to be in the cytoplasmic loop of MotA, which contains the charged residues that interact with FliG.[167] A plausible

model, therefore, is one in which protonation of Asp-32 in MotB drives a conformational change that forces the cytoplasmic loop of MotA to push against FliG, resulting in rotation of the flagellar motor.[167]

The work reported here was to discover more about MotA, MotB, and their function as a proton channel. It has been previously proposed that a portion of MotB may be involved in blocking the flow of protons through the MotAB channel when it is not in contact with a flagellar motor, but that this block is removed upon contact with the motor, perhaps due to a conformational change induced by contact with the basal body, thus allowing the channel to assume its open, proton-conducting state.[120,164] It was believed that if the block is artificially removed, slower growth phenotypes would be observed, as had been seen previously.[98,99,166] Fusions of MotB to PhoA, single residue substitutions, and deletions of residues were performed and assayed by looking at the growth phenotypes of these mutants compared to wild-type and is presented in Chapter II. Chapter III outlines work to determine whether groups of oppositely charged residues in the C-terminus of MotA and the N-terminus of MotB interact to stabilize MotB or to position MotA relative to the rotor. If such an interaction between these two regions exists, then altering the charges of the residues in these regions should disrupt the interaction leading to MotB being unstable even in the presence of MotA. Chapter IV details work that was performed to understand the translational coupling between *motA* and *motB* and whether that coupling is responsible for generating the 2:1 intracellular ratio of MotA to MotB. Chapter V presents preliminary work performed to test the hypothesis that MotB interacts with the peptidoglycan layer of the cell wall. This

hypothesis is based on the presence of a conserved peptidoglycan binding motif in MotB that is found in other known peptidoglycan binding proteins.

CHAPTER II

THE *E. coli* MotAB PROTON CHANNEL UNPLUGGED

Introduction

We have presented a model for insertion of the MotA/MotB complex into the flagellar motor.[120] We proposed that MotA and MotB exist in the membrane in an inactive form in which part of the complex, possibly the periplasmic domain of MotB, blocks proton flow through the channel. This pre-assembled form of the complex can diffuse within the membrane until it collides with a rotor. Once the complex contacts a motor, a conformational change removes the block and activates the channel. In either a coupled or separate event, the peptidoglycan-binding domain of MotB attaches to the cell wall.

Here, we report experiments that confirm the first part of the model. We have identified a short segment in the periplasmic domain of MotB that acts as a plug to block the proton channel. Residues 52 through 65 form an amphipathic helix flanked by Pro residues. Our analysis of this region inspired a model for control of proton flow through the MotAB complex. The ability to block proton flow through MotAB channels not yet incorporated into flagellar motors could represent a significant selective advantage to the cells.

Results

Generation of MotB-PhoA fusion proteins. Alkaline phosphatase (PhoA) is only active in the periplasm.[175] PhoA, lacking the cleavable signal sequence needed for

export, has been fused to membrane proteins to probe their topology,[176] and this approach has been successfully applied to MotB.[97] We therefore decided to use MotB-PhoA fusions to determine how much of MotB is required to cause proton leakage in the presence of excess MotA.

PhoA was fused to MotB after residues 308 (full-length MotB), 233,190, 140, 110, 90, 80, 70, 65, 60, 50, 35, and 20 to generate the MotB-$PhoA_{308}$ through MotB-$PhoA_{20}$ hybrid proteins. Residue 20 normally resides in the cytoplasm, residue 35 is in the TM region, and the remaining residues are located in the periplasm.[97] We placed the fusion genes after an intact plasmid-borne *motA* gene that is under control of the *araBAD* promoter. Plasmids containing the various fusion constructs were introduced into strain MM5000 (Δ*motAB*), and the transformed cells were plated onto LB agar plates containing Amp (50 μg per ml). These same cells were also plated onto LB agar plates containing the chromogenic PhoA substrate 5-bromo-4-chloro-3-indolyl phosphate (BCIP) and 0.2% L-arabinose to screen for PhoA activity. Stable dark blue colonies were obtained when cells were transformed with plasmids encoding hybrids with fusions at position 70 or later in MotB. Stable white colonies were obtained for cells transformed with plasmids encoding hybrids with fusions at positions 20 or 35, as expected, since PhoA in these chimeras should not localize to the periplasm. Fusions at positions 50, 60, and 65 allowed normal growth of pale blue colonies only in the absence of arabinose. Only the MotB-$PhoA_{308}$ hybrid supported motility, a result consistent with previous mutational analyses.[120,177]

To quantify how deleterious the fusion proteins were, we monitored growth in tryptone broth (TB) at 30°C in MM5000 cells containing the various p*araBAD* plasmids. Induction of $MotB_{308}$-PhoA, $MotB_{190}$-PhoA, $MotB_{70}$-PhoA, $MotB_{35}$-PhoA, and $MotB_{20}$-PhoA together with MotA did not decrease the growth rate below that of cells expressing wild-type MotA and MotB. In contrast, cells expressing $MotB_{65}$-PhoA grew slower, and expression of $MotB_{60}$-PhoA and $MotB_{50}$-PhoA resulted in complete cessation of growth within 1 h of the addition of arabinose (**Fig. 2.1A**). About the same amount, on a per cell basis, of fusion protein of the size expected was detected in immunoblots of whole-cell extracts from induced cultures probed with PhoA antibody (data not shown). Nearly identical growth defects were seen when synthesis of the $MotB_{50}$-PhoA, $MotB_{60}$-PhoA, and $MotB_{65}$-PhoA fusions were induced in strain RP3098, which does not make any flagellar proteins (data not shown). The growth defects were seen only in the presence of functional MotA (data not shown).

To test whether the growth defects were attributable to proton influx rather than a general disruption of the membrane, we introduced the $MotB_{D32N}$ substitution into the chimeras. All growth defects were eliminated, and cells expressing the formerly toxic fusions now grew slightly faster than cells expressing wild-type MotAB (**Fig. 2.1A**). This result indicates that a proton leak through the large number of MotA/MotB-PhoA complexes not associated with flagellar basal bodies is responsible for the growth defects observed.

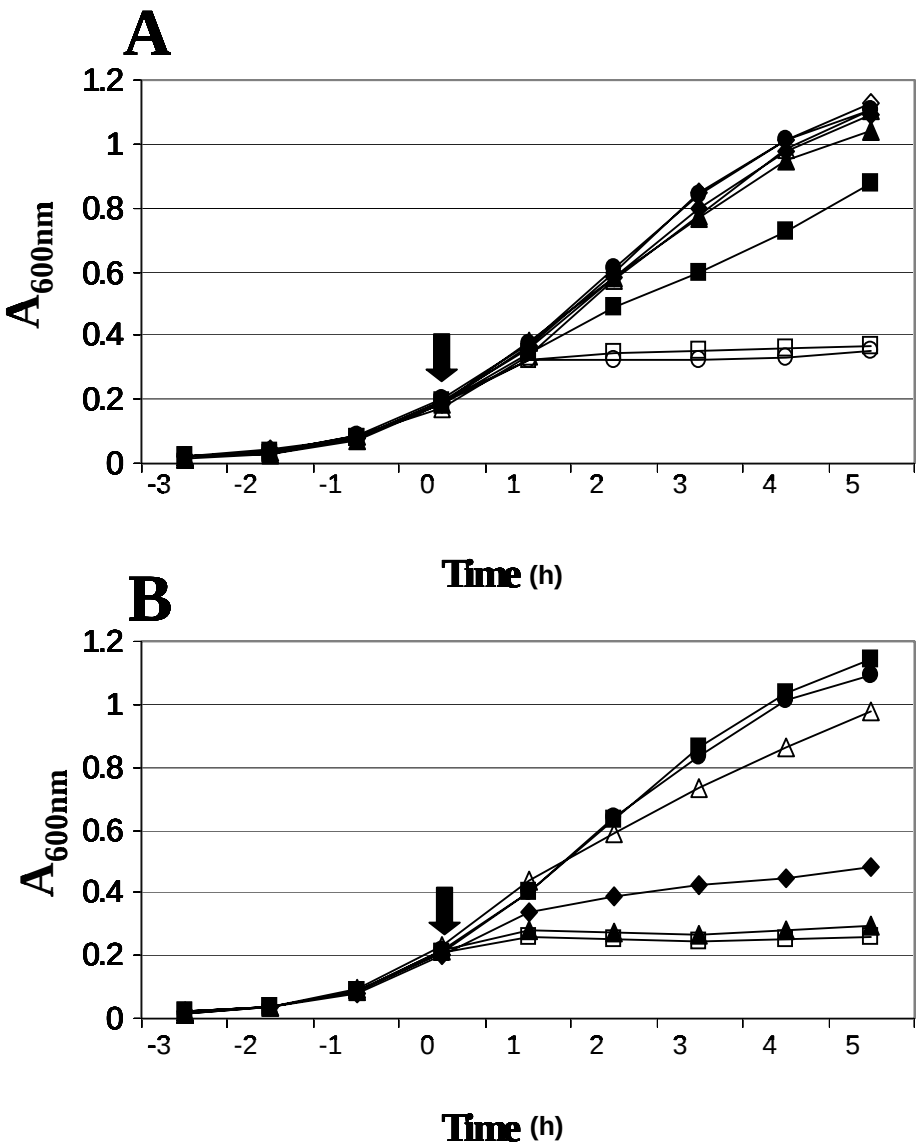

Figure 2.1. Growth curves of cells expressing MotAB-PhoA fusions and internal MotB deletions. (A) Growth curves of Δ*motAB* cells expressing MotA and C-terminal MotB fusions to PhoA. Growth curves were performed as described in Materials and Methods. A_{600nm} was measured after the initial dilution (-3 h) and then every hour (time points -2 h to 5 h). Arabinose (0.2%) was added after 3 h (arrow; t = 0 h). MM5000/p*motAB* (—●—); AB_{308}-PhoA (—◆—); AB_{70}-PhoA (—▲—); AB_{65}-PhoA (—■—); AB_{60}-PhoA (—○—); AB_{50}-PhoA (—□—); $AB_{D32N/60}$-PhoA (—△—); AB_{35}-PhoA (—◇—). (B) Growth curves of Δ*motAB* cells expressing MotA and MotB containing residue deletions within or near the proposed "plug" of MotB. Cultures were grown as above. MM5000/p*motAB* (—●—); $AB_{\Delta 51\text{-}60}$ (—◆—); $AB_{\Delta 51\text{-}70}$ (—▲—); $AB_{D32N/\Delta 51\text{-}70}$ (—■—); $AB_{\Delta 61\text{-}70}$ (—□—); $AB_{\Delta 71\text{-}90}$ (—△—).

The effect of internal *motB* deletions on cell growth. To determine which residues of MotB block proton flow through the MotAB proton channel, various in-frame internal deletions were introduced into *motB*. Cells induced to express the $MotB_{\Delta 51\text{-}70}$, $MotB_{\Delta 51\text{-}80}$, $MotB_{\Delta 51\text{-}90}$, and $MotB_{\Delta 61\text{-}70}$ proteins along with MotA stopped growing (**Fig. 2.1B**; category 4 growth in **Table 2.1**), and induction of the $MotB_{\Delta 51\text{-}60}$ protein and MotA led to a dramatic decrease in growth rate (category 3 in **Table 2.1**). In contrast, the $MotB_{\Delta 71\text{-}90}$ protein had a relatively minor effect (category 2 in **Table 2.1**). All mutant proteins were present at normal levels (data not shown). Growth was inhibited similarly when proteins were expressed in strains MM5000 and RP3098, and the $MotB_{D32N}$ substitution again eliminated all growth defects (data not shown).

Inspection by phase-contrast microscopy showed that MM5000 cells expressing MotA and wild-type MotB, or any of the internally deleted MotB proteins, became motile within 15 min after induction with arabinose (data not shown). At least some cells remained motile for at least several hours after induction, long after some cultures stopped growing.

The MotB sequence was analyzed by the program PredictProtein (available at http://cubic.bioc.Columbia.edu), which predicted an α-helix between Pro-52 and Pro-65. Previous analysis of MotB-PhoA fusions places this helix in the periplasm.[97] with Pro-52 located approximately five residues after the single TM of MotB. A helical wheel projection of the helix shows that it is amphipathic (**Fig. 2.2**). Because of the discrete structure and function of this region, we refer to it as the plug of the MotAB channel.

Table 2.1. Mutant MotB proteins grouped according to their effect on growth phenotype.

Category 1[a]	Category 2[b]	Category 3[c]	Category 4[d]
MotAB	B_{65}-PhoA	Δ51-60	B_{60}-PhoA
B_{308}-PhoA	Δ71-90	E60C	B_{50}-PhoA
B_{70}-PhoA	K53C	I58A	Δ51-70
B_{35}-PhoA	L55A	Y61R	Δ51-80
B_{20}-PhoA	Y61W	R63E	Δ51-90
K53A	F62Y	P52A/P65A	Δ61-70
E54A			E54C
I56A			L55C
Q57A			I56C
E60A			Q57C
R63A			I58C
T64A			A59C
K53E			Y61C
Y61F			F62C
T64S			R63C
P52A			T64C
P65A			Y61A
			F62A
			L55E
			I58E
			Y61S
			Y61Q
			Y61E
			F62S
			F62E
			F62R
			F62L
			F62Q
			F62W

[a] Category 1: wild-type growth.
[b] Category 2: slightly slower than wild- type growth.
[c] Category 3: significantly slower than wild-type growth.
[d] Category 4: growth ceases within 1 h of arabinose addition.

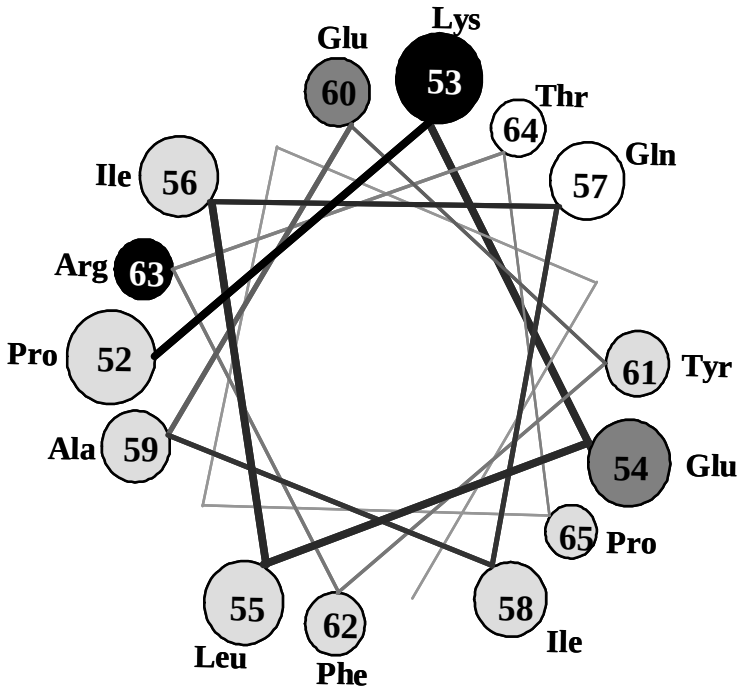

Figure 2.2. Helical-wheel projection of the predicted α-helix extending from residues Pro-52 to Pro-65 of MotB. Polar, uncharged residues are shown in white; nonpolar residues in light gray; acidic residues in dark gray; and basic residues in black.

The behavior of MotB proteins with Cys substitutions in the plug. When the proton channel opens, the two plugs in the $MotA_4MotB_2$ complex might come close enough to form a disulfide bond between introduced Cys residues. To test this possibility, we introduced Cys at each of the residues 53 to 64 of MotB by site-directed mutagenesis and then monitored the growth of cells expressing these proteins and MotA (**Fig. 2.3A**; **Table 2.1**). Induction of $MotB_{K53C}$ had a modest effect on cell growth (category 2), and induction of $MotB_{E60C}$ severely decreased growth (category 3). Induction of every other Cys-substituted protein blocked growth completely (category 4). The effects on growth were identical in strains MM5000 and RP3098, and the MM5000 cells remained motile for several hours.

Immunoblots of whole-cell extracts in strain MM5000 revealed that all of the Cys-substituted MotB proteins dimerize spontaneously (**Fig. 2.3B**). An identical result was obtained with strain RP3098 (data not shown). With the $MotB_{L55C}$, $MotB_{I58C}$, $MotB_{A59C}$, $MotB_{Y61C}$, $MotB_{F62C}$, and $MotB_{R63C}$ proteins, very little monomer remained. Only $MotB_{K53C}$ remained primarily as a monomer. This result shows that MotB-dimer formation does not require the presence of flagellar motors, even as a catalyst. The peaks of crosslinking at intervals of 3 to 4 residues is consistent with the idea that the plug is an α–helix and suggests the two plugs align in a parallel orientation.

If locking channels "open" causes the growth defects observed with the Cys-substituted proteins, reduction of the disulfide bonds could reverse the effect. Accordingly, 2 mM DTT was added to growing cultures 2 h after induction. All but three of the mutants resumed growth (**Fig. 2.3C**). The exceptions were $MotB_{I58C}$,

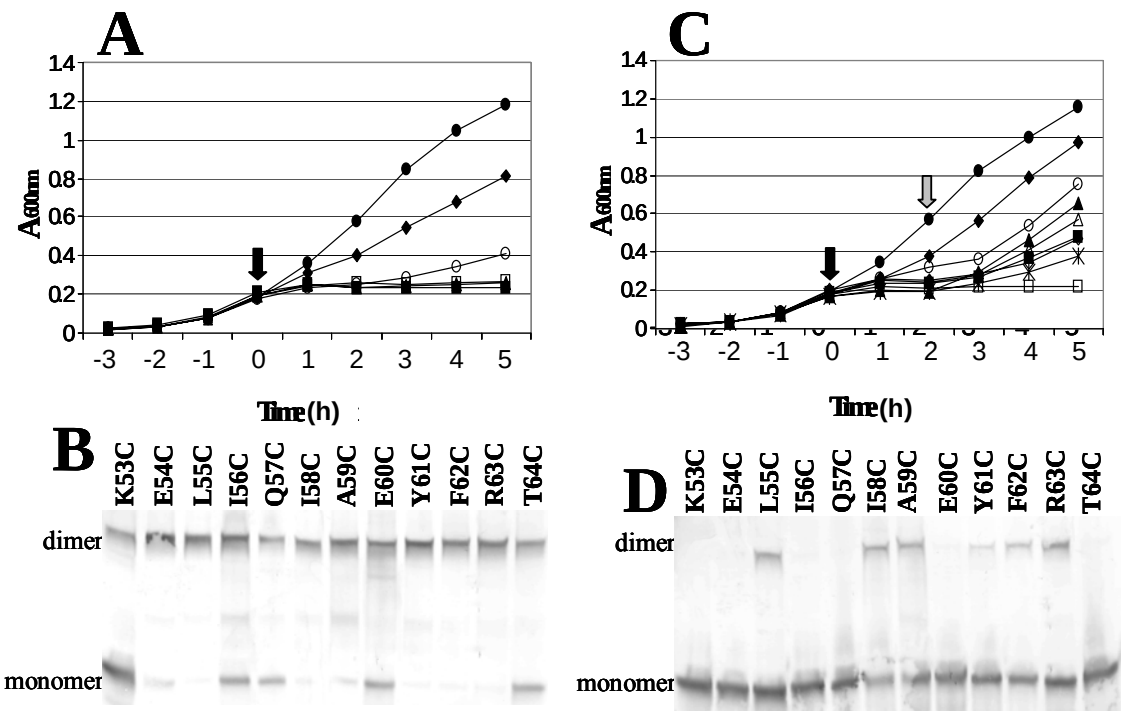

Figure 2.3. Effect of single Cys substitutions within the proposed α-helical region of MotB. (A) Single Cys residues were introduced into the proposed α-helical region of MotB at positions K53 to T64. Proteins were expressed and growth monitored as in Figure 2.1. Representative samples of different effects on growth are shown. Refer to Table 2.1 for a complete list. MM5000/p*motAB* (—●—); /K53C (—◆—); /I56C (—▲—); /A59C (—■—); /E60C (—○—); /Y61C (—□—). (B) Immunoblot of whole-cell extracts of a Δ*motAB* strain expressing MotA and Cys-substituted MotB. Extracts were prepared and subjected to SDS-PAGE as described in Materials and Methods. Proteins were visualized by immunoblotting with MotB antibody. (C) Growth effects observed as in (A) except that 2 mM DTT was added at 2 h (gray arrow). MM5000/p*motAB* (—●—); /K53C (—◆—); /E54C (—△—); L55C (—◇—); /I56C (—▲—); /A59C (—■—); /E60C (—○—); /Y61C (—□—); and /R63C (···■···). (D) Immunoblot of whole cell extracts of a Δ*motAB* strain expressing MotA and Cys-substituted MotB. Extracts were prepared and subjected to SDS-PAGE as described in Materials and Methods. Proteins were visualized by immunoblotting with MotB antibody.

$MotB_{Y61C}$, and $MotB_{F62C}$. Immunoblots of whole cell extracts subjected to non-reducing SDS-PAGE showed that 2 mM DTT nearly completely eliminated dimers of the $MotB_{53C}$, $MotB_{E54C}$, $MotB_{I56C}$, $MotB_{Q57C}$, $MotB_{E60C}$, and $MotB_{T64C}$ proteins (**Fig. 2.3D**). In the absence of crosslinking, these Cys-substituted plugs can apparently close the MotAB proton channel. Significant levels of crosslinked dimer remained with $MotB_{L55C}$, $MotB_{I58C}$, $MotB_{A59C}$, and $MotB_{R63C}$, and low levels of dimer were seen with $MotB_{Y61C}$, and $MotB_{F62C}$.

The effect of Ala substitutions at residues 53 to 64 of MotB. The inability of cells producing $MotB_{I58C}$, $MotB_{Y61C}$, and $MotB_{F62C}$ to resume growth after addition of DTT could be due to loss of the native residue or retention of crosslinked MotB dimer. The second explanation seems unlikely, because $MotB_{L55C}$ and $MotB_{R63C}$ retain much crosslinking in the presence of DTT, although DTT restores the growth of cells producing these proteins. To address this point directly, we replaced residues 53 through 64 of MotB with Ala. Cells producing all of the Ala-substituted proteins except $MotB_{L55A}$, $MotB_{I58A}$, $MotB_{Y61A}$, and $MotB_{F62A}$ grew like cells producing wild-type MotB (**Table 2.1**). Cells producing $MotB_{L55A}$ showed category 2 growth, $MotB_{I58A}$ caused category 3 growth, and $MotB_{Y61A}$ and $MotB_{F62A}$ completely eliminated growth (category 4) (**Table 2.1**). All of the mutant proteins were present at normal levels, based on immunoblot analyses (data not shown). Thus, residues Tyr-61 and Phe-62, and to a lesser extent Leu-55 and Ile-58, may be uniquely important for proper function of the plug.

The MotB plug does not interact specifically with the periplasmic loops of MotA. The non-polar face of the plug helix contains a number of charged residues (**Fig. 2.2**), as does the periplasmic loop between TM3 and TM4 of MotA, which has the sequence DRPAAEL. To determine whether electrostatic interactions are important for plug function, we converted the charged residues in the TM3-TM4 loop to Ala or residues of opposite charge (Arg or Glu, respectively, for acidic or basic residues), singly and in combination. None of these changes affected the growth of cells producing the mutant MotA together with wild-type MotB (data not shown). We also converted the Lys-53 and Arg-63 residues of the MotB plug to Ala or Glu and the Glu-54 and Glu-60 residues to Ala. Only the $MotB_{R63E}$ substitution had a detectable effect; it led to category-3 growth (**Table 2.1**).

We next investigated whether hydrophobic interactions between the plug and MotA might be involved in plug function. No substitution of hydrophobic residues with Ser, singly or in combination, in either periplasmic loop of MotA affected growth (data not shown), suggesting that direct protein/protein interactions are not key to plug function.

The effect of converting residues in the TM3-TM4 loop of MotA or residues 53 through 64 of MotB to other amino acids. An alternative mechanism for function of the plug is that it might bury its hydrophobic face in the membrane to block the channel. If so, mutations that disrupt association of the plug with the membrane might cause growth defects. To test this prediction, we made site-directed mutations that target

codons specifying residues 53 through 64 of MotB and measured the growth of strains producing these proteins (**Table 2.1**). The K53E, Y61F, and T64S substitutions had no deleterious effect on growth. The Y61W and F62Y substitutions impaired growth somewhat (category 2). The Y61R and R63E substitutions resulted in category-3 growth. Finally, the L55E, I58E, Y61S, Y61Q, Y61E, F62S, F62E, F62R, F62L, F62Q, and F62W substitutions completely abolished growth. MM5000 cells producing these mutant proteins became motile within 15 min of induction with arabinose, except for cells expressing $MotB_{Y61F}$, which remained non-motile. All of the mutant MotB proteins were produced at normal levels (data not shown). These results reinforce the notion that Leu-55, Ile-58, Tyr-61, and Phe-62 are important for plug function and are consistent with a membrane-interaction hypothesis (**Fig. 2.4A**). Tyr-61 and Phe-62 seem especially critical.

Cys-crosslinking of MotB may occur during membrane assembly. The most likely reason for the uniquely non-motile phenotype of cells expressing $MotB_{Y61F}$ might be that the Y61F plug does not readily come out of the membrane. If so, then cells expressing the $MotAB_{A59C/Y61F}$ doubly substituted protein might have their growth less impaired than cells expressing the $MotAB_{A59C}$ complex because the crosslinks form less readily. However, growth of the single and double mutants after arabinose induction was identical and led to complete (category 4) inhibition of growth, and the degree of crosslinking seen in the absence of DTT was identical for the two Cys-substituted proteins (data not shown). A simple explanation for this result is that the disulfide bond

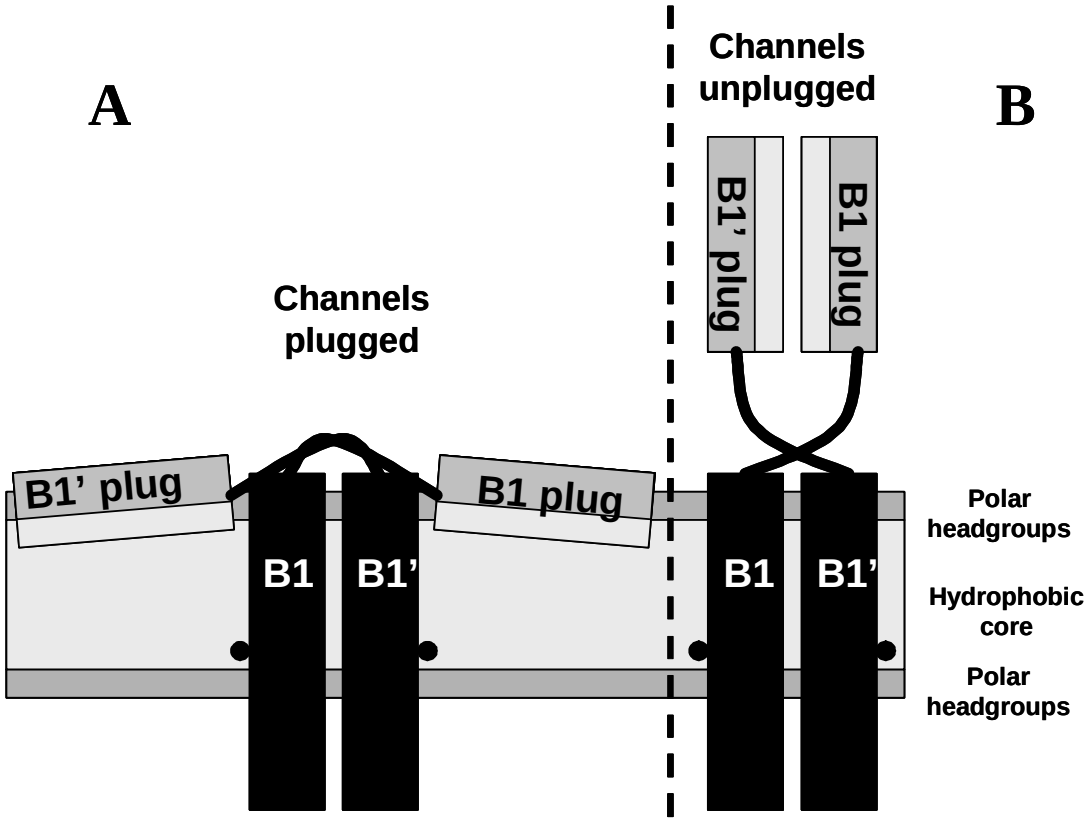

Figure 2.4. Schematic to show the position of the plug in the closed and open states of the channel. Only the MotB TMs and plugs are shown, in a view parallel to the plane of the cell membrane. The plugs are depicted in the *trans* configuration. Asp-32 is shown as a black dot. The interior hydrophobic core of the membrane is indicated with light gray, the layers containing the polar head groups of the membrane phospholipids are shown in dark gray. Similarly, the hydrophobic face of the amphipathic plug helix is shown in light gray and the remainder of the plug helix is shown in dark gray. (A) In the closed state, the hydrophobic faces of the plug helices are in contact with the hydrophobic core of the membrane, and the amphipathic Tyr-61 residue resides in the interfacial zone between the hydrophobic core and the polar head groups. (B) In the open state, the hydrophobic faces of the two plug helices may pack against one another in the periplasm to stabilize the open channel. The conformational change that opens the channel may also allow the peptidoglycan-binding domain of MotB to attach to the cell wall (not shown).

between the two Cys-59 residues forms early during assembly of the MotB dimer, before the plug enters the membrane. Other possibilities are considered in the Discussion.

The MotB plug can act in *trans*. The active Mot protein complex is believed to contain two copies of MotB and 4 copies of MotA and is likely to contain two proton-conducting channels. Each channel requires Asp-32 for function, and each should have a plug. This configuration affords two non-mutually exclusive possibilities: the plug acts in *cis* to block the channel containing the MotB of which it is a part (**Fig. 2.5A**), or it acts in *trans* to block the channel containing the other copy of MotB (**Fig. 2.5B**).

Neither the MotAB nor $MotAB_{\Delta 51\text{-}70/D32N}$ complex impairs growth when expressed alone. To determine whether the plug functions in *trans*, we employed a strategy used to study interaction of aspartate and maltose-binding protein with the Tar chemoreceptor.[178] Expression of p*tacmotA*$^{+}$*B*$^{+}$ and p*araBADmotA*$^{+}$*motB*$_{\Delta 51\text{-}70/D32N}$ was induced with 1 mM IPTG and 0.2% arabinose, respectively, from compatible plasmids. Since the two MotB proteins are expressed at about the same level (data not shown) and should dimerize equally well, half of the MotAB complexes should be heterodimers. Even if the levels of expression are somewhat different, a significant number of heterodimers should be made. If the plugs act in *cis*, then no difference in growth would be expected, since no constitutively open channels are present (**Fig. 2.6A**). However, if they act in *trans*, slower growth is expected since the plug of the wild-type MotB would serve to block proton flow through the inactive $MotAB_{D51\text{-}70/D32N}$ channel, but the wild-type MotAB channel would remain constitutively open due to the lack of a plug (**Fig.**

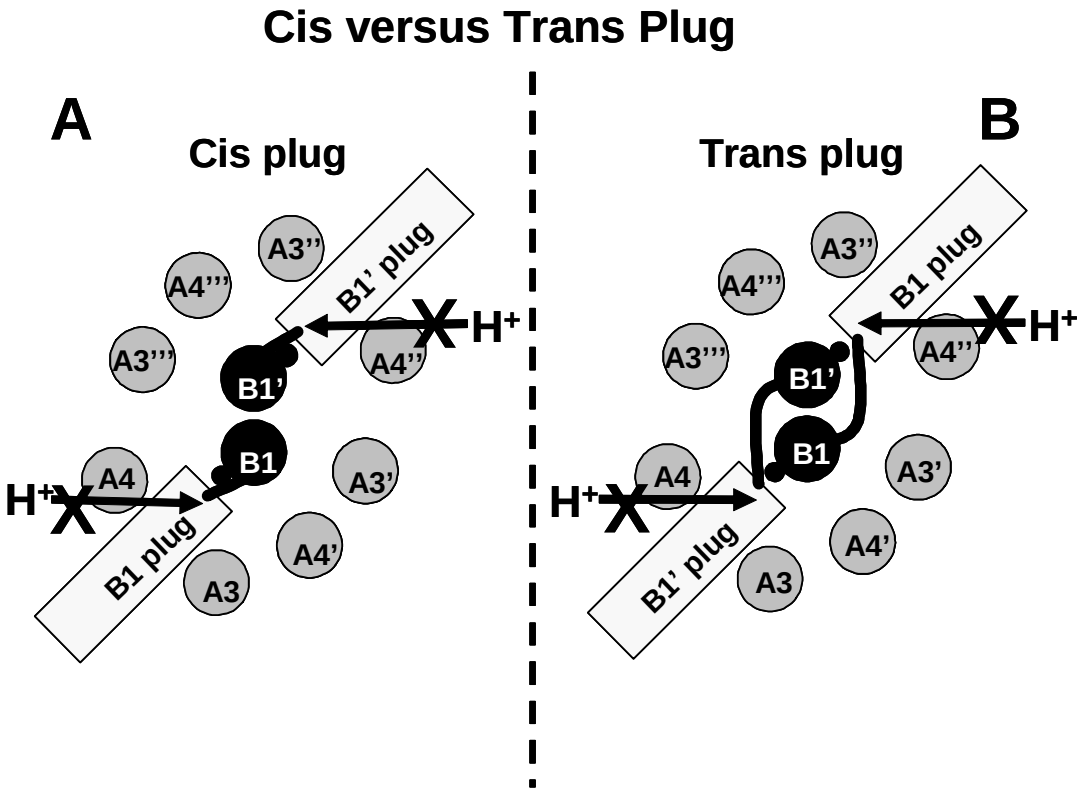

Figure 2.5. Schematic of how the plug may function in *cis* or in *trans* within the $MotA_4MotB_2$ complex. The complex is viewed perpendicular to the plane of the membrane from the periplasmic side. The arrangement of helices is as shown in Braun[164]. The Asp-32 residue is depicted as a black dot. The TM1 and TM2 helices of MotA are excluded for the sake of clarity. (A) Each plug blocks the channel containing the MotB TM helix that is part of the same polypeptide. (B) Each plug blocks the channel containing the MotB TM helix that is not part of the same polypeptide.

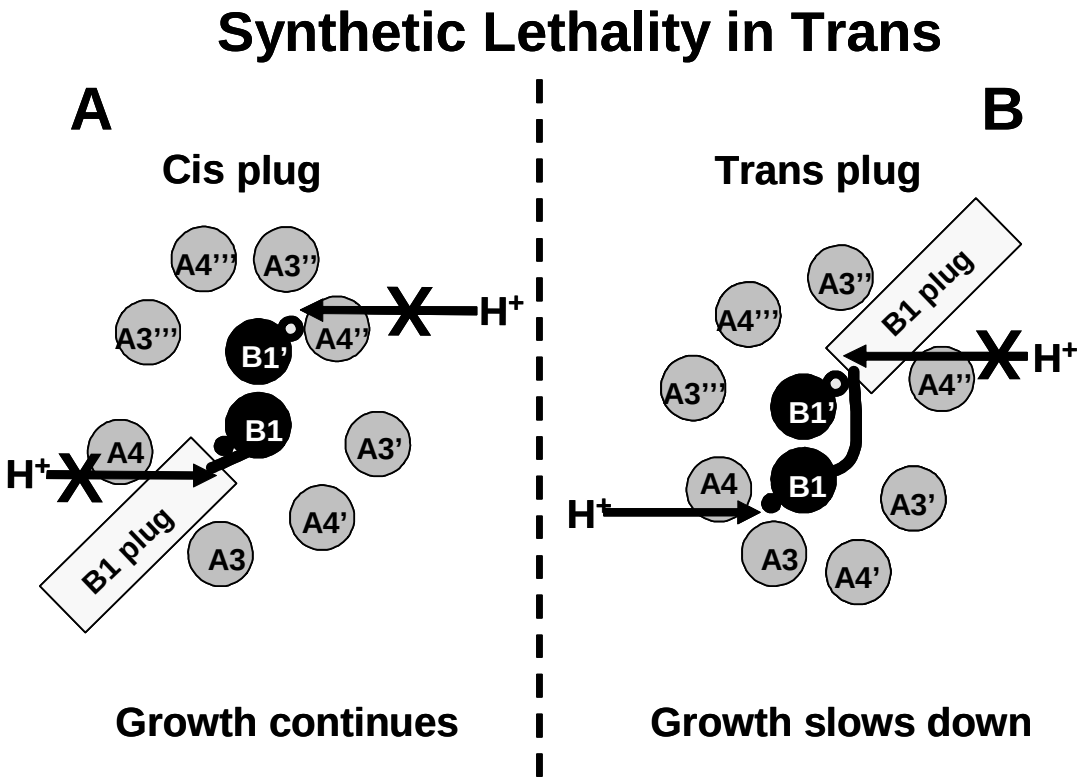

Figure 2.6. Schematic explaining the MotB synthetic-lethality test. The view is the same as in Figure 2.5. When wild-type MotB and $MotB_{\Delta 51\text{-}70/D32N}$ are overexpressed in equal amounts, along with MotA, from two compatible plasmids, one quarter of the $MotA_4MotB_2$ complexes will contain two copies of wild-type MotB, one quarter will contain two copies of $MotB_{\Delta 51\text{-}70/D32N}$, and one half should contain one wild-type MotB and one $MotB_{\Delta 51\text{-}70/D32N}$. Neither wild-type MotB nor $MotB_{\Delta 51\text{-}70/D32N}$ impairs growth significantly when overexpressed together with MotA. Asp-32 is shown as a black dot, Asn-32 is indicated by a black-ringed gray dot. (A) If the plugs act in *cis*, neither channel will conduct protons. One is plugged and the other contains the D32N substitution. (B) If the plugs act in *trans*, the channel that contains Asp-32 will be unplugged and the non-functional D32N channel will be plugged.

2.6B). When this experiment was done, growth declined to the category 2 level (**Fig. 2.7**). We conclude that at least some of the wild-type MotAB channels must be open in these cells because the $MotAB_{\Delta 51\text{-}70/D32N}$ subunit failed to block the wild-type channels in *trans*. The plugs of the wild-type MotB in such heterodimers would block non-functional channels containing Asn-32.

Pro-52 and Pro-65 are important for plug function. The Pro residues flanking the amphipathic helix might help position the plug in the channel. To test this possibility, P52A and P65A single substitutions and the double substitution were introduced by site-directed mutagenesis. Although the single replacements had no significant effect, expression of the doubly substituted MotB protein severely impaired growth (category 3) when it was expressed with MotA (**Table 2.1**). Cells of all three mutants were motile after induction with arabinose and exhibited wild-type levels of protein (data not shown).

Proton leakage through MotAB does not collapse Δp. An unplugged MotAB complex might inhibit growth by allowing an uncontrolled proton influx that collapses Δp. We calibrated this effect by titration with the Δp-uncoupler dinitrophenol (DNP). Cells were grown with 100 μM to 1 mM DNP. Increasing concentrations of DNP up to 400 μM caused a stepwise decrease in the growth rate of cells expressing wild-type MotAB (**Fig. 2.8A**). Higher concentrations led to an essentially immediate and complete cessation of growth.

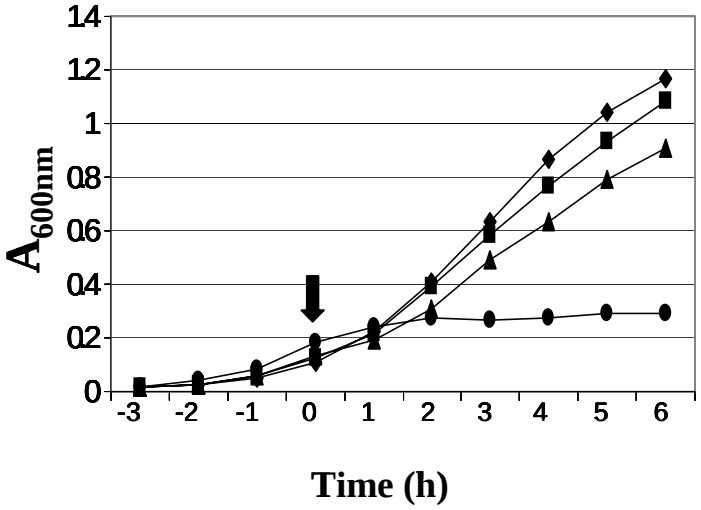

Figure 2.7. Testing *cis* vs *trans* orientation of the plug. Growth curves of Δ*motAB* cells expressing plasmid pairs pBAD30-*motAB*$_{\Delta 51\text{-}70/D32N}$ and pHSG575 (—◆—), pBAD30-*motAB* and pHSG575-*motAB* (—■—), pBAD30-*motAB*$_{\Delta 51\text{-}70/D32N}$ and pHSG575-*motAB* (—▲—), and pBAD30 and pHSG575-*motAB* (—●—). Growth was monitored as in Figure 2.1. Arabinose (0.2%) and IPTG (1 mM) were added at 0 h (arrow).

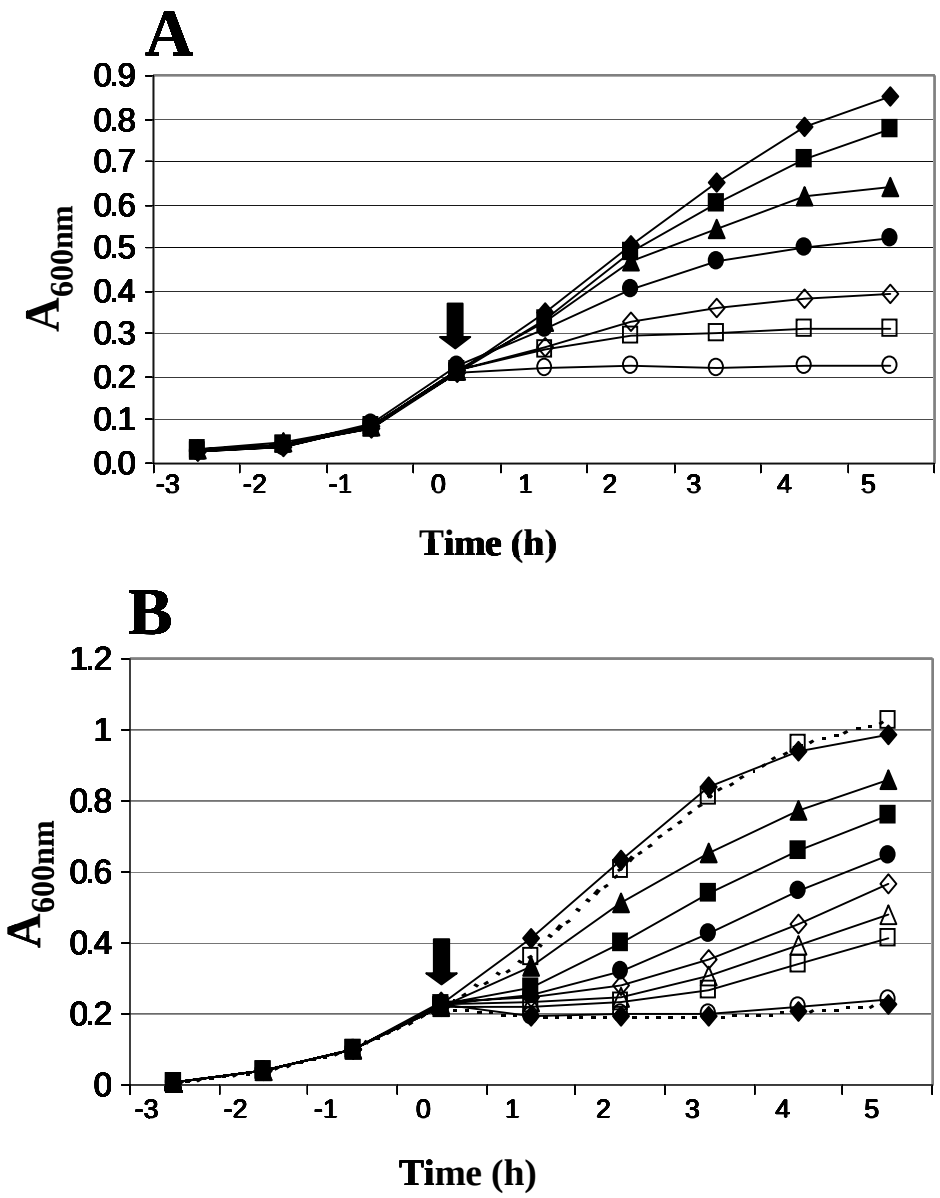

Figure 2.8. Effect of dinitrophenol (DNP) and sodium acetate on growth of RP437/p*motA*$^{+}$*B* $^{+}$ cells. (A) Growth curves in the presence of increasing concentrations of the uncoupler DNP. Growth was monitored as in Figure 2.1. Arabinose (0.2%) and DNP in 1% ethanol were added at 0 h (arrow). Symbols: no DNP control (—◆—); 1% ethanol control (—■—); 100 μM DNP (—▲—); 200 μM (—●—); 300 μM (—◇—); 400 μM (—□—); 1 mM (—○—). (B) Growth curves in the presence of increasing concentrations of sodium acetate (pH 7.0). Growth was monitored as in Figure 2.1 with arabinose (0.2%) and sodium acetate or 180 mM NaCl added at 0 h (arrow). Symbols: no sodium acetate control (—◆—); 180 mM NaCl (···□···); 40 mM sodium acetate (—▲—); 60 mM (—■—); 80 mM (—●—); 100 mM (—◇—); 120 mM (—△—); 140 mM (—□—); 160 mM (—○—); 180 mM (···◆···).

Cells expressing *motB* genes with any of the deletions or point mutations that inhibited growth became motile after induction of MotAB synthesis with 0.2% arabinose. However, the motility of those cells was tumblier than that of cells induced for expression of wild-type MotAB. We therefore performed a tethered cell assay to determine if the speed of flagellar rotation decreased. The rotation speed of tethered cells of a motile *Streptococcus* strain[124,125] and of *E. coli*[179] is directly proportional to the value of Δp from 0 mV to -180 to -200 mV (the physiological value). We previously measured the rotation speed of tethered *E. coli* cells as a function of DNP concentration and showed that rotation speed decreases linearly with increasing DNP concentration.[180]

Cells of the receptorless, smooth-swimming strainVB13, which rotates its flagella only CCW, were tethered in a flow cell[181] and bathed with TB warmed to 37°C. These cells contained plasmids encoding either wild-type MotAB, $MotAB_{D32N}$, or $MotAB_{\Delta 51\text{-}70}$. (Induction of $MotAB_{\Delta 51\text{-}70}$ inhibits the growth of VB13 cells with the same kinetics as it inhibits the growth of MM5000 cells; data not shown). These cells contain wild-type copies of *motAB* in the chromosome, so the assay measures the effect of newly synthesized MotAB complexes on the performance of pre-existing motors. Cells of all three strains continued to spin at the original rates after the addition of 0.2% arabinose (data not shown), by which time induction of $MotAB_{\Delta 51\text{-}70}$ completely blocks growth. Since a decrease in Δp should be reflected in a reduced rotation speed, this result indicates that the $MotAB_{\Delta 51\text{-}70}$ complex does not inhibit growth by collapsing Δp. Because the speed of flagellar rotation remained nearly constant even when the

$MotAB_{D32N}$ complex was overproduced, we also conclude that incorporation of the newly synthesized Mot proteins into pre-existing motors is negligible.

Lowering the cytoplasmic pH with acetate phenotypically mimics unplugged MotAB complexes. Exposure to acetate or benzoate, which permeate the cell membrane only in their protonated state, can lower bacterial growth rates by acidifying the cytoplasm, since they equilibrate the external and in internal pH.[182] Acidification of the cytoplasm also initiates CW flagellar rotation in a response mediated by the Tsr chemoreceptor.[183-185] To assess the effects of sodium acetate on growth, motility, and chemotaxis, we used wild-type strain RP437 harboring the $motA^{+}B^{+}$ plasmid and added different concentrations of sodium acetate at pH 7. Expression of the plasmid-borne genes was induced by addition of 0.2% arabinose. Increasing concentrations of sodium acetate decreased growth rates (**Fig. 2.8B**); at 160 mM and 180 mM growth stopped. In contrast, 180 mM NaCl had no effect (**Fig. 2.8B**), implying that sodium acetate inhibits growth by acidifying the cytoplasm rather than by changing osmolarity or ionic strength.

E. coli cells respond to acid stress by the induction of a large set of RpoS-regulated genes.[186] Thus, one might expect cells experiencing an acidification of their cytoplasm would initiate such a response and recover. When cultures of strain RP437 harboring the $motA^{+}B^{+}$ plasmid were exposed to 100 mM sodium acetate and then incubated continuously, with shaking, at 30^{o}C, they never recovered at pH 6.0, recovered partially (to around 50% of their original growth rate) at pH 7.0, and returned to their original growth rate after 2 h at pH 7.5 (**Fig. 2.9A**). When MM5000 cells harboring the

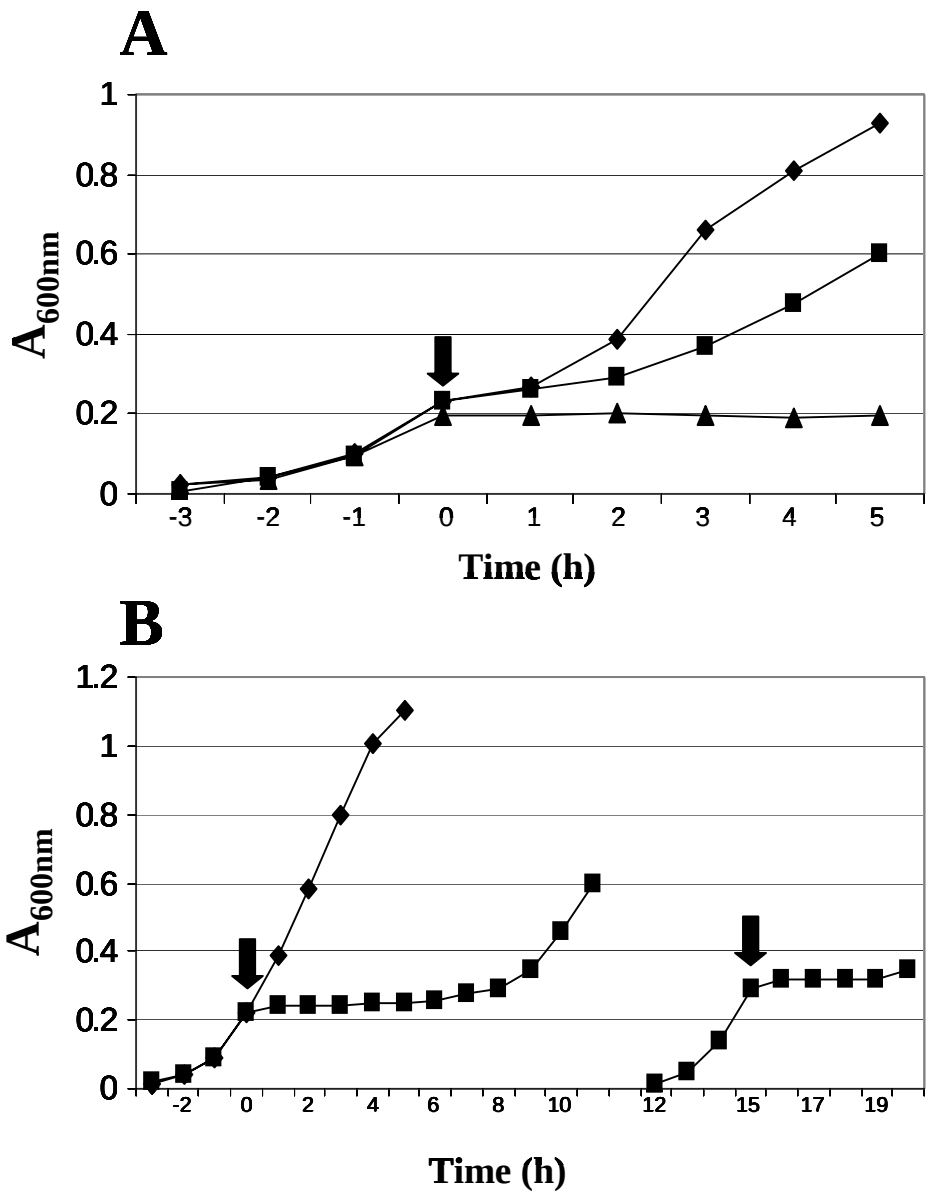

Figure 2.9. Effect of external pH on inhibition of growth by sodium acetate and recovery of cells from induction of $MotB_{\Delta 51\text{-}70/D32N}$. Growth curves are as in Figure 2.1. (A) Growth of strain RP437/ p*motA*$^{+}$*B* $^{+}$ in the presence of 100 mM sodium acetate and 0.2% arabinose added after 3 h of growth at the following pH values: 6.0 (—▲—); 7.0 (—■—); 7.5 (—◆—). (B) Extended growth curves of RP437/ $MotB_{\Delta 51\text{-}70/D32N}$ cells after induction with arabinose (arrow). Cells started to grow again ca. 8 h after addition of 0.2% arabinose. They were then back-diluted 100 fold (time point 17) and 0.2% arabinose was added again after 3 h (arrow at 15 h).

$MotAB_{\Delta 51\text{-}70}$ plasmid were induced with 0.2 % arabinose, they stopped growing (**Fig. 2.1B**) for about 8 h and then recovered to nearly their original growth rate over the next three hours (**Fig. 2.9B**). The cells that eventually grew had not lost the plasmid, because when they were re-grown without arabinose and then exposed to 0.2% arabinose, they again ceased growth within less than an hour. Thus, cells recover phenotypically from induction of $MotAB_{\Delta 51\text{-}70}$ in much the same way as they recover from acidification with 100 mM sodium acetate at an external pH somewhere between 6.0 and 7.0.

Acidification of the cytoplasm is perceived as a repellent (tumble-inducing) signal by the Tsr receptor.[183-185] Strains RP437 and SW10 (Δ*tsr*) harboring plasmids encoding wild-type MotAB, $MotAB_{D32N}$, $MotAB_{\Delta 51\text{-}70}$, or $MotAB_{P52A/P65A}$ were tethered in TB and exposed to 0.2% arabinose. In either strain, induction of wild-type MotAB or $MotAB_{D32N}$ had no effect on the ratio of CW to CCW rotation or on the switching frequency of cells for 1 h after addition of 0.2% arabinose (data not shown). The same result was obtained when $MotAB_{\Delta 51\text{-}70}$ or $MotAB_{P52A/P65A}$ was produced in strain SW10. However, induction of $MotAB_{\Delta 51\text{-}70}$ (**Fig. 2.10A**) or $MotAB_{P52A/P65A}$ (**Fig. 2.10B**) in RP437 cells increased CW rotation and flagellar switching frequency. Induction of $MotAB_{\Delta 51\text{-}70}$ in RP437 cells caused some cells to begin reversing more often within 20 min. By 25 min a few cells became "twitchy," failing to complete a full rotation before switching direction, and by 30 min the tethered flagellum began to turn only CW on a few cells. The same effect was seen in RP437 cells induced for synthesis of $MotAB_{P52A/P65A}$, but the changes were delayed by 10 min (**Fig. 2.10B**), a result

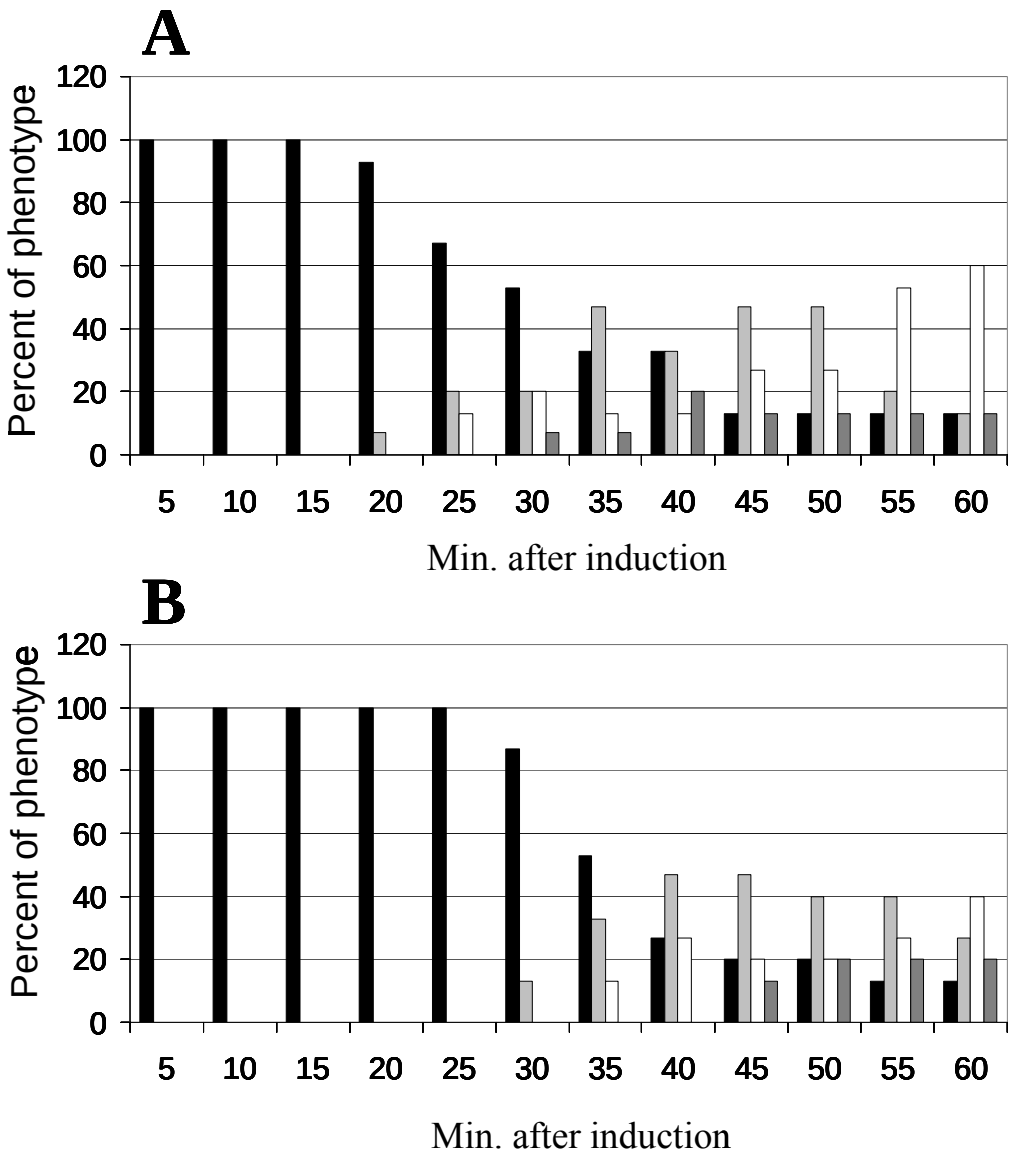

Figure 2.10. Rotational behavior of tethered cells expressing mutant MotB proteins. (A) A tethered-cell assay was performed using strain RP437/p*motAB*$_{\Delta 51\text{-}70}$. The assay was performed as outlined in Material and Methods. The rotation of 20 cells was analyzed. Cells showing wild-type reversal frequencies are indicated by the black bar, cells with increased-switch frequencies are indicated by light gray bars, cells that are constantly switching and making few complete rotations are indicated by white bars, and cells that rotate exclusively CW are indicated by dark gray bars. (B) A tethered-cell assay with strain RP437/p*motAB*$_{P52A/P65A}$. The assay was done and the symbols used as in (A).

consistent with the observation that $MotAB_{P52A/P65A}$ inhibits growth less than $MotAB_{\Delta 51-70}$.

We attempted to look at the effect of sodium acetate on tethered cells as well, but the high ionic strength washed the cells off the coverslip. However, free-swimming RP437 cells exposed to 160 mM or 180 mM sodium acetate had the same tumbly motility as RP437 cells that overexpress $MotAB_{\Delta 51-70}$. In contrast, the motility of free-swimming SW10 cells was unaffected by sodium acetate. These results indicate that sodium acetate, $MotAB_{\Delta 51-70}$, and $MotAB_{P52A/P65A}$ inhibit cell growth and lead to increased switching and CW rotation. Since sodium acetate lowers cytoplasmic pH, it seems likely that leaky MotAB complexes do the same.

Unplugged MotAB complexes lead to acidification of the cytoplasm. Because addition of sodium acetate to wild-type cells and the proton-leaky mutants produce the same phenotype, the internal pH of the cells expressing mutant MotAB complexes was measured. The first experiment compared MM5000 cells expressing MotAB and $MotAB_{\Delta 51-70}$ grown in TB medium buffered to a pH of 7.0. Because of the short time required to determine the internal pH using radioactive salicylic acid, growth curves and salicylate uptake were determined by taking measurements at 15-min intervals (**Fig. 2.11A**). Cells expressing $MotAB_{\Delta 51-70}$ stopped growing after induction with arabinose. The internal pH of the cells with the wild-type MotAB plasmid, either induced or uninduced, or with the uninduced $MotAB_{\Delta 51-70}$ plasmid remained constant (**Fig. 2.11B**).

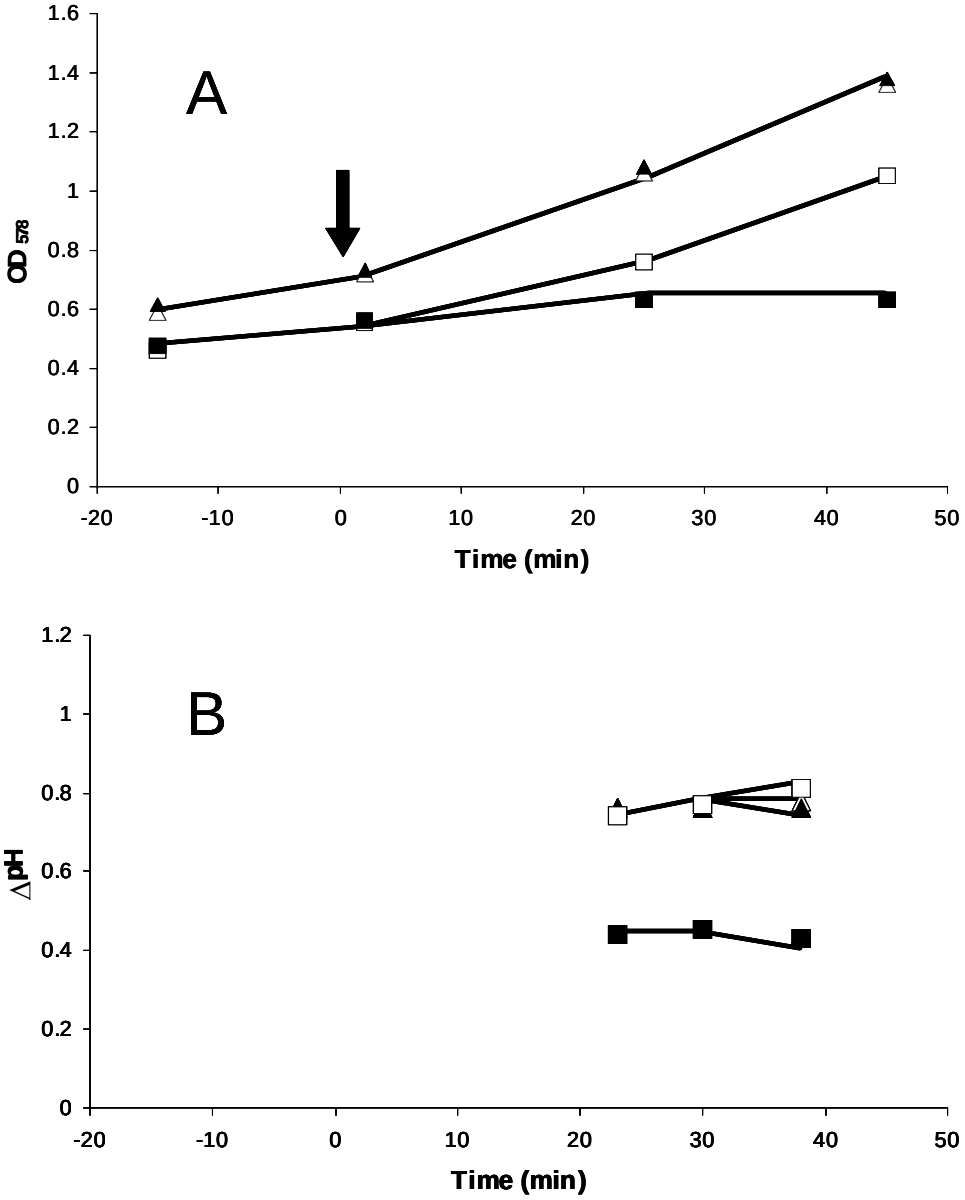

Figure 2.11. Determination of ΔpH for cells expressing MotAB and $MotAB_{\Delta 51\text{-}70}$ at an external pH of 7.0. (A) Growth was monitored beginning 15 min prior to induction and followed for 45 min after induction. Arabinose at 0.2% was added at t=0. Induced strains: MM5000/AB(—▲—) and /Δ51-70 (—■—). Uninduced strains: MM5000/MotAB (—△—) and /$MotAB_{\Delta 51\text{-}70}$ (—□—). (B) The ΔpH values for the strains in (A) were determined as outlined in Materials and Methods.

However, there was a drop in ΔpH by approximately 0.4 units, from 0.8 to 0.4, with the induced $MotAB_{\Delta 51\text{-}70}$ cells (**Fig. 2.11B**).

The experiment was repeated in TB medium buffered to a pH of 6.5. The same change in growth rates after addition of arabinose was observed (**Fig. 2.12A**) as had been seen in unbuffered TB medium (**Fig. 2.1** and **Table 2.1**). Cells producing wild-type MotAB, $MotAB_{D32N}$, $MotAB_{\Delta 51\text{-}70/D32N}$, and the vector only control were unaffected by arabinose. In contrast, growth of $MotAB_{P52A/P65A}$ slowed and growth of $MotAB_{\Delta 51\text{-}70}$ stopped completely. The ΔpH values for the first four strains after arabinose induction remained between 1.1 and 1.2 units (**Fig. 2.12B**). The ΔpH value of cells expressing $MotAB_{P52A/P65A}$ dropped by 0.2 units to around 0.9, and the ΔpH value for cells expressing $MotAB_{\Delta 51\text{-}70}$ dropped 0.4 units to 0.7 (**Fig. 2.12B**). Proton-leaky cells also lost K^+, decreasing from about 650 nmol/mg dry weight in cells expressing MotAB to about 450 nmol/mg dry weight in cells expressing $MotAB_{\Delta 51\text{-}70}$ and 475 nmol/mg dry weight in cells expressing $MotAB_{P52A/P65A}$, respectively (**Fig. 2.12C**). There was also some water loss, from about 4.25 μl/mg dry weight in cells expressing MotAB to 3.60 μl/mg dry weight in cells expressing $MotAB_{\Delta 51\text{-}70}$ and 3.75 μl/mg dry weight in cells expressing $MotAB_{P52A/P65A}$. The other four strains in the presence of arabinose, and all six strains in the absence of arabinose, retained their original internal K^+ levels at 600-650 nmol/mg dry weight and their water content at 4.0-4.25 μl/mg dry weight. The combination of K^+ and water loss meant that the intracellular K^+ concentration decreased by about 20% in the proton-leaky cells.

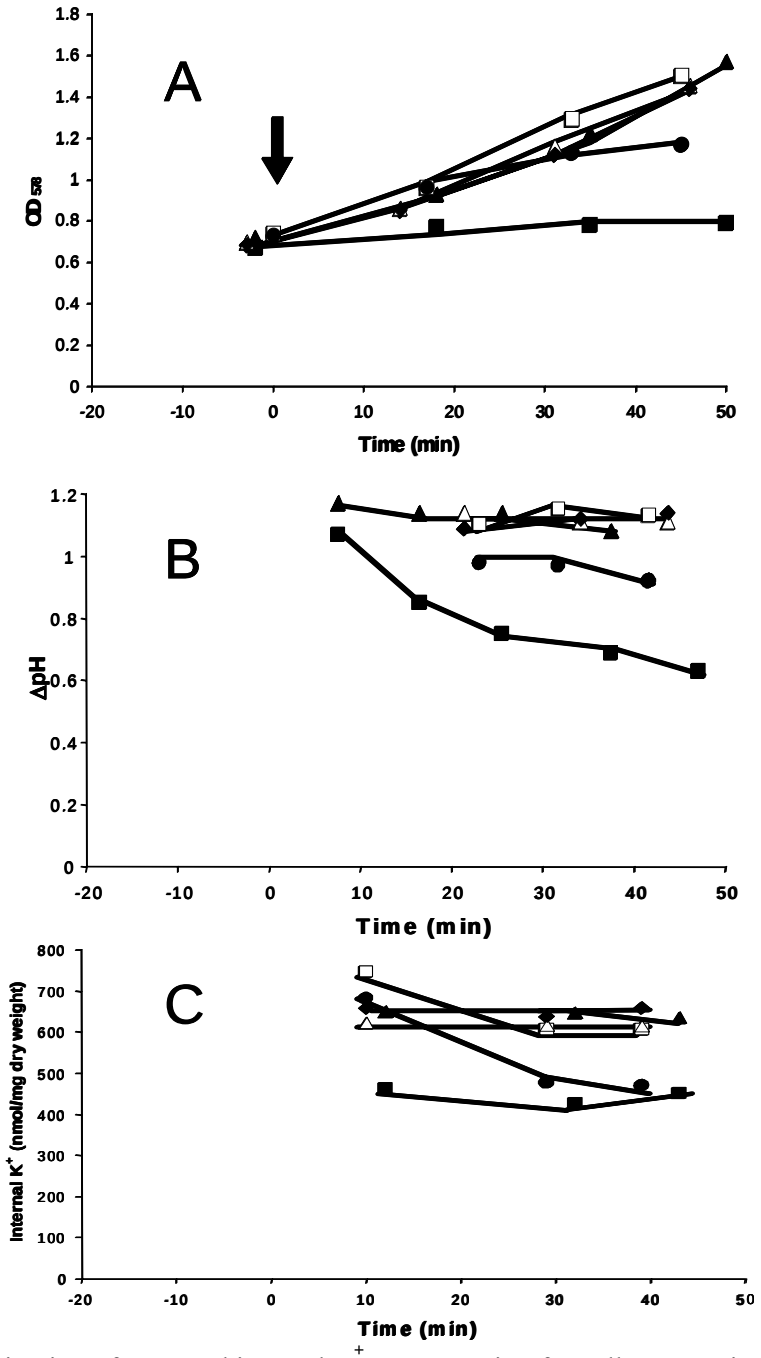

Figure 2.12. Determination of ΔpH and internal K^+ concentration for cells expressing various MotAB complexes at an external pH of 6.5. (A) Growth was monitored beginning 5 min prior to induction and followed for 50 min after induction. Arabinose at 0.2% was added at t=0. MM5000/MotAB (—▲—), /$MotAB_{D32N}$ (—△—), /$MotAB_{P52A/P65A}$ (—●—), /$MotAB_{\Delta 51\text{-}70}$ (—■—), $MotAB_{\Delta 51\text{-}70/D32N}$ (—□—) and vector control pBAD30 (—◆—). (B) The internal pH values of the strains in (A) were determined as outlined in Materials and Methods. (C) The internal K^+ levels of the strains in (A) were determined as outlined in Materials and Methods.

Discussion

Accumulation of wild-type MotAB at up to 50-fold greater levels than normal in the *E. coli* cell membrane does not substantially decrease cell growth rate.[173] However, high-level expression of MotA with a fusion protein joining the first 60 residues of MotB to a 50-residue stretch of polar residues encoded by plasmid pBR322 decreases the cell growth rate by about 80%.[99] This effect requires a functional MotA protein and is abolished by dominant-negative mutations targeting the TM region of *motB*.[166] Some MotB-PhoA fusions also impair growth when co-expressed with MotA.[97] However, stable MotB nonsense fragments of 110 or more residues do not have much effect on cell growth.[99,120] These results suggest that uncontrolled proton flow through the MotAB proton channel inhibits growth, but that this flow is blocked until the MotAB complex assembles into a flagellar motor.

To identify the region in MotB that regulates proton flow, we generated a series of MotB-PhoA hybrid proteins. Induction of the synthesis of the $MotB_{50}$-PhoA, $MotB_{60}$-PhoA, or $MotB_{65}$-PhoA proteins completely blocked the growth of cells (**Fig. 2.1A**). Similarly, strains encoding MotB proteins with internal, in-frame deletions of residues 61-70 of MotB underwent a rapid cessation of growth upon induction, and expression of MotB deleted for residues 51-60 caused severe growth impairment (**Fig. 2.1B**). Inhibition required co-expression of MotA, and normal growth was restored by introduction of the $MotB_{D32N}$ substitution (**Fig. 2.1A**), which blocks proton flow through MotAB.[166] Similar phenotypes were obtained when these mutant proteins were expressed in a strain that lacks any flagellar proteins. We conclude that the mutant MotB

proteins form active MotAB channels, even in the absence of flagella, that allows an uncontrolled flux of protons across the cell membrane.

Residues 52 to 65 of MotB may form an amphipathic helix flanked by Pro residues (**Fig. 2.2**). This sequence is just C-terminal to the TM of MotB (residues 27 to 49). Conversion of either Pro to Ala did not affect growth, but induction of the $MotB_{P52A/P65A}$ double mutant decreased growth dramatically. We speculate that the two Pro residues allow the amphipathic helix to orient parallel to the plane of the membrane to form a plug for the proton-conducting channel. The finding that co-expression of MotAB and $MotAB_{\Delta 51\text{-}70/D32N}$ inhibits growth (**Fig. 2.7**) implies that at least some of the MotB plugs function in *trans* within the $MotA_4$:$MotB_2$ complex.

Site-directed mutagenesis was used to convert each of the residues 53 to 64 to Cys. Expression of most of these proteins abolished growth, and expression of $MotB_{E60C}$ severely decreased the growth rate. However, the $MotB_{K53C}$ protein slowed growth only modestly (**Fig. 2.3A and Table 2.1**). In each case, disulfide-linked dimers of MotB, which arise spontaneously in the periplasm, were observed (**Fig. 2.3B**). In fact, the $MotB_{L55C}$, $MotB_{I58C}$, $MotB_{A59C}$, $MotB_{Y61C}$, $MotB_{F62C}$, and $MotB_{R63C}$ proteins were present only as dimers. This 3-4 residue repeat pattern supports the idea that the plug forms an α–helix and indicates that the two plugs of a MotB dimer can come into close contact (**Fig 2.4B**).

It is uncertain when the disulfide bonds form, but we suspect that it is early during the assembly of the MotAB complex. This conclusion is based on the observation that, under oxidizing conditions, cells expressing $MotAB_{A59C/Y61F}$ behave just like cells

expressing $MotAB_{A59C}$. Since the Y61F replacement probably makes it difficult for the plug to leave the membrane, the only time the two Cys-59 residues should come into close proximity is during the initial assembly of the MotB dimer. Alternatively, the plug may "breathe" in and out of the membrane even in the presence of the Y61F substitution, or the Cys-59 residues may crosslink while still in the membrane. However, the first interpretation is unsatisfying because of the tight non-motile/no-growth-impairment phenotype of cells expressing $MotAB_{Y61F}$, and the second seems unlikely because a MotAB complex containing $MotB_{A59C}$ still supports good motility under oxidizing conditions, although the cells expressing it do not grow.

Exposure to DTT 2 h after induction of the Cys-substituted proteins restored growth to strains expressing all of the proteins except $MotB_{I58C}$, $MotB_{Y61C}$, and $MotB_{F62C}$ (**Fig. 2.3C**). This finding implies that crosslinking locks the MotAB complex in an open state. It also indicates that the Cys-58, Cys-61, and Cys-62 residues, even in their reduced state, impair MotB plug function.

A variety of substitutions were introduced at residues 53 through 64. Ala substitutions had little effect except at positions 55, 58, 61, and 62 (**Table 2.1**), and only the $MotB_{Y61A}$ and $MotB_{F62A}$ proteins completely stopped growth. These two residues were very sensitive to change. Induction of $MotB_{F62L}$ and $MotB_{F62W}$ inhibited growth completely, and even the seemingly conservative Y61W and F62Y changes compromised plug function to some degree.

The only change at these positions that was innocuous for growth was Y61F. However, cells expressing Y61F are non-motile, suggesting that the Y61F plug cannot

be removed from the proton channel. The probable explanation is that Phe has a stronger tendency to remain buried in the hydrophobic core of the membrane than does Tyr, which prefers to reside at the hydrophobic/hydrophilic interfacial zone.[187--190] In summary, the transition from the plugged (closed) state, to the unplugged (open) state of the channel, seems to be very finely calibrated.

The ability of the MotB plug to block proton flow presumably involves some interaction with MotA. However, site-directed mutagenesis targeting the TM1-TM2 and TM3-TM4 loops of MotA did not reveal residues uniquely important for plug function. These negative data, and the amphipathic nature of the MotB 53-64 helix, encourage us to think that the plugs insert into the proton channel and that the hydrophobic face of the plug interacts with the membrane. Our mutagenic analysis of the plug supports this interpretation. Aromatic residues Tyr-61 and Phe-62 are especially important. In looking at the helical-wheel projection of the plug helix (**Fig. 2.2**), the hydrophobic Leu-55, Ile-58, Ala-59, and Phe-62 residues are positioned to be buried in the non-polar core of the membrane. The amphipathic Tyr-61 residue might localize to the interfacial zone between the hydrophobic core and the polar head groups of the phospholipids, and the polar Lys-53, Glu-60, Arg-63 and Thr-64 residues could interact with the polar head groups[187-190] (**Fig. 2.4A**).

A schematic model of how the inactive channel may be organized is depicted in **Figure 2.13A**, and possible conformations of the active MotAB complex are shown in **Figure 2.13B**. The two plugs in the open complex are shown with their hydrophobic faces in close apposition. The two $MotA_2$:MotB components of a stator element are

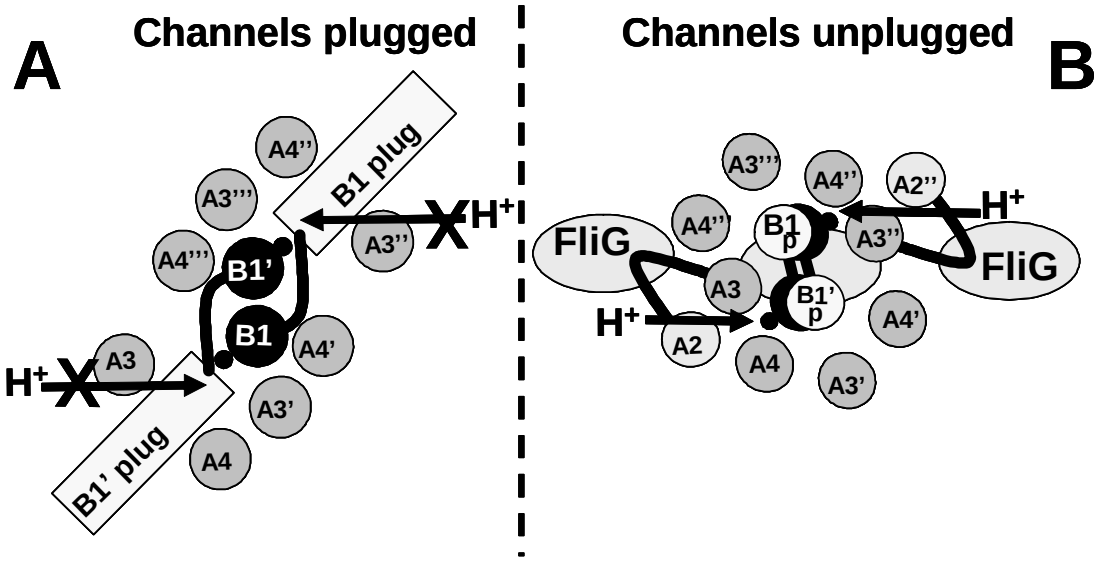

Figure 2.13. Schematic of how the wild-type $MotA_4MotB_2$ complex may be activated by contact with the flagellar basal body. The view is the same as in Figure 2.5. The TM1 and TM2 helices of MotA are excluded for the sake of clarity, except that a TM2 helix that is part of a MotA subunit involved in an active channel is shown. The curved black line connecting TM2 and TM3 is the cytoplasmic loop of MotA that contacts FliG.[109] (A) As the $MotA_4MotB_2$ complex diffuses through the cell membrane, both of the channels are plugged. (B) When the complex contacts a flagellar basal body (which would be above, in this view), a conformational signal is initiated, perhaps by an interaction of the cytoplasmic domains of MotA with FliG in the rotor, that leads to removal of the plug. Both channels open and the two plugs interact as shown in Figure 2.4B. In this geometry, both channels would be able, in principle, to participate in generating torque at the same time, since the cytoplasmic loops connecting TM2 and TM3 of each channel are more or less in line to interact sequentially with the FliG ring.[167, 195] Three subunits of FliG are shown as gray ovals (below the $MotA_4MotB_2$ complexes), but it must be emphasized that the actual position of the TM2-TM3 loops relative to the FliG ring is unknown.

depicted with rotational symmetry because that configuration is most consistent with the crosslinking data.[167] It remains an open question whether any of the various periplasmic peptidylprolyl isomerases interact with the peptide bonds N-terminal to Pro-52 and Pro-65 to effect a *cis* to *trans* (or vice versa) transition during activation.[191,192]

Another question is how inappropriately open MotAB channels interfere with cell growth. We initially thought that the proton motive force (Δp) would collapse. However, cells expressing MotB proteins with impaired plug function remain fully motile for an hour after induction of the offending proteins. Since the uncoupler DNP abolishes motility[180] at concentrations that inhibit growth (**Fig. 2.8A**), Δp cannot be collapsed in the stricken cells. The explanation instead seems to be that a proton leak acidifies the cytoplasm to an extent incompatible with growth. Addition of sodium acetate, which acidifies the cytoplasm,[182,193] had the same effect on cell growth as induction of unplugged MotAB complexes (compare **Fig. 2.1** and **Fig. 2.8B**). Furthermore, unplugged MotAB channels (**Fig. 2.10**) and sodium acetate[183-185,194] (data not shown) generate prolonged repellent responses that required the cytoplasmic pH-sensing chemoreceptor Tsr.

Most convincingly, direct measurement of internal pH showed that it was about 0.4 units lower in the induced $MotAB_{\Delta 51\text{-}70}$ cells than in wild-type cells (**Fig. 2.11B** and **2.12B**). A drop in the internal pH of cells, or accumulation of H^+ within the cell, can lead to efflux of K^+ ions.[196-199] We observed about a 30% decrease in cellular K^+ content in cells in which $MotAB_{\Delta 51\text{-}70}$ were induced (**Fig. 2.12C**). There was also a decrease of 15 % in the cell water content. With cells expressing $MotAB_{P52A/P65A}$, whose induction

produces only a partial growth defect, the loss of K^+ (**Fig. 2.12C**) and water was slightly less.

It was unexpected that the unplugged MotAB channel could lower cytoplasmic pH without dissipating Δp, since H^+ ions entering the cell must deplete both the ΔΨ and ΔpH components of Δp. An exchange of H^+ into the cells and K^+ out of the cells may be what allows them to increase ΔΨ to keep Δp essentially constant,[196-199] although the loss of K^+ is quite modest. The observed growth defect may be primarily due to the acidification of the cytoplasm, but it might also be caused by a cascade of effects, including efflux of K^+ and water, that ensues upon a lowering of cytoplasmic pH.[182] Whatever the explanation, it will require a careful rethinking of pH and membrane potential homeostasis, since our data are very clear.

In retrospect, the existence of a plug was presaged by the phenotypes of MotB-PhoA and MotB-TetA fusion proteins.[97,99] However, earlier analysis had shown that deletion of residues 50 to 90 of *Salmonella* MotB has no obvious motility or cell-growth phenotype when the protein is made at normal levels.[177] This result is consistent with our observation that unplugged MotAB complexes support motility. Only under conditions of MotA and MotB overexpression does an unplugged channel become catastrophic for the cell.

This observation raises the question of what selective pressure led to evolution of a plug. Cells induced for expression of plasmid-encoded $MotA^+B^+$ proteins grew 0.8% slower than cells of the same strain expressing the $MotA^+B_{D32N}$ proteins (data not

shown). This difference should reflect the cost of proton flow through the motor. A 0.8% faster growth rate translates into a two-fold higher population after 90 generations. The difference might be considerably greater under the nutrient-limiting conditions that typically prevail in the natural environment of *E. coli*. For comparison, MM5000 cells expressing wild-type MotAB had a growth disadvantage of 1.8% per generation relative to RP3098 (Fla^-) cells expressing wild-type MotAB (data not shown). The latter strain neither sustains proton flow through MotAB channels nor expends resources on flagellar assembly. Thus, these results suggest that flagellar synthesis imposes an additional 1% decrease in growth rate.

Presumably, an open MotAB channel not associated with a flagellum will conduct protons at least as fast as a channel incorporated into a motor. Although we do not know how many MotAB complexes there are in the membrane, or for what portion of the cell cycle they are present, if they conduct protons freely they would produce a significant drain on the resources of the cell. The number of functional channels in a wild-type cell can be calculated if one assumes that wild-type MotAB channels open only when incorporated into flagella and that open MotAB complexes not associated with motors conduct protons at least as fast as complexes associated with motors. Taking the upper limit of 7 flagella per *E. coli* cell[200] and 12 $MotA_4B_2$ complexes per flagellum,[21] 168 proton channels (7 flagella x 12 stator complexes/flagellum x 2 channels per stator complex) might function under these conditions, or 84 channels if only one channel per complex functions at a time. Thus, there could be as many as 5,000

to 10,000 open channels in the membrane of arabinose-induced cells containing the plasmid encoding $MotAB_{\Delta 51\text{-}70}$.

A sequence alignment of *E. coli* MotB with ten MotB sequences from a range of Gram-negative proteobacteria revealed that Pro-65 is conserved in all sequences (**Fig. 2.14**). Pro-52 is conserved in seven of the sequences. Y61 and F62 are conserved in all eleven sequences, possibly indicating their critical role as membrane anchors for the plug in the closed state. Likewise, either Ile or Val is present at position 58. The majority of the MotB transmembrane domain is also highly conserved in all eleven sequences. The high degree of conservation within the proteobacteria of residues that are crucial for plug function in *E. coli* indicates that this regulatory mechanism for MotAB-channel inactivation is apt to be a general phenomenon.

How is the MotAB channel activated when the stator complex assembles into a motor? One alternative is that contact between the cytoplasmic domain of MotA and FliG initiates a conformational change that opens the channel. To test this option, we altered the conserved Arg-90 and Glu-98 residues of MotA,[147] thinking that electrostatic interactions with oppositely charged residues in the motility domain of FliG might constitute the trigger. If so, reversing the charges at positions 90 and 98 of MotA, which abolishes motility, should prevent activation of the channel. However, in a growth-competition experiment, cells expressing $MotA_{R90E/E98R}B^{+}$ had no competitive advantage over cells expressing $MotA^{+}B^{+}$, and they were out-competed by cells expressing $MotA^{+}MotB_{D32N}$ (data not shown). Thus, this assay provided no evidence for a role of Arg-90 or Glu-98 in the cytoplasmic loop of MotA in triggering opening of the channel.

Figure 2.14. Alignment of amino acid sequences of MotB extending from the transmembrane domain through the predicted α-helix. The number in parentheses indicates the residue number for the first position in the sequence shown. Pro residues that flank the plug are highlighted in black. Residues highlighted in light gray are identical in all of the sequences. Boldface type indicates positions at which residues are chemically conserved. The beginning and end of the MotB TM is marked by asterisks.

Another possibility is that association of the peptidoglycan-binding domain of MotB with the cell wall activates the MotAB channel. Since the channels are not open until they incorporate in a flagellar motor, this model requires that the cell wall in the vicinity of the P ring has some specific feature that enables MotB to attach stably there, and there only. There is no evidence for such specificity, but because FlgJ is a flagellum-specific muramidase,[61] it is possible that the peptidoglycan surrounding the P ring has a unique structure. We have argued for an inverted order of events, in which activation of the MotAB channel releases the peptidoglycan-binding domain to interact with the cell wall,[120] but there is no compelling evidence for or against that hypothesis. Thus, important questions remain about how the MotAB complex assembles into the flagellar motor and how it is activated once it gets there.

Materials and Methods

Media. Media were prepared as described previously.[201] Tryptone broth (TB) contains 1% (w/v) tryptone extract and 0.8% (w/v) NaCl. Luria broth (LB) contains 1% tryptone and 0.5% (w/v) yeast extract. LB agar contains, in addition, 1.5% (w/v) Difco agar. Liquid cultures and agar plates were incubated at 37°C for LB or 30°C for TB. Media were supplemented with ampicillin (Amp, 50 μg per ml), chloramphenicol (Cm, 30 μg per ml), tetracycline (Tet, 15 μg per ml), and kanamycin (Kan, 30 μg per ml), as needed. Arabinose (0.2%, w/v) and 1 mM IPTG were used for induction of the *araBAD* promoter and the *tac* promoter, respectively.

Strains and plasmids. Strain RP437[202] is wild type for motility. Strain MM5000[120] (Δ*motAB*) is a derivative of RP437 that contains an internal, non-polar deletion spanning *motA* and *motB* (J. S. Parkinson, personal communication). Strain RP3098[203] [Δ*flhA-flhD*] contains a deletion removing part of the *flhBAE* operon and all of the *meche*, *mocha*, and *flhDC* operons. In the absence of the *flhDC* gene products, cells make no flagellar proteins. Strain SW10 (Δ*tsr*) is a *thr*$^+$ Δ*tsr7021* derivative of RP437 (S. Ward, personal communication). Strain VB13[204] is a *thr*$^+$ *eda*$^+$ *tsr7201 trg::Tn10* Δ(*tar*-tap)5201 version of RP437. Plasmid pBAD30-*motAB* was constructed by cutting pHSG575-*motAB*[120] and pBAD30[205] (Amp^r, arabinose inducible) with EcoRI and HindIII. A 1.8 Kb fragment of *motAB* was ligated into pBAD30, and proper orientation was confirmed by sequencing.

The pBAD30-*motABphoA* plasmid was constructed by using primers to insert SmaI and KpnI restriction sites downstream of *motB* in pHSG-*motAB.* Plasmid pMA632,[206] which carries *phoA* deleted for the PhoA signal sequence, and pBAD30-*motAB* (with the SmaI and KpnI sites), were double-digested with SmaI and KpnI. A 1.4 Kb fragment of *phoA* was ligated into the doubly digested pBAD30-*motAB* and confirmed by sequencing. A TGA stop codon was inserted in-frame at the end of *phoA*. Finally, the intervening sequence between the end of *motB* and the beginning of *phoA* was deleted to fuse *phoA* in frame with *motB*.

Site-directed mutagenesis. In-frame truncated MotB-PhoA fusions and point mutations were generated in pBAD30-*motAB* using Quick-Change mutagenesis

(Stratagene) according to the manufacturer's protocol. Mutagenized p*motAB* plasmids were introduced into strain MM5000 or RP3098. Transformants were selected on LB-Amp agar. Mutations were confirmed using the ABI Prism Dye-Terminator Cycle Sequencing Ready Kit with AmpliTaq DNA polymerase (PE Applied Biosystems).

Colorimetric detection of PhoA activity. MM5000 cells containing MotB-PhoA fusions were plated onto LB plates containing 0.2% arabinose, 50 μg per ml ampicillin, and 40 μg per ml 5-bromo-4-chloro-3-indolyl phosphate (BCIP; Sigma). Plates were screened to identify blue and white colonies.

Growth curves. Growth curves were performed as described previously[166] while overexpressing *motAB* from plasmid pBAD30 in MM5000 or RP3098 cells. Overnight cultures were grown at 30°C in TB supplemented with Amp, then diluted 1:100 in 5 ml fresh TB+Amp with swirling at 30°C. Arabinose (0.2%) was added after 3 h, and the A_{600nm} was measured every hour. To study growth under reducing conditions, 2 mM DTT was added after 5 h.

DNP and sodium-acetate treatment. Growth curves for strain MM5000/pBAD30-*motAB* were recorded after adding 0.2% arabinose and dinitrophenol (DNP) dissolved in 100% ethanol, after 3 h incubation, to final concentrations of 100 μM, 200 μM, 300 μM, 400 μM, 500 μM, 600 μM, 700 μM, 800 μM, 900 μM, and 1 mM. A control with 1% (50 μL) of 100% ethanol was also run. Sodium acetate at pH 7.0

was added to 40 mM, 60 mM, 80 mM, 100 mM, 120 mM, 140 mM, 160 mM, and 180 mM. A control with 180 mM NaCl (pH 7.0) was also run.

Competition growth experiment. Chromosomal kanamycin or tetracycline resistance markers were introduced into strains MM5000 and RP3098 by phage $P1_{vir}$ transduction to create strains MM5000K, MM5000T, RP3098K, and RP3098T, respectively. These strains were transformed with plasmid pBAD30 carrying either wild-type *motAB* or $motAB_{D32N}$. All possible differently resistance-tagged combinations of MM5000K, MM5000T, RP3098K, and RP3098T carrying the respective plasmids were grown overnight five times in TB+Amp. Cultures were back-diluted 1:100 before each round of growth. After each round of growth, 0.1 ml aliquots of 10^6 dilutions of the mixed cultures were plated onto LB agar containing Amp and either Tet or Kan. Plates were incubated overnight at 37^oC, colonies were counted, and titers of Tet- and Kan-resistant cells determined.

Data were plotted as the log ratio of Kan^r/Tet^r cells in each round *vs*. the round of growth. (Each round represents 6.64 generations.) To account for differences in the growth rates of Kan^r and Tet^r cells, the reciprocal pairings of strains with different antibiotic-resistance markers were examined, and the relative growth rates were corrected accordingly.

Tethered-cell assay. Strain VB13, in which the flagellum rotates only CCW, strain RP437, and the Δ*tsr* strain SW10 were used for tethered cell assays. Overnight cultures of cells carrying either p*ara*BAD-*motAB*, p*ara*BAD-$motAB_{\Delta 51\text{-}70}$, or the

p*ara*BAD-*motAB*$_{P52A/P65A}$ were grown in TB+Amp at 30^{o}C. Overnight cultures were diluted 1:100 into 10 mL TB+Amp and shaken at 30^{o}C until the culture reached an A600$_{nm}$ of 0.8. The cells were sheared and tethered with flagellar antibody as described previously[119] and observed in a flow chamber[181] by reverse phase-contrast microscopy. Solutions were flowed through the chamber as described previously.[180] All solutions were prewarmed to 38^{o}C. The cells were initially equilibrated at a flow rate of 0.4 ml/min. At t_0, expression of *motAB* was induced by flow of TB with 0.2% arabinose. Every 5 min the flow was stopped for 30 sec to record the rotation of individual cells for later analysis. Twenty cells were observed for each strain, and the same cells were analyzed for each time point for one hour.

SDS-PAGE and immunoblots. Whole-cell extracts were prepared from cultures at the completion of growth curves. Cells at an A_{600nm} of 0.8 were collected by centrifugation, washed once in 1 ml TE, and resuspended in 50 µl SDS loading buffer [2% (w/v) SDS, 5% (v/v) 2-mercaptoethanol, 8.5% (v/v) glycerol, 60 mM Tris (pH 6.8), 0.0004% (w/v) bromophenol blue]. Freeze-thaw extracts were prepared from these cells, prior to loading, by three alternating cycles of 5 min at -80°C and 5 min boiling. Proteins were separated by 12% acrylamide SDS-PAGE and transferred to polyvinylidene difluoride membranes (PVDF). Anti-MotB, anti-MotA,[149] and anti-PhoA (Abcam) polyclonal antibodies were used to probe the immunoblots. Proteins were visualized with PhoA-conjugated goat anti-rabbit antibody (BioRad). The blot was developed using SigmaFast.

In experiments involving cysteine-substituted MotB proteins, 20 mM N-ethylmaleimide (NEM; Sigma) was added to cultures for 10 min before harvesting to block free sulfhydryl groups. Whole-cell extracts were prepared as above. Samples were electrophoresed under non-reducing conditions (loading buffer lacking 2-mercaptoethanol), then transferred and developed as above.

Determination of *cis vs. trans* function of the MotB plug. MM5000 cells were co-transformed with the plasmid pair pBAD30-$motAB_{\Delta 51\text{-}70/D32N}$ and pHSG575-*motAB*, pBAD30-$motAB_{\Delta 51\text{-}70/D32N}$ and pHSG575, pBAD30 and pHSG575-*motAB*, and pBAD30-*motAB* and pHSG575-*motAB*. Double-transformants were plated onto LB agar containing Amp and Cm. Growth curves were performed as above, with 0.2% arabinose and 1 mM IPTG added after 3 h.

Determination of internal pH and K^+ concentration. Plasmid-containing cells were grown overnight at 37^{o}C under aerobic conditions in tryptone-K10-glycerol medium, which contains 46 mM Na_2HPO_4, 23 mM NaH_2PO_4, 0.4 mM $MgSO_4$, 8 mM $(NH_4)_2SO_4$, 10 mM KCl, 0.6 μM $FeSO_4$, 8 g/L tryptone, 2 g/L glycerol, and 50 mg/L ampicillin. The pH of this medium was set at 7.0 or was brought to 6.5 with concentrated HCl. The cells were diluted into 50 ml fresh growth medium to an OD_{578nm} value of 0.05 and grown under the same conditions as the overnight cells. After the OD_{578nm} had

reached a value of about 0.7, synthesis of the MotAB proteins was induced by the addition of .2% L-arabinose.

The ΔpH value, defined as $[H^+]_{in}$ minus $[H^+]_{out}$, was determined by growing cells as described previously,[207,208] except that [^{14}C-]-benzoic acid, which is no longer commercially available, was replaced by [^{14}C]-salicylic acid. Five ml of cell suspension was transferred to a 50 ml Erlenmeyer flask, and $^{3}H_2O$ and [^{14}C]-salicylic acid were added to final concentrations of about 1 and 0.2 μCi/ml, respectively. At different times, the cells were separated from the medium by centrifugation through silicone oil, and the internal pH was calculated from the ratio of radioactivity of [^{14}C]/[^{3}H] in the cell pellet and the supernatant fraction.[209] Cell K^+ was determined by flame photometry of the cell pellet from 1 ml of growing cells centrifuged through silicone oil.[207,208] The pH value of the suspension was checked immediately after the last samples had been centrifuged through the oil. It was within 0.05 units of the value measured before the medium was autoclaved.

CHAPTER III

ROLE OF CYTOPLASMIC CHARGED RESIDUES IN MotA/MotB INTERACTIONS IN THE *E. coli* FLAGELLAR MOTOR

Introduction

Genetic suppression analysis has shown that the periplasmic regions of MotA and MotB may interact.[119,150,160] This same analysis also showed that mutations in MotB are suppressible by changes in the motility domain of FliG,[119] indicating that FliG interacts directly with the MotAB proton channel complex. Based on these analyses, it appears that proper positioning of MotA relative to MotB and FliG is crucial for proper torque generation, since mutations in MotA and MotB are suppressed by residue changes separated by relatively large distances and/or by the cell membrane.[119,150,160]

The C-terminal tail of MotA has a net negative charge, and the cytoplasmic N-terminal tail of MotB has a net positive charge. In *Rhodobacter sphaeroides*, however, there is a net positive charge at the C-terminus of MotA and a net negative charge at the N-terminus of MotB. In either case, the suggestion is that interaction between oppositely charged residues is important for proper assembly and function of the MotAB complex.

In previous work,[120] we proposed that these regions interact to facilitate membrane insertion and to stabilize MotB. Here, we report experiments that tested whether the charged C-terminus of MotA and N-terminus of MotB play an important functional role in the Mot protein complex. Charged residues were systematically replaced with neutral or oppositely charged residues, and some of these changes were

associated with severe defects in motility. We also found that many of these mutations can be suppressed by changes in the other protein or at distant sites in the primary sequence of the same protein. However, we found no evidence that the charge interactions are necessary for stabilization of MotB, since levels of that protein were normal in all of the mutants.

Results

Sequence alignments of *E. coli* MotB and MotA from diverse bacteria. An alignment of the *E. coli* MotB amino acid sequence with MotB from six other bacterial species identified clusters of conserved positively charged residues in the cytoplasmic N-terminus (**Fig. 3.1A**). A stretch from residue 12 to 17 of *E. coli*, with the sequence KRRKAK, was the most notable. When a similar alignment was made with MotA, areas of conservation of negatively charged residues were noted at the cytoplasmic C-terminus (**Fig. 3.1B**). The first region corresponded to the sequence ELEE at residues 275-278 of *E. coli* MotA, and the second consisted of residues E293 and E294.

A seventh bacterium used in the alignment, *Rhodobacter sphaeroides*, had groups of charged residues in the same general regions described above, except that the MotB residues were negatively charged (**Fig. 3.1A**) and the MotA residues were positively charged (**Fig. 3.1B**). The apparent importance of these charged regions, indicated by their conservation in species as distantly related as *E. coli* and the gram-positive *Bacillus subtilis*, suggested it might be worthwhile to investigate their role in more detail.

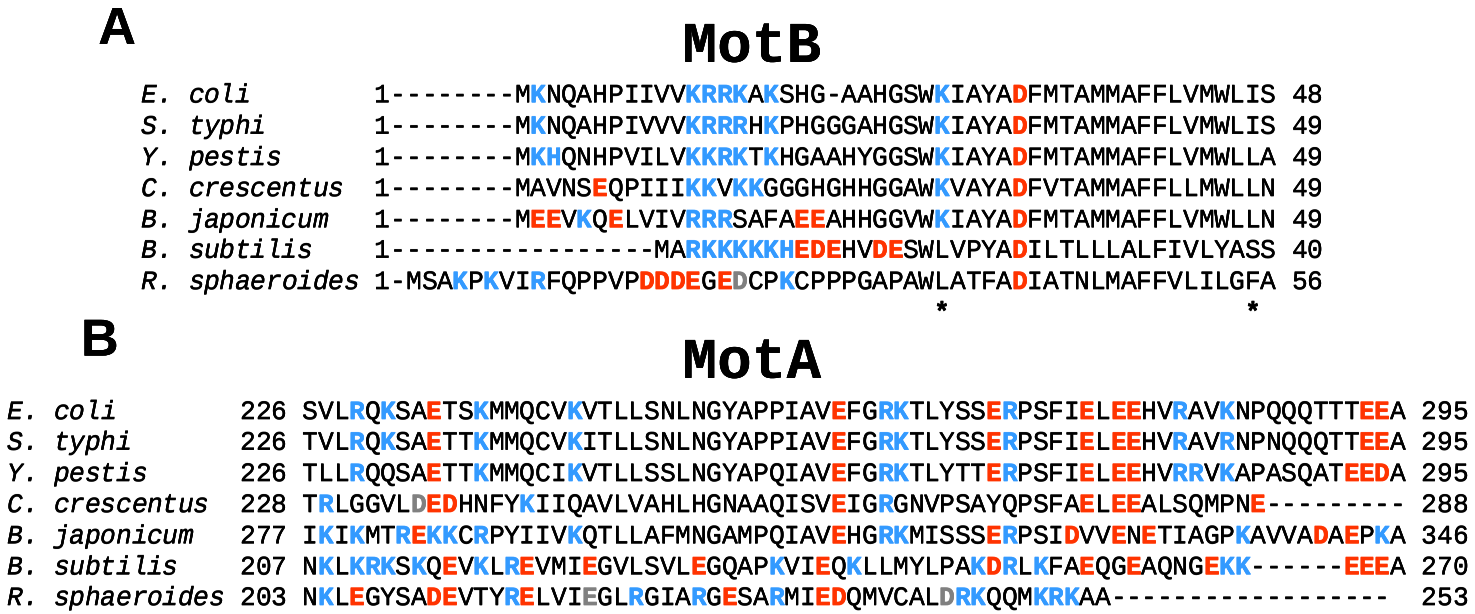

Figure 3.1. Sequence alignments of MotB and MotA. (A) Alignment of amino acid sequences of MotB extending from the first residue through the transmembrane (TM) domain. The numbers indicate the positions of the first and last residues in the sequence. Positively charged residues are highlighted blue, negatively charged residues are in red. The beginning and end of the TM domain is marked by asterisks. The aligned sequences are from *Escherichia coli*, *Salmonella typhi*, *Yersinia pestis*, *Caulobacter crescentus*, *Bradyrhizobium japonicum*, *Bacillus subtilis*, and *Rhodobacter sphaeroides*. (B) Alignment of amino acid sequences of MotA extending from just after the fourth TM domain through the C-terminus of the protein. The numbers indicate the positions of the first and last residues in the sequence. The highlighting and alignments are as in (A).

Mutation of negatively charged residues at the C-terminus of MotA. To determine the importance of the negatively charged Glu residues at the extreme C-terminus of MotA, their codons were mutated to Ala codons in the IPTG inducible p*HSG-motAB* plasmid. Instead of looking one residue at a time, we substituted Glu-275, Glu-277, and Glu-278 together as one group, and Glu-293 and Glu-294 as a second group. The mutant plasmids were then introduced into strain MM5000 (Δ*motAB*), and the motility phenotypes of the transformants were screened. The E293A/E295A double mutant ($MotA_{293\text{-}295A}B$) had a swarm diameter in tryptone semi-solid agar 95% that of strain MM5000 complemented with p$motA^{+}B^{+}$ (data not shown). However, the triple mutant E275A/E277A/E278 ($MotA_{275\text{-}278A}B$) had a relative swarm diameter only 5% that of the wild-type strain (**Fig. 3.2**). We also made the E275K/E277K/E278K triple mutant ($MotA_{275\text{-}278K}B$) (**Table 3.1**), which led to a completely non-motile phenotype (data not shown). Wild-type levels of both MotA and MotB were detected on immunoblots for all of these strains (data not shown).

Suppressors of the *motA* mutations. Suppressors of $MotA_{275\text{-}278A}B$ and $MotA_{275\text{-}278K}B$ were isolated as described in Materials and Methods. After 36 hours of incubation of colonies in tryptone semi-solid agar, six motile flares were found with $MotA_{275\text{-}278A}B$ (**Table 3.1**), and three were found with $MotA_{275\text{-}278K}B$ (**Table 3.1**). The plasmids were isolated and reintroduced into MM5000, and a motile phenotype was again observed, indicating that the suppressing mutations were plasmid borne. DNA sequencing revealed that all of the plasmids contained a second-site mutation in the *mot*

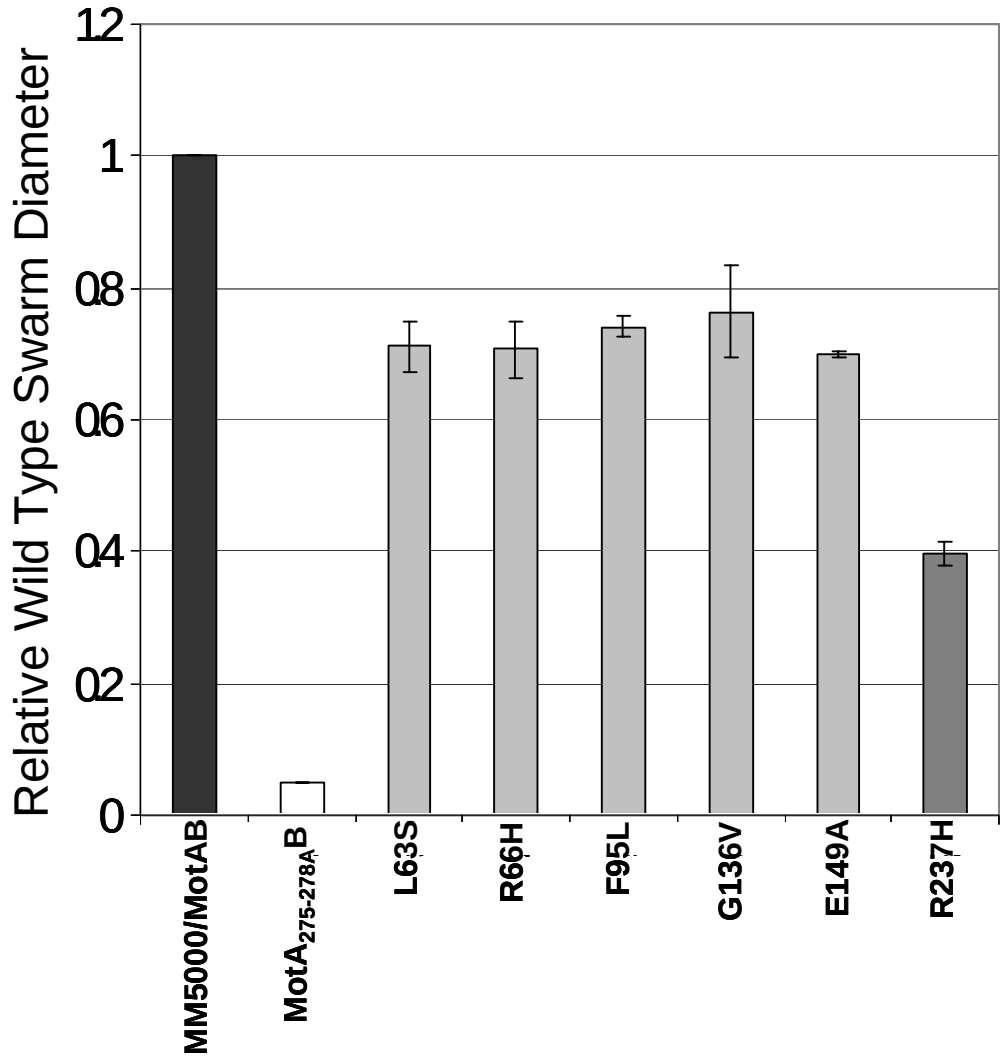

Figure 3.2. Motility of MM5000 (Δ*motAB*) cells that contain p*motAB*, the p*motA*$_{275\text{-}278A}$B mutation, and motile suppressors of the p*motA*$_{275\text{-}278A}$B mutation. Swarm diameters are expressed relative to the diameter of swarms formed by MM5000 cells harboring p*motAB*. The swarm assay was carried out as described in Materials and Methods. Each bar of the graph was calculated from the mean diameter of ten swarms. MM5000/p*motAB* is black, the MM5000/p*motA*$_{275\text{-}278A}$*B* mutant (**Table 3.1**) is white, *motA* suppressors of MM5000/p*motA*$_{275\text{-}278A}$*B* are light gray, and the *motB* suppressor of MM5000/p*motA*$_{275\text{-}278A}$*B* is dark gray. Error bars represent the standard deviation.

Table 3.1. Mutations made during this study.

	Sequence		Suppressors Found	
Mutation[a]	**Wild Type**[b]	**Mutated**[c]	**Total**[d]	**Independent**[e]
$MotA_{275\text{-}278A}B$	275-ELEE-278	275-ALAA-278	6	6
$MotA_{275\text{-}278K}B$	275-ELEE-278	275-KLKK-278	3	2
$MotAB_{12\text{-}14A}$	12-KRK-14	12-AAA-14	8	7
$MotAB_{12\text{-}17A}$	12-KRKKAK-17	12-AAAAAA-17	8	2
$MotAB_{12\text{-}17D}$	12-KRKKAK-17	12-DDDDAD-17	1	1

[a] Name of mutation as it appears in the text.
[b] Wild-type sequence of the region being changed. Numbers indicate the first and last residues altered.
[c] Same as *a* except showing the mutated sequence.
[d] Number of motile flares isolated from each mutant.
[e] Number of unique suppressor mutations found.

genes. Five of the six suppressors of $MotA_{275\text{-}278A}B$ were in *motA* and one was in *motB* (**Fig. 3.2**). With $MotA_{275\text{-}278K}B$, two independent suppressor mutations in *motA* were identified (**Table 3.1**), one of which was isolated twice.

Swarm assays in tryptone semi-solid agar were run to determine the relative motility of the suppressed strains compared to wild type. All of the $MotA_{275\text{-}278A}B$ suppressors in *motA*, which generated the residue changes L63S, R66H, F95L, G136V, and E194A, restored swarming to about 70% of the wild-type level (**Fig. 3.2**). The lone $MotA_{275\text{-}278A}B$ suppressor in *motB* created the change R237H, and the strain bearing this mutation formed a swarm with 40% the diameter of the wild type (**Fig. 3.2**). The E142K suppressor of $MotA_{275\text{-}278K}B$ restored a relative swarm diameter of 35%, whereas the E144K suppressor of $MotA_{275\text{-}278K}B$ led to a relative swarm diameter of 19% (data not shown). Wild-type levels of both MotA and MotB were present on immunoblots for all of the suppressed mutants (data not shown), demonstrating that it was not an increase in production of MotA or MotB that restored motility.

Mutation of positively charged residues at the N-terminus of MotB. Residue replacements were also made in the cluster of positively charged residues near the N-terminus of MotB. Again, instead of looking at each residue one at a time, we mutated the first three positively charged residues (Lys-12, Arg-13, and Arg-14) and the last two residues (Lys-15 and Lys-17) to Ala in two separate groups, to create the $MotAB_{12\text{-}14A}$ (**Table 3.1**) and $MotAB_{15\text{-}17A}$ mutants. These two groups were also combined to create the mutant $MotAB_{12\text{-}17A}$ (**Table 3.1**). The mutated p*HSG-motAB* plasmids were then

introduced into strain MM5000 (Δ*motAB*), and their motility phenotypes were determined. The $MotAB_{12\text{-}14A}$ mutant resulted in a non-motile phenotype, but the $MotAB_{15\text{-}17A}$ mutant still had a swarm diameter 73% as large as wild type (**Fig. 3.3**). The quintuple mutant, $MotAB_{12\text{-}17A}$, was also non-motile (**Fig. 3.4A**). The same positively charged residues were also changed to Asp residues to create mutant $MotAB_{12\text{-}17D}$ (**Table 3.1**), which was non-motile (**Fig. 3.4A**). When a plasmid was constructed that combined the reversed charges in MotA and MotB ($MotA_{275\text{-}278K}$/$MotB_{12\text{-}17D}$) in an attempt to mimic the reversed-charge situation of *R. sphaeroides* MotAB (**Fig. 3.1**), the transformed cells remained non-motile (data not shown).

Suppressors of the *motB* mutations. Suppressors were also sought, in the same manner as for the *motA* mutations, with the *motB* mutations that eliminated motility. Eight motile flares were isolated from the non-motile stabs of mutant $MotAB_{12\text{-}14A}$ (**Table 3.1**). Seven of the eight plasmids restored motility when reintroduced into strain MM5000 (Δ*motAB*) (**Table 3.1**). Of these, three had second-site mutations in *motA* (M237I, Q239R and L246R) and four had second-site mutations in *motB*, causing the H138Y, I152V, and R173C replacements. (H138Y was independently isolated twice.) The eighth plasmid did not confer motility to strain MM5000, and it contained no second-site mutation in the plasmid-borne *mot* genes. Whatever the suppressing mutation is, it must be located on the chromosome of the original isolate.

The suppressors changing residues in MotA (M237I, Q239R, and L246R) had relative swarm diameters 60-70% that of wild type (**Fig. 3.3**). The *motB* suppressors

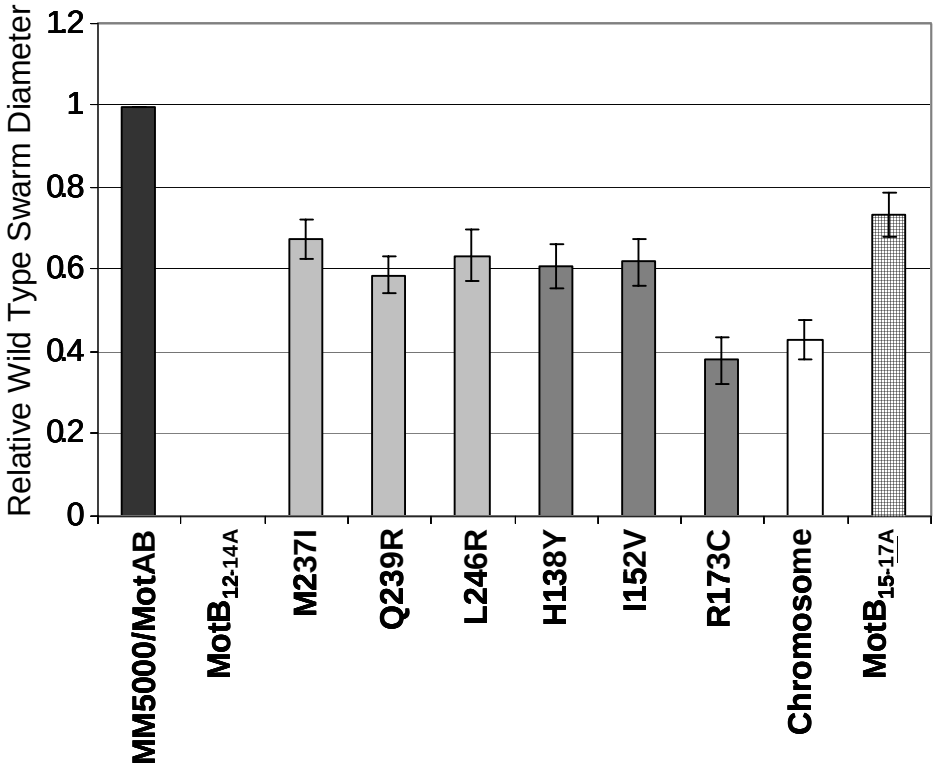

Figure 3.3. Motility of MM5000 cells that contain p*motAB*, the p*motAB*$_{12\text{-}14A}$ mutant, motile suppressors of the p*motAB*$_{12\text{-}14A}$ mutant, and p*motAB*$_{15\text{-}17A}$. Assays were conducted and data are expressed as in Figure 3.2. MM5000/p*motAB* is shown in black, MM5000/p*motAB*$_{12\text{-}14A}$ and MM5000/p*motAB*$_{15\text{-}17A}$ mutants are textured, *motA* suppressors of MM5000/p*motAB*$_{12\text{-}14A}$ are light gray, the *motB* suppressors of MM5000/p*motAB*$_{12\text{-}14A}$ are dark gray, and the chromosomal suppressor of MM5000/p*motAB*$_{12\text{-}14A}$ is white. Absence of a bar means that no swarming was observed. Error bars represent the standard deviation.

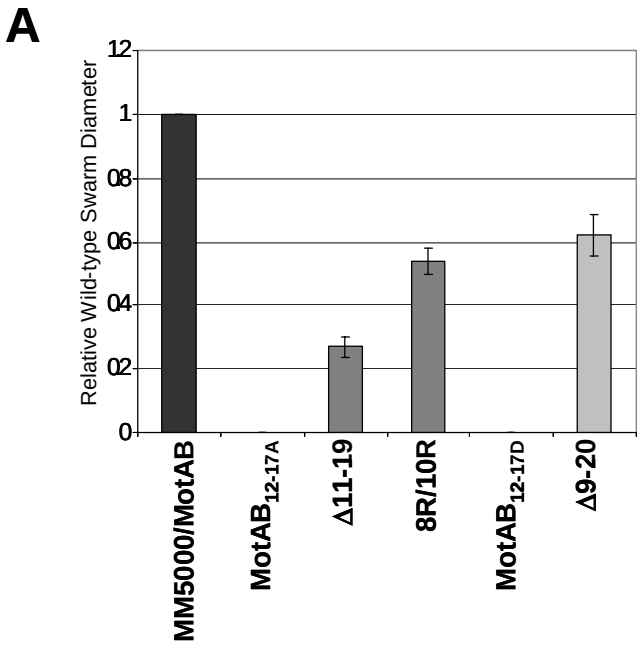

B

Wild Type MotB

1-M***K***NQA***H***PIIVV***KRRK***A***K***SHGAAHGSWKIAYADFMTAMMAF 40 **MotB**

Suppressors of 5000/AB$_{12\text{-}17A}$

(Δ11-19) 1-M***K***NQA***H***PIIVGAAHGSWKIAYADFMTAMMAF 40 **MotB**

(8R/10R) 1-M***K***NQGSS***R***I***R***LLSSAAASHGAAHGSWKIAYADFMTAMMAF 40 **MotB**

Suppressor of 5000/AB$_{12\text{-}17D}$

(Δ9-20) 1-M***K***NQAHPIAA***H***GSWKIAYADFMTAMMAF 40 **MotB**

Figure 3.4. Motility of p*motAB*$_{12\text{-}17A}$, p*motAB*$_{12\text{-}17D}$, their suppressors and a sequence alignment of these suppressors. (A) Motility of MM5000 cells that contain p*motAB*, the p*motAB*$_{12\text{-}17A}$, suppressors of p*motAB*$_{12\text{-}17A}$, the p*motAB*$_{12\text{-}17D}$, and a motile suppressor of p*motAB*$_{12\text{-}17D}$. Assays were conducted and data are expressed as in Figure 3.2. MM5000/p*motAB* is shown in black, MM5000/p*motAB*$_{12\text{-}17A}$ and MM5000/p*motAB*$_{12\text{-}17D}$ are hatched, and suppressors of MM5000/p*motAB*$_{12\text{-}17A}$ are light gray and the suppressor of MM5000/p*motAB*$_{12\text{-}17D}$ is shown in light gray. Absence of a bar means that no swarming was observed. (B) Comparison of the N-terminal MotB sequences of the suppressors of MM5000/p*motAB*$_{12\text{-}17D}$, MM5000/p*motAB*$_{12\text{-}17A}$, and wild-type MotB. The sequences are aligned with reference to the TM domain (underlined) to highlight the effect of the deletions on the position of the positively charged residues (bold italics). The altered amino acids in the 8R/10R suppressor are shown in gray. The mutated K15A and K17A residues from the original mutant are still present.

causing the H138Y and I152V substitutions showed the same efficiency, whereas the R173C substitution led to a swarm with 38% the diameter of wild type (**Fig. 3.3**). The chromosomal suppressor was 43% efficient (**Fig. 3.3**). All of the suppressed mutants had wild-type levels of MotA and MotB (data not shown).

Eight independent motile flares were identified with the $MotAB_{12\text{-}17A}$ mutant (**Table 3.1**). A deletion in MotB of codons 11-19 was found in seven of the eight plasmids (**Fig. 3.4B**). The eighth suppressor, which we have termed 8R/10R, inserted eight additional bases between the first and second bases of codon five and deleted eight bases, including codons 12 and 13 and the first two bases of codon 14. These changes alter the amino acid sequence of residues 5 through 14 of *motB* (**Fig. 3.4B**). Two new codons for positively charged Arg residues appear in this altered region at positions eight and ten. Compared to wild type, the relative swarm diameter for strains expressing $MotAB_{\Delta 11\text{-}19}$ was 27% and for $MotAB_{8R/10R}$ was 54% (**Fig. 3.4A**). Only one motile flare appeared with the $MotAB_{12\text{-}17D}$ mutant (**Table 3.1**). The plasmid isolated from the suppressed mutant contained a deletion of codons 9-20 of MotB. The swarm diameter of the suppressed mutant was 62% of the wild-type value (**Fig. 3.4A**). Once again, all of the suppressed mutants had wild-type levels of MotA and MotB protein (data not shown).

Discussion

Alignment of MotA and MotB sequences from six disparate bacterial species revealed a conserved cluster of negative charges at the C-terminus of MotA and of positive charges at the N-terminus of MotB. In a seventh species, *Rhodobacter*

sphaeroides, these charges are reversed such that the equivalent portion of the C-terminus of MotA has a net positive charge and the N-terminus of MotB has a net negative charge (**Fig. 3.1**). This conservation of charged residues inspired us to ask whether there is a functionally important interaction between them, which might be predicted to help in the association of MotA and MotB during membrane insertion.

Replacement of residues Glu-293 and Glu-294 with Ala had very little effect on motility. In contrast, conversion of residues Glu-275, Glu-277, and Glu-278 to Ala (mutant $MotA_{275\text{-}278A}B$) in plasmid-encoded MotA lowered motility to only 5% that of a strain containing the wild-type *motA* gene (**Fig. 3.2**). Changing these same residues to Lys (mutant $MotA_{275\text{-}278K}B$) resulted in a non-motile phenotype (data not shown). Suppressing mutations that dramatically increased the motility of cells expressing these two mutant proteins were found (**Fig. 3.2**). The suppressing mutations changed residues in MotA (L63S, R66H, F95L, G136V, and E149A) and MotB (R237H) for the $MotA_{275\text{-}278A}B$ mutant (**Fig 3.2**), but only in MotA (E142K and E144K) for the $MotA_{275\text{-}278K}B$ mutant.

All seven of the suppressors in *motA* target residues in the large cytoplasmic loop between TM2 and TM3 of MotA (**Fig. 3.5**). The sites of four of these changes flank the two charged residues, Arg-90 and Glu-98, which have been shown to interact electrostatically with opposite charges in FliG,[109] whereas the Phe-95 residue is located between them. The suppressing change in MotB, R237H, is located shortly after the proposed peptidoglycan-binding domain (**Fig. 3.5**).

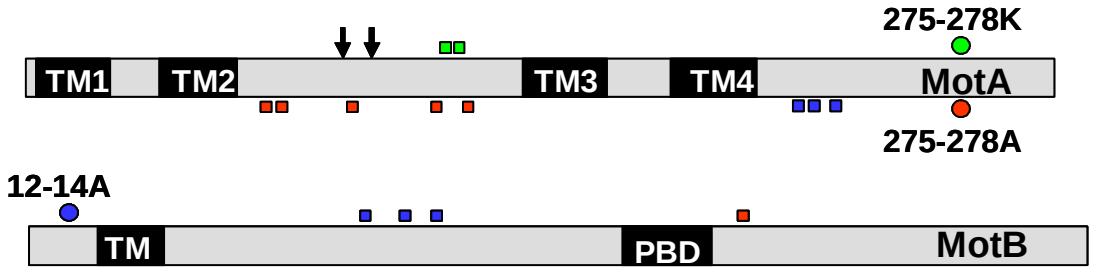

Figure 3.5. Position of the point mutations that suppressed charge-altering residue changes in MotA and MotB. Mutations are indicated by their name and their location within the protein is indicated by a circle. The location of the corresponding suppressors are highlighted by squares of the same color as the circle representing the original mutation. The location of the TM domains of MotA and MotB, and the proposed peptidoglycan-binding domain (PBD) of MotB are labeled. Residues Arg-90 and Glu-98 of MotA, which interact electrostatically with FliG,[109] are indicated by the two downward-facing arrows.

Part of our original hypothesis, based largely on the observation that MotB is unstable in the absence of MotA, was that charge interactions between MotA and MotB might facilitate their association prior to and during insertion into the cell membrane. However, neither the original mutations nor the suppressors had any significant affect on the levels of either of the two Mot proteins (data not shown). The location of the original mutations in the cytoplasmic tail of MotA and of the suppressing mutations in the cytoplasmic loop instead suggests that the suppressors exert their effect by restoring an interaction between these two regions that is disturbed by the original mutations. One compelling explanation is that the original charge reversals alter the interaction in such a way that residues Arg-90 and Glu-98 are no longer able to interact effectively with the motility domain of FliG. The suppressing mutations would restore a more-normal orientation between these residues and FliG.

Changing residues Lys-12, Arg-13, and Arg-14, or residues Lys-15 and Lys-17 of MotB to Ala (the $MotAB_{12\text{-}14A}$ and $MotAB_{15\text{-}17A}$ mutants) led to a complete loss of motility or a decrease to 73% of wild-type motility, respectively. Seven different suppressors restored motility to the strain expressing $MotAB_{12\text{-}14A}$ (**Fig. 3.3**). Three altered residues in the C-terminal tail of MotA (M237I, Q239R, and L246R), three affected residues in the periplasmic domain of MotB (H138Y, I152V, and R173C), and one was chromosomal (**Fig. 3.5**), perhaps in *fliG*. These data imply that the N-terminus of MotB indeed interacts with the C-terminus of MotA, in this case perhaps by indirectly affecting the orientation of the cytoplasmic loop of MotA via an altered conformation of the cytoplasmic tail of MotA.

The existence of suppressors of both $MotA_{275-278A}B$ and $MotB_{12-14A}B$ that target the periplasmic domain of MotB suggests a further step, in which the position of the N-terminus of MotB relative to MotA depends on the conformation of the periplasmic domain. Previous suppressor studies found that specific mutations affecting the periplasmic domains of MotA or MotB were suppressed by mutations in either *motA*, *motB*, or *fliG*.[119,150,160] The residue substitution H138Y, in fact, suppresses both the $MotAB_{12-14A}$ mutation (**Fig. 3.3**) and the mutation causing the V207M substitution in TM4 of MotA.[150]

The suppressors described here and in previous studies from this laboratory may cause a conformational readjustment that restores function to a previously misaligned MotAB proton channel. The idea is that the cell wall, the periplasmic domain of MotB, the transmembrane domains, the cytoplasmic N-terminus of MotB, the C-terminal tail of MotA, the cytoplasmic loop of MotA, and the region around residues Arg-90 and Glu-98 are connected in the order presented. Each of these connections may contribute to the proper positioning of the region around residues Arg-90 and Glu-98 relative to the motility domain of FliG. A precise alignment of each of these components may be necessary to induce the rotor to turn when the cytoplasmic N-terminus of MotB flexes in response to protonation of Asp-32 (**Fig. 3.6**).

It is less clear what the suppressors of the rather drastic $MotAB_{12-17A}$ and $MotAB_{12-17D}$ mutants are doing (**Fig 3.4A**). The suppressors involve deletions of the mutated region of *motB* or a double frameshift that alters the amino acid sequence between residues 5 and 14 of MotB (**Fig. 3.4B**). The common theme to all of these

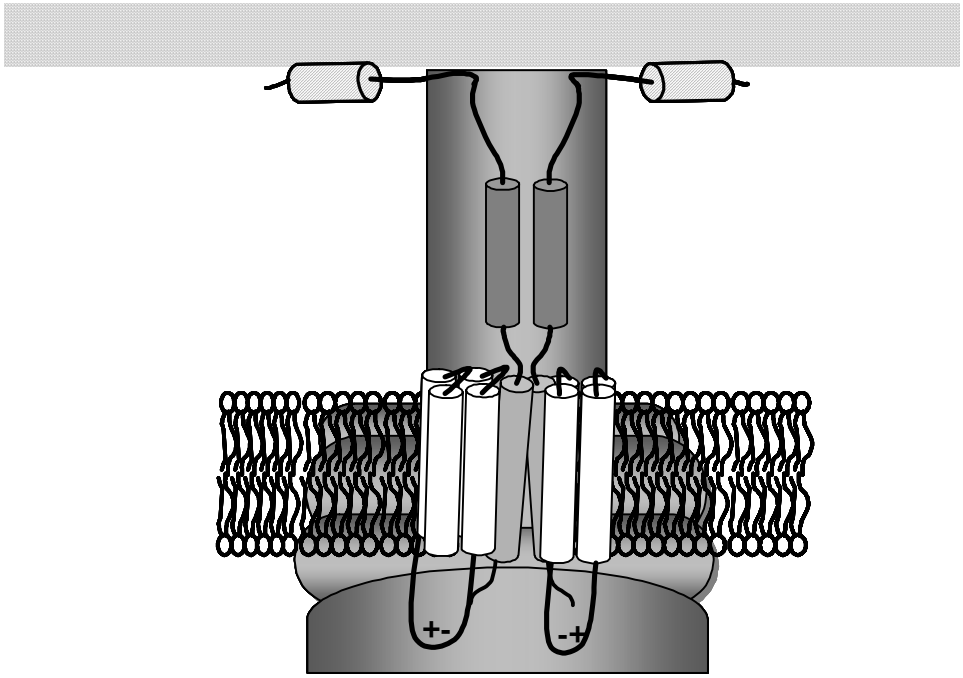

Figure 3.6. Schematic of the MotAB proton channel in the open conformation after contact with a flagellar motor. It shows the "connections" between the periplasmic domain of MotB with peptidoglycan, the transmembrane domains of MotA and MotB, the cytoplasmic N-terminus of MotB, the C-terminal tail of MotA, and the cytoplasmic loop of MotA which contains the residues Arg-90 and Glu-98 shown by the +/- that interacts with FliG.[109]

suppressors is that they eliminate the introduced neutral or negatively charged residues at positions 12-17 and/or bring other positively charged residues closer to the N-terminus of MotB (**Figs. 3.4B**). The take-home message seems to be either that a positively charged extreme N-terminus of MotB is important for proper channel function or assembly or that a neutral or negatively charged C-terminus is bad for motility. (The $MotAB_{\Delta 9\text{-}20}$ suppressor may suggest that the latter explanation holds). Again, none of these mutations affect the steady-state levels of MotB in the cell. Instead, one is led to conclude that the composition of the N-terminal cytoplasmic extension of MotB plays a crucial role in the coupling between protonation of Asp-32 of MotB and movement of the cytoplasmic loop of MotA.

Materials and Methods

Media. Routine media were prepared as described previously.[201] Tryptone broth (TB) is 1 % (w/v) tryptone extract and 0.8 % (w/v) NaCl. Luria broth (LB) contains 1 % tryptone extract, 0.5 % (w/v) yeast extract. LB solid agar contains 1.5 % (w/v) Difco agar and TB swarm plates contain 0.325% (w/v) Difco agar. Liquid cultures and agar plates were incubated at 37°C for LB or 30°C for TB. Media were supplemented with chloramphenicol (Cm, 30 μg per ml) and 1 mM Isopropyl β-D-1-thiogalactopyranoside (IPTG) for induction of the *tac* promoter of p*HSG*, as needed.

Strains and plasmids. Strain MM5000 (Δ*motAB*)[120] is a derivative of RP437[202] containing an internal, non-polar deletion within *motA* and *motB* (J. S. Parkinson,

personal communication). Construction of pHSG575-*motAB* was previously described.[120]

Site-directed mutagenesis. All mutations were introduced into pHSG575-*motAB* using the Quick-Change mutagenesis kit (Stratagene) according to the protocol supplied by the manufacturer. Mutagenized p*motAB* plasmids were transformed into MM5000. Transformants were selected on LB-Cm agar. Mutations were confirmed by dideoxynucleotide sequencing using the ABI Prism Dye-Terminator Cycle Sequencing Ready Kit with AmpliTaq DNA polymerase (PE Applied Biosystems).

Motility assay. The motility of each strain was assessed by inoculating colonies into TB swarm plates. Plates were incubated at 30°C for six to eight hours, and the diameter of each swarm was measured. Ten colonies of each strain were inoculated on one plate, and the swarming ability of a mutant was calculated as the ratio of the mean diameter of the ten swarms to the diameter of the swarms formed by the appropriate control strain MM5000/p$motA^{+}B^{+}$.

Isolation of suppressors. Eight colonies of each mutant were stabbed into a swarm plate and four to five swarm plates were prepared for each mutant. The plates were placed in an incubator at 30°C and observed for up to 36 hours. The plates were watched for motile flares emanating from the non-motile stab. Cells from each motile flare were streaked and isolated on LB+Cm plates. Plasmids were isolated from cultures

inoculated with cells from a single colony that was isolated from each flare and sequenced. Plasmids found to have a second site mutation were transformed into MM5000 and a swarm plate motility assay was performed as outlined above.

SDS-PAGE and immunoblots. Whole cell extracts were taken at the completion of growth curves. A_{600} of .8 were collected by centrifugation, washed once in 1 ml TE and resuspended in 50 μl SDS loading buffer (2 % (w/v) SDS, 5 % (v/v) 2-mercaptoethanol, 8.5 % (v/v) glycerol, 60 mM Tris (pH 6.8), 0.0004 % (w/v) bromophenol blue). Freeze-thaw extracts were prepared from these resuspended cells by three alternating cycles of five minutes at −80 °C and five minutes of boiling prior to loading on gels for SDS-PAGE. Proteins were separated by 12 % acrylamide SDS-PAGE and transferred to polyvinylidene difluoride membranes (PVDF). Anti-MotB[149] was used to probe the immunoblots, and the cross-reacting protein was visualized with alkaline phosphatase-conjugated, goat anti-rabbit antibody (BioRad). The blot was developed using SigmaFast (Sigma).

CHAPTER IV

MECHANISM OF TRANSLATIONAL COUPLING BETWEEN THE *E. coli motA* AND *motB* GENES

Introduction

The *motA* and *motB* genes are part of the *mocha* operon and are co-transcribed.[22] They are thought to be translationally coupled because the UGA stop codon of *motA* overlaps the AUG start codon of *motB* such that the overlapping sequence is AUGA.[173] This same overlap exists for *nifL* and *nifA* of *Klebsiella pneumoniae*.[210] Translational coupling means that the translation of the second (downstream) gene depends on the translation of the first in some more direct way than conventional transcriptional polarity.[211,212] Under conditions in which transcriptional polarity should be minimal, three to four fold more MotB is found in cells when the *motB* is downstream of *motA* with an in-frame deletion than when *motB* is downstream of *motA* with an out-of-frame deletion.[173] This result certainly points to the existence of functional translation coupling between MotA and MotB.

One possible mechanism for translational coupling is that ribosomes reading the upstream gene melt a strong secondary structure in the mRNA that otherwise inhibits translation initiation of the downstream gene by occluding the Shine-Dalgarno (SD) sequence and/or start codon.[211] However, SD recognition by free 30S ribosomal subunits can allow for very low levels of independent translation without melting the secondary structure.[213,214] It has also been proposed that when the downstream gene has a poor SD

sequence, its translation occurs via a reinitiation mechanism by the ribosome that has just finished translating the first gene. A translational reinitiation mechanism has been proposed for the translation of the coat and lysis genes of the phages MS2 and fr,[213,215] RNA phage GA coat and lysis genes,[216] and the regulatory genes of nitrogen fixation, *nifL* and *nifA*, of *Klebsiella pneumoniae*.[210] A third possibility combines the first two such that translation of the first gene melts secondary structure to allow free ribosomes to recognize the SD sequence to augment reinitiation.[217-221]

The SD sequence of the *motB* gene is GAGGAA, which is not far from the AGGAGGU consensus. However, this sequence is located only two bases in front of the AUG start codon of *motB*, far less than the canonical 7 to 11 bases. Thus, one would expect the *ab initio motB* translation start to be rather inefficient. Since a functional Mot complex has a strict 2:1 ratio of MotA to MotB, it seems selectively advantageous for some coordinated control of the expression of the two genes. Translational coupling provides one mechanism for exercising this control.

The work reported here was undertaken to determine whether reinitiation, *ab initio* initiation, or a combination of the two processes is responsible for the 2:1 stoichiometry of MotA relative to MotB. Translational *motA-lacZ* and *motB-lacZ* fusions were employed to eliminate concerns about the degradation of the inherently unstable MotB protein. The data show that *motB* is translated primarily by reinitiation, with a moderate contribution by *ab initio* translation, resulting in a final ratio of 1.5:1 in the translation of *motA* relative to *motB*.

Results

Impetus to study translational coupling of *motA* and *motB*. To examine the role of positively charged residues near the N-terminus of MotB, the AAG codon for Lys-2 of MotB in the sequence AUGAAG (**Fig. 4.1A**) was changed to the GCA codon for Ala, creating the sequence AUGGCA (*motAB*$_{K2A}$) (**Fig. 4.1B**). The site-directed mutation was made on the IPTG-inducible pHSG575-*motAB* plasmid, which was then introduced into strain MM5000 (Δ*motAB*). Remarkably to us at the time, this one-codon change abolished motility (**Table 4.1**), eliminated production of MotB and of normal-length MotA (data not shown), and led to the production of a longer form of MotA.

After some initial excitement, it became clear that the explanation had nothing to do with the K2A substitution *per se*. Instead, the UGA stop codon of *motA* had been converted into a UGG Trp codon (**Fig. 4.1B**). This change created a run-on, out-of-frame (with respect to MotB) MotA protein and led to dramatically decreased translation of MotB.

Before this realization was reached, pseudorevertants of the original mutant had been isolated. One, which restored motility to a wild-type level, generated the sequence AUGACA, which restores the UGA stop codon and produces the MotAB$_{K2T}$ substitution (**Table 4.1** and **Fig. 4.1C**). These cells produced normal levels of both MotA and MotB (data not shown). This finding demonstrated the non-essential nature of Lys-2 of MotB. The second pseudorevertant (*motAB*$_{AUA/K2A}$), which barely restored detectable motility (**Table 4.1**), generated the sequence AUAGCA (**Fig. 4.1D**). These cells made normal amounts of normal-length MotA, but their levels of MotB were greatly decreased (data

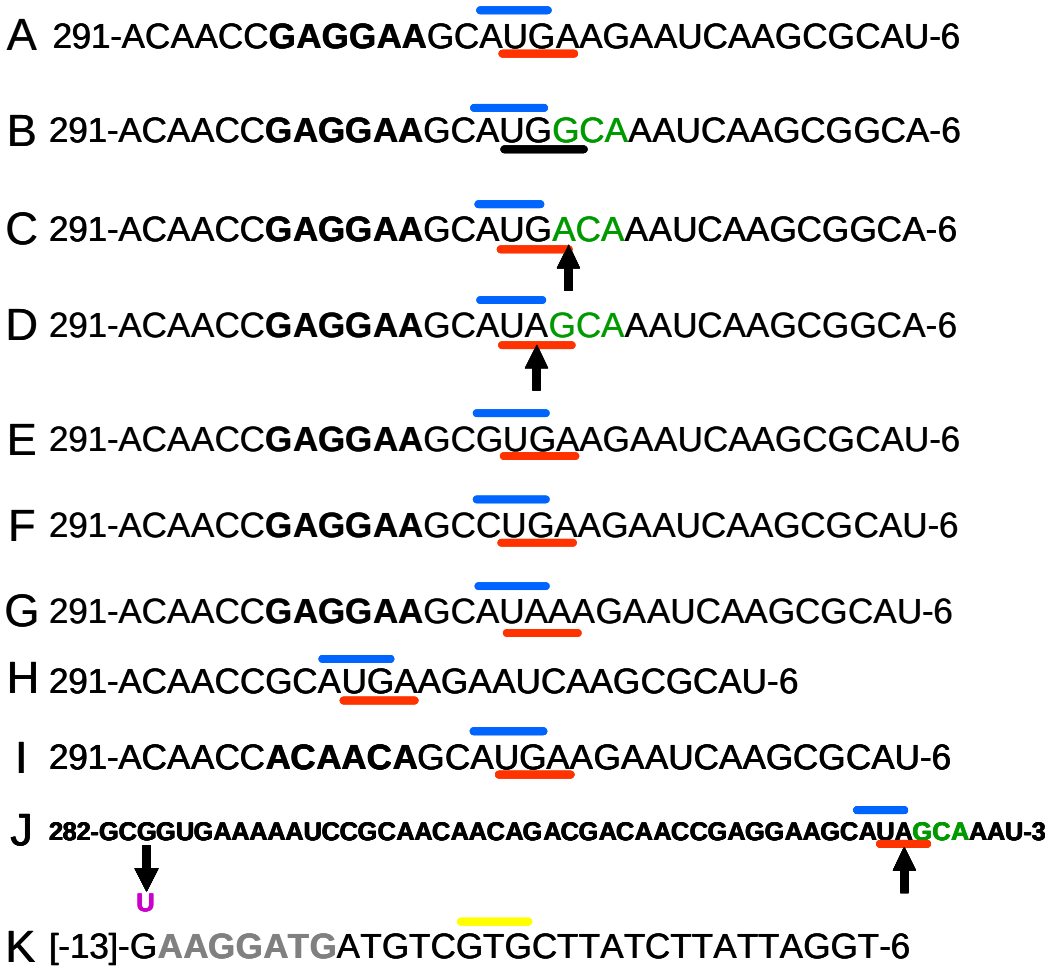

Figure 4.1. Base sequences of mutants and mutations studied. (A) Base sequence showing the native *motA/motB* overlap. (B) Original *motAB*$_{K2A}$ base sequence showing the change of the *motA* UGA stop codon to UGG (Trp codon, black bar). (C) Base sequence of a suppressor that restored a UGA stop codon by creating MotAB$_{A2T}$ from the original mutant shown in (B). (D) Suppressor of the sequence shown in (B) that altered the start codon from AUG to AUA. (E-G) Base sequence of *motAB* with alternative start codons for *motB*. (H) Base sequence with the *motB* SD sequence deleted. (I) The *motB* SD sequence has been altered to ACAACA. (J) Base sequence around the *motA*/*motB* overlap. The sequence is an extension of (A) that shows the change of the wild-type *motA*$_{282}$ codon of GCG changed to GCU (purple). The blue bar highlights the *motB* start codon. The red bar highlights the *motA* stop codon. The green-highlighted residues show the original K2A mutation. The bold residues make up the *motB* Shine-Dalgarno sequence. The block arrows indicate the bases altered by the suppressors that were isolated. (K) Base sequence of the region around the *motA* start codon highlighted by a yellow bar. The gray residues make up the *motA* Shine-Dalgarno (SD) sequence.

Table 4.1. Relative swarm diameters of mutants measured in this study.

Mutant	Relative Swarm Diameter[a]					
	motAB	$motAB_{\Delta SD}$[b]	$motAB_{SD\ (Thr)}$[b]	$motAB_{SD\ (Thr)\ new/SS}$[b]	$motA_{282}B$[b]	$motA_{282}B_{\Delta SD}$[b]
$motAB_{AUG}$	100%[c]	94 ± 6%	83 ± 4%[c]	97 ± 6%[c]	97 ± 4%	79 ± 5%
$motAB_{GUG}$	78 ± 5%[a]	84 ± 5%	82 ± 3%	92 ± 4%	86 ± 4%	86 ± 1%
$motAB_{CUG}$	22 ± 3%[c]	51 ± 2%	45 ± 5%[c]	65 ± 4%[c]	44 ± 4%	68 ± 1%
$motAB_{AUA}$	3 ± 0%[c]	23 ± 2%	18 ± 0%[c]	49 ± 2%[c]	17 ± 2%	47 ± 1%
$motA_{P286Q}B_{AUG}$	94 ± 6%				90 ± 0 %	
$motA_{P286Q}B_{GUG}$	85 ± 6%				80 ± 6%	
$motA_{P286Q}B_{CUG}$	39 ± 3%				21 ± 2%	
$motA_{P286Q}B_{AUA}$	18 ± 4%				3 ± 1%	
$motAB_{K2A}$	0%					
$motAB_{K2T}$	81 ± 5%					
$motAB_{AUA/K2A}$	3 ± 1%					
$motA_{P286P}B_{AUG}$	95 ± 6%					
$motA_{P286P}B_{GUG}$	86 ± 7%					
$motA_{P286P}B_{CUG}$	40 ± 4%					
$motA_{P286P}B_{AUA}$	14 ± 2%					
$motA_{AUG}B_{AUG}$	77 ± 4%					
$motA_{CUG}B_{AUG}$	21 ± 2%					
$motA_{AUA}B_{AUG}$	86 ± 4%					

[a] Swarm diameters are expressed as a percentage of the diameter of the swarm of the wild-type $motA^+B^+$ strain.
[b] These mutations were combined with the mutations listed in the first column.
[c] Value was used to create Figure 4.3.

not shown). Clearly, AUA had to be serving as a start codon for *motB*, however inefficiently. We hypothesized that this situation could arise only in the context of translational coupling, a prediction that led to the series of experiments described here.

Efficiency of alternative start codons in initiation of *motB* translation. To assess the intrinsic function of various potential start codons, we used site-directed mutagenesis to introduce potential start codons (**Fig. 4.1E-G**) into the pHSG575-*motAB* plasmid (*cis*) and determined the effect on motility. The swarm diameters in tryptone semi-solid agar compare to the initial AUG was 78% with GUG, 22% with CUG, and 3% with AUA (**Table 4.1**). No motility was seen when the start codon was CUA, GUA, or UUA (data not shown). The GUG start codon allowed normal amounts of MotB to be made, but the amount of MotB present was much lower with CUG and AUA (data not shown), and no MotB was seen for CUA, GUA, or UUA (data not shown).

Utilizing the Δ*motB* strain MM5003 and the IPTG-inducible pHSG575-*motB* plasmid, we also studied the effects of the different start codons on motility when *motB* was not translationally coupled to *motA* (*trans*). With the AUG start codon, swarm diameters were 73% of the diameter seen when MotB was expressed in *cis* with MotA from pHSG575-*motAB* (data not shown), and the amount of MotB relative to MotA was lower (data not shown). When AUG was substituted with GUG, CUG, and AUA, cells were non-motile (data not shown). No protein was seen with CUG or AUA start codons in *trans*, and only GUG produced any detectable level of MotB (data not shown).

For comparison, we also looked at the effect of different codons on MotA production. The native start codon for *motA* is GUG, but *motA* possesses a good SD sequence, as would be expected for *ab initio* translation (**Fig. 4.1K**). When the GUG was replaced in the p*motAB* plasmid with AUG, the swarm diameter decreased to 77% of the wild-type level, with AUA it was 86%, with CUG it was 21%, and no motility was seen with CUA (**Table 4.1**). Even with AUA, the protein level was only moderately lower than with GUG (data not shown).

These findings lead to two conclusions. First, AUA functions much better as a start codon when it is paired with a good SD sequence. Second, having the maximum level of translation initiation, as would be expected with the AUG start codon, does not necessarily result in the highest motility. It remains to be seen whether the latter conclusion is true only for the somewhat artificial situation in which the Mot proteins are overexpressed from an inducible, plasmid-borne set of *motAB* genes.

Effect of altering the *motB* Shine-Dalgarno sequence in *cis* and *trans*. The presumptive SD sequence for *motB* (GAGGAA) spans codons 293-294 of *motA* and is located only two bases from the *motB* AUG start codon (**Fig. 4.1A**). We previously showed that replacing the existing *motB* SD sequence with a consensus sequence at optimal spacing has little effect on swarm size when *motB* is expressed in *trans* relative to *motA*.[120] However, removing the mRNA secondary structure in the vicinity of the native translation-start site of motB expressed in *trans* led to a moderate increase in swarm diameter, and a restoration of swarming equivalent to that seen when *motB* is

expressed in *cis* with *motA* was seen when the secondary structure was removed and a consensus SD sequence replaced the original one.[120]

We therefore decided to look at the effect of removing (**Fig. 4.1H**) or altering (**Fig. 4.1I**) the SD sequence of *motB* when it was together with *motA* in *cis*. With an AUG start codon and the *motB* SD sequence removed, the swarm diameter relative to wild-type *motAB* was 94%, with GUG as the start codon it was 84%, with CUG it was 51%, and with AUA it was 23% (**Table 4.1**). MotB levels appeared normal with the AUG or GUG start codons, and there appeared to be an increase in MotB above the original low levels seen with CUG and AUA when the SD sequence was still present (data not shown).

The GAGGAA SD sequence of *motB* was also changed to ACAACA. Besides eliminating the SD sequence, this change replaces Glu-293 and Glu-294 of MotA with Thr [SD (Thr)] (**Fig. 4.1I**). The swarm diameter with the AUG start codon was 83% of wild type, with GUG it was 82%, with CUG 45%, and with AUA was 18% (**Table 4.1**), virtually the same result seen when the SD sequence was deleted. However, when this same change was made in pHSG575-*motB* and motility examined in strain MM5003, the relative swarm diameter fell to 45% with AUG (data not shown), and no motility is seen with the GUG, CUG, or AUA start codons (data not shown).

The role of mRNA secondary structure in *motB* translation initiation. The mRNA sequence at the *motAB* boundary was submitted into the *mfold* 3.2 program (www.bioinfo.rpi.edu/applications/mfold/rna/form1-2.3.cgi) to predict the mRNA

secondary structure. The stop/start overlap of *motAB* exists in a hairpin loop (**Fig. 4.2A**), as does the presumptive SD sequence. The SD (Thr) sequence opens the secondary structure around the SD sequence (**Fig. 4.2B**). The secondary structure with SD (Thr) can be restored by changing codons 6 and 7 of *motB* to CAGTTG from CATCCG [SD (Thr)w/ SS] (**Fig. 4.2C**). When the secondary structure is restored, the relative swarm diameters are 97% with AUG, 92% with GUG, 65% with CUG, and 49% with AUA (**Table 4.1**). Thus, the maximum reduction of the expected efficacy of *ab initio* translation from the *motB*, by eliminating the resident SD sequence and strengthening the mRNA secondary structure, leads to the highest level of motility. This result suggests that, in the native situation, there is competition between free 30S ribosomal subunits binding to the *motB* SD sequence and read-through translation by ribosomes that have finished translating *motA*.

Translation efficiency measured with *motB-lacZ* translational fusions.

Several problems arise when *motB* translation efficiency is measured by motility assays or immunoblots for MotB. In the first case, there is no assurance that the extent of motility is directly proportional to the production of MotB, particularly from an inducible, plasmid-borne gene. In the second case, aside from the inherent problems associated with quantifying protein levels from immunoblots, the intrinsic lability of MotB may lead to underestimates of its translation. To circumvent these difficulties, the *lacZ* sequence was inserted in-frame after residue 13 of MotB. Relative to the native case with the AUG start codon for *motB*, a GUG start codon resulted in β-galactosidase

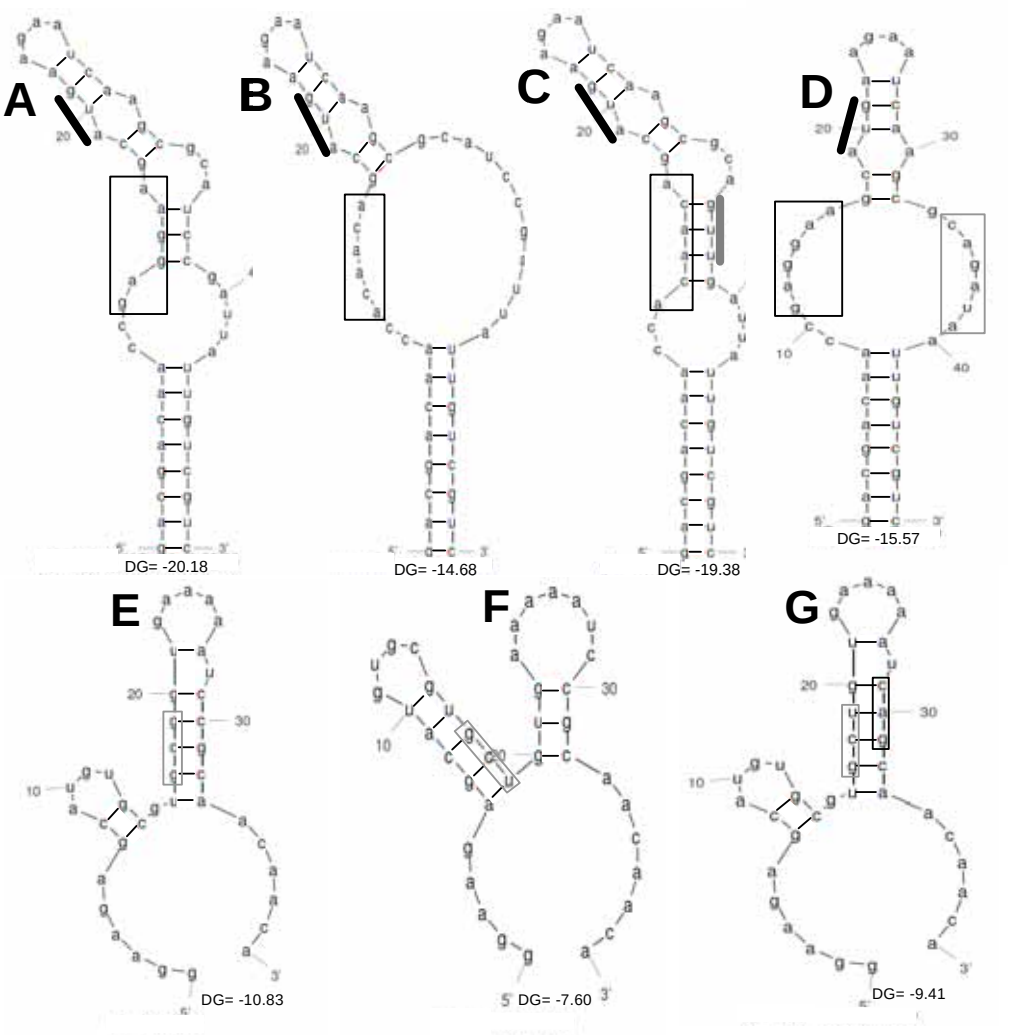

Figure 4.2. The mRNA secondary structure predictions of the stop/start overlap of *motAB* and a region upstream of the overlap. Secondary structure predictions were obtained by submitting the base sequence of *motAB* to the *mfold* 3.2 program (www.bioinfo.rpi.edu/applications/mfold/rna/form1-2-3.cgi). (A) Secondary structure prediction of the area around the stop/start overlap of wild-type *motAB*. The AUG start codon is highlighted by a black bar and the SD sequence is black boxed. (B) Secondary structure prediction of the same area shown in (A) after the Shine-Dalgarno sequence of *motB* was altered [SD (Thr)]. The altered SD sequence is black boxed. (C) Secondary structure prediction of the same area shown in (B) after the Shine-Dalgarno sequence of *motB* was altered [SD (Thr)] and specific mutations were placed into *motB* that restored the secondary structure to nearly the wild-type form. The specific mutations introduced at codons 6 and 7 of MotB are highlighted by a gray bar. (D) Secondary structure prediction of the same area in (A) after specific mutations were introduced into *motB* to open up the secondary structure. The specific mutations introduced into codons 6 and 8 (codon 7 was deleted) are highlighted by the gray box. (E) Secondary structure prediction of a hairpin loop just upstream of the stop/start overlap of *motAB*. The codon for MotA residue Ala-282 is highlighted by a gray box. (F) Secondary structure prediction of the same area shown in (E) after a mutation at codon 282 of MotA that changes the sequence from GCG to GCU was introduced that resulted in a reduction of the hairpin loop. The altered codon of $MotA_{282}$ is highlighted by a gray box. (G) Secondary structure prediction of the same area shown in (F) after a mutation is placed into codon 286 of MotA that restores the hairpin loop to nearly the wild-type form. The mutated $MotA_{P286Q}$ codon is highlighted by a black box.

activity 31% that of wild type, whereas with CUG and AUA the activities were only 1.5%, and 0.5% of wild type (**Table 4.2**). In the pHSG575-*motB* plasmid, the AUG start codon yielded a relative β-galactosidase activity of only 8% (data not shown), while the GUG, CUG and AUA start codons supported no detectable β-galactosidase activity (data not shown). These results show that swarm diameters tend to underestimate the decrease in *motB* translation caused by various manipulations of the translation start site. Placing an opal (UGA) stop codon after residue 250 of *motA*, which stops *motA* translation prematurely and should eliminate any translational coupling, yielded a relative β-galactosidase activity 12% that of the wild-type level (**Table 4.2**), similar to that seen when *motB-lacZ* was expressed in *trans*.

When the *motB* SD sequence was changed from GAGGAA to ACAACA [SD (Thr)], the relative β-galactosidase activities were 93% with AUG, 2.5% with CUG, and 1% with AUA (**Table 4.2**). When SD (Thr) was combined with the mutations that restore the secondary structure around the SD sequence of *motB*, the β-galactosidase activity was 99% with AUG, 5% with CUG, and 4% with AUA (**Table 4.2**). This same change in the SD sequence in pHSG575-*motB* resulted in a relative β-galactosidase activity of 4% (data not shown).

We also looked at β-galactosidase activities when the last base of codon 287 of MotA was deleted ($motA_{287fs}B$). In this case, the ribosome translating *motA* reads out of frame through the UGA stop codon of *motA* and is also out of frame with the *motB-lacZ* ORF, effectively uncoupling translation. The relative β-galactosidase activity of a strain in which pHSG575-*motAB* carries this mutation with the wild-type AUG start codon is

Table 4.2. Relative β-galactosidase activity of mutants analyzed in this study.

Mutant	Relative β-galactosidase Activity [a]						
	motA^{+}*B*$^{+}$	*motAB*$_{\text{SD (Thr)}}$ [b]	*motAB*$_{\text{SD (Thr) newSS}}$ [b]	*motA*$_{282}$*B* [b]	*motAB*$_{\text{openSS}}$ [b]	*motA*$_{287\text{fs}}$*B* [b]	*motA*$_{\text{openSS-287fs}}$*B* [b]
motAB$_{\text{AUG}}$ [c]	100% [e]	93 ± 1% [e]	99 ± 6% [e]	93 ± 9% [e]	156 ± 14%	2 ± 0%	65 ± 3%
motAB$_{\text{GUG}}$ [c]	31 ± 3% [e]				39 ± 7%	0%	11 ± 1%
motAB$_{\text{CUG}}$ [c]	1.5 ± 0% [e]	2.5 ± 0% [e]	5 ± 0% [e]	2 ± 0% [e]	2 ± 0%		
motAB$_{\text{AUA}}$ [c]	0.5 ± 0% [e]	1 ± 0% [e]	4 ± 0% [e]	1 ± 0% [e]	0%		
motA$_{\text{UGA(250)}}$*B*$_{\text{AUG}}$ [c]	12 ± 1%						
motA$_{\text{AUG/consSD}}$*B*$_{\text{AUG}}$ [c]	223 ± 9%					1 ± 0%	
motA$_{\text{CUG}}$*B*$_{\text{AUG}}$ [c]	11 ± 0%						
motA$_{GUG}$ [d]	149 ± 9%						
motA$_{\text{CUG}}$ [d]	2 ± 0%						
motA$_{\text{AUG/consSD}}$ [d]	455 ± 20%						

[a] Activities are expressed as a percentage of the activity supported by the wild-type *motAB-lacZ* fusion.
[b] These mutations were combined with the mutations listed in the first column.
[c] Activities in these rows are from the *motB-lacZ* translational fusion.
[d] Activities in these rows are from the *motA-lacZ* translational fusion.
[e] Value was used to create Figure 4.3.

only 2%, and with GUG as the start codon, no *motB* β-galactosidase activity at all was detected (**Table 4.2**). This result confirms the observation made with the original fortuitous mutant that eliminated the UGA stop codon.

Effect of the level of *motA* translation on *motB-lacZ* expression. The level of translation of *motA* should influence translation of *motB* if the two processes are coupled. To test this prediction, the start codon of *motA*, normally GUG, or the *motA* SD sequence was modified to modulate the extent of *motA* translation. When the GUG start codon was changed to CUG, the β-galactosidase activity of the MotB-LacZ fusion fell to 11% of the normal level (**Table 4.2**). With an AUG start codon and a consensus SD sequence for *motA*, β-galactosidase activity increased to 223% of the wild-type level (**Table 4.2**). With this same *motA* translation start, if *motA* and *motB* translation were uncoupled by the frameshift mutation in codon 287 of *motA* (*motA*$_{287fs}$*B*), the β-galactosidase activity dropped to 1% of that seen in wild type (**Table 4.2**).

Expression of *motA-lacZ* fusions coupled to different *motA* translation starts. To insure that the changes in the *motA* translation start were having the effects that we anticipated, we also fused *lacZ* in frame after codon 8 of *motA*. With the wild-type translation start, the β-galactosidase activity was 149% of that seen with the *motB-lacZ* fusion in a wild-type setting. With a CUG start, the value was only 2% of that normally seen with the *motB-lacZ* fusion (**Table 4.2**). In contrast, changing the Shine-Dalgarno sequence of *motA* to a consensus sequence, from AGGATG to AGGAGG, and

introducing an AUG start codon resulted in a β-galactosidase activity 455% of that seen with the *motB-lacZ* fusion (**Table 4.2**).

Effect of secondary structure *per se* on expression of *motB-lacZ*. Based on the prediction of *motAB* mRNA secondary structure, it is possible to open up the secondary structure around the translation start while retaining the SD sequence by mutating codons 6 and 8 and deleting codon 7 of *motB* (**Fig. 4.2D**) and express *motB* in *cis* and *trans*. When this was done with the native AUG start codon for *motB* in pHSG575-*motAB*, the relative β-galactosidase was 156%, with GUG it was 39%, with CUG it was 2%, and no activity was seen with AUA (**Table 4.2**). With the same change in pHSG575-*motB*, the relative β-galactosidase activity compared to that produced by the wild-type fusion in *cis* was 65% with AUG, 1% with GUG, and undetectable with CUG or AUA (data not shown). If pHSG575-*motAB* also contained the uncoupling frameshift at codon 287 of *motA*, the relative β-galactosidase activity was 65% with the AUG start codon for *motB*, 11% with GUG (**Table 4.2**), and undetectable with either CUG or AUA (data not shown). The implication is that the secondary structure in the region of the SD sequence is important for efficient translational coupling and that the resident SD sequence interferes with translational coupling when it is not sequestered in secondary structure.

Sequences in *motA* far from the MotAB overlap effect translational coupling. The original AUA mutation in *motB* would never have been identified by

itself, since it increases swarming to only 3% of the wild-type level (**Table 4.1**). The plasmid actually had a second mutation that converts the GCG of codon 282 of *motA* to GCU (**Fig. 4.1J**). This mutation does not change the Ala residue at position 282 of MotA, but it does increase the swarm diameter to 17% of the wild-type level (**Table 4.1**). When the $MotA_{282}$ was combined with *motB* start codons of AUG, GUG and CUG, the relative swarm diameters were 97%, 86%, and 44%, respectively (**Table 4.1**), compared to swarm diameters of 100%, 78%, and 22%, respectively, without the $MotA_{282}$ change (**Table 4.1**). The β-galactosidase activity in the presence of the $MotA_{282}$ mutation was 93% with AUG, 2% with CUG, and 1% with AUA (**Table 4.2**), whereas without the $MotA_{282}$ mutation they were 100%, 1.5%, and 0.5%, respectively (**Table 4.2**).

When the $MotA_{282}$ mutation was combined with the deletion of the SD sequence, relative swarm diameters of 68% and 47% were seen with the CUG and AUA start codons, respectively (**Table 4.1**). With GUG as the *motB* start codon, the swarm diameters were 86% of wild type (**Table 4.1**), and with AUG as the *motB* start, the relative swarm diameter fell to 79% (**Table 4.1**). MotB protein levels were unchanged with AUG and GUG as start codons in the presence of the $MotA_{282}$ mutation and the SD deletion, but with CUG and AUA there appears to be an increase in the level of MotB (data not shown).

The secondary structure prediction suggests that the third base of residue 282 can pair with the second base of codon 286 (**Fig. 4.2E**). The mRNA made by the $MotA_{282}$ mutant cannot form this bond, resulting in a weakening of the hairpin loop (**Fig. 4.2F**).

When the codon of MotA residue 286 is changed from CCG to CAG, causing the P286Q residue change, the hairpin loop should be restored when combined with $MotA_{282}$ (**Fig. 4.2G**) but causes a similar reduction in secondary structure as $MotA_{282}$ (**Fig. 4.2F**) when not combined. The $MotA_{P286Q}$ mutation by itself results in relative swarm diameters of 94% with an AUG start codon, 85% with GUG, 39% with CUG, and 18% with AUA (**Table 4.1**). If codon 286 of *motA* is changed from CCG to CCT, which keeps the Pro residue but reduces the strength of the hairpin loop in the same manner as the $MotA_{282}$ (**Fig. 4.2F**) or $MotA_{P286Q}$ mutation (data not shown), relative swarm diameters of 95% with AUG, 86% with GUG, 40% with CUG and 14% with AUA are seen (**Table 4.1**). However, combining the $MotA_{282}$ and $MotA_{P286Q}$ mutations to restore the hairpin loop structure (**Fig. 4.2G**) results in relative swarm diameters of 90% with AUG, 80% with GUG, 21% with CUG, and 3% with AUA (**Table 4.1**), values nearly identical to those observed with the original hairpin intact (**Table 4.1**). Thus, structural elements in the *motA* mRNA well upstream of the translation start site of *motB* can still have significant effects on the extent of translational coupling.

Discussion

The data presented in the Results section come across as rather bewildering on first glance because of the large set of different combinations of mutations. Therefore, the Discussion will present each of the six main conclusions, roughly in order of importance, as the lead sentence in a paragraph. Each paragraph will continue with a

brief discussion of the evidence that supports the conclusion. The final paragraph considers the global implications of the results.

First, the AUGAAG overlap of the *motA* stop codon and the *motB* start codon leads to efficient translational coupling of the two genes (**Fig. 4.1A**). The conversion of this sequence to AUGGCA (**Fig. 4.2B**) almost completely eliminates intracellular MotB. Although the run-on MotA protein may well be non-functional for motility, even though it is still present, it might be expected to be capable of forming a complex with MotB to stabilize it.[120] Moreover, some of the intrinsically unstable MotB should remain even in the absence of MotA.[120,173] The almost total absence of MotB suggests that one significant effect of ribosomes not stopping at the UGA codon is that translational coupling is eliminated. The same conclusion can be reached based on the frameshift mutation introduced at codon 287 near the very end of MotA (*motA*$_{287fs}$*B*). Again, translation of *motB* is uncoupled from *motA* so the ribosome will not stop at the UGA codon, and under these conditions translation of *motB* decreases to 2% of its normal level (**Table 4.2**). It should be noted that in both instances, the resident site for *ab initio* translation of *motB* is unaffected by the mutations.

Second, *motB* is translated mainly through reinitiation by the 30S subunits of ribosomes that have just completed translating *motA*. With the normal AUG start codon present, there is still a small contribution (< 10%) to MotB production due to *ab initio* translation from the intrinsic *motB* translation start (**Table 4.2**, data for the ACAACA *motB* SD [SD (Thr)]). In the absence of any translational coupling, *ab initio* translation of *motB* from its own ribosome-binding site also supports translation at about 10% of the

normal level (**Table 4.2,** data for UGA at *motA* codon 250 and wild-type *motB* SD in *trans*). With the alternative start codons GUG, CUG, and AUA, virtually all of the translation of *motB* is due to read-through by ribosomes that have translated *motA*. Furthermore, the resident Shine-Dalgarno (SD) sequence of *motB* is incapable of initiating significant levels of translation with GUG, CUG, or AUA start codons when *motB* is uncoupled from *motA* (**Table 4.2**). The conclusion that ribosomes translating *motA* reinitiate is also supported by the fact that, in two different constructs (**Fig. 4.1B** and the frameshift mutation in codon 287 of *motA*, ribosomes reading through the *motA* stop codon drastically decrease *motB* translation. The upstream ribosomes must stop near the *motB* translation start, not just melt secondary structure there.

Third, the extent of translation of the upstream *motA* gene is proportional to the translation of the downstream *motB* gene. For example, when the start codon for MotA was changed to CUG, which reduced the translation of *motA* to less than 2% of its normal level (**Table 4.2**), the translation of *motB* dropped to 12% of its wild-type level, about the same as when translational coupling was eliminated altogether. When translation of *motA* was increased more than four fold by replacing the normal GUG start codon with AUG and introducing a perfect SD sequence at the optimal separation from the start codon, *motB* translation increased by 225% (**Table 4.2**). These findings are consistent with the idea that ribosomes reading *motA* reinitiate translation of *motB* with a fixed efficiency. There is no clear reason this proportionality would be seen if the only role of the upstream ribosomes were to melt secondary structure involving the *motB* translation start site.

Fourth, the resident SD sequence of *motB* can act as a negative regulator of *motB* translation. The canonical SD sequence is AGGAGGU, whereas the sequence GAGGAAGC lies just upstream of the AUG start codon of *motB* (**Fig. 4.1A**). The most crucial residues of a SD sequence are GGAGG. Of these, four out of five are present in the *motB* SD sequence. Presumably, the reason that intrinsic translation initiation is so poor for *motB* (**Table 4.1** and **Table 4.2**) is that the SD sequence is sequestered in secondary structure (**Fig. 4.2A**) and also located too close to the start codon (two bases before rather than the optimal 7 to 11). Whatever capacity for *ab initio* translation of *motB* remains, it is apparently somewhat independent of the SD sequence and can occur only with the AUG start codon (**Table 4.2**), as reported for other systems.[222-225] When the *motB* SD sequence is deleted or eliminated through sequence alteration (**Fig. 4.1H,I**), production of MotB by translational coupling increases significantly with the weak start codons CUG and AUA, and reintroducing secondary structure in this region without the SD sequence further enhances translation with CUG and AUA (**Table 4.1** and **Table 4.2**). Thus, the GGAGG sequence may recruit 30S ribosomal subunits that block reinitiation by 30S subunits of ribosomes that have translated *motA* but not be able to initiate translation themselves. The same effect presumably occurs when the AUG codon is present, but it is compensated by *ab initio* translation that is independent of a functional SD sequence.

Fifth, secondary structure in *motA* mRNA upstream of the *motB* translation start can affect the efficiency of translational coupling. Replacing the native AUGAAG sequence at the *motAB* overlap with AUGGCA completely eliminated translational

coupling, but the mutation of this sequence to AUAGCA partially restored it. The pseudorevertant with this change was found only because of a second, fortuitous mutation in Ala codon 282 of *motA* (**Fig. 4.1J**) that diminished the strength of RNA secondary structure well upstream of the *motB* translation start, which encompasses codons 293-295 of *motA*. This seemingly innocuous, synonymous codon change is predicted to weaken a RNA hairpin stem (compare **Fig. 4.2E and F**). Although no significant difference in *motB* translation was seen when the mutation at codon 282 was combined with the native *motB* translation start, pausing of ribosomes at the upstream secondary structure could diminish translational coupling under some circumstances.

Sixth, relative swarm diameters, and presumably other measures of the motility of swimming cells, are poor quantitative measures of intracellular levels of Mot proteins. This idea is not novel. It is explicitly predicted by observations of the resurrection of rotation to flagella operating at different external loads,[127-132,137] which suggest that far fewer Mot complexes are needed under conditions of low external torque (*e.g.*, swimming cells) than at high external torque (*e.g.*, tethered cells). However, **Figure 4.3** presents the first quantitative comparison that correlates the translation level of a Mot protein (in this case MotB) with a measure of swimming motility (here swarm diameter). Admittedly, the levels of IPTG-inducible MotB expression from the p*HSG* plasmids do not coincide with physiological levels of MotB expression from the chromosomal gene, but they do provide a qualitative demonstration of the non-linearity of the relationship between the number of functional Mot complexes and swimming motility.

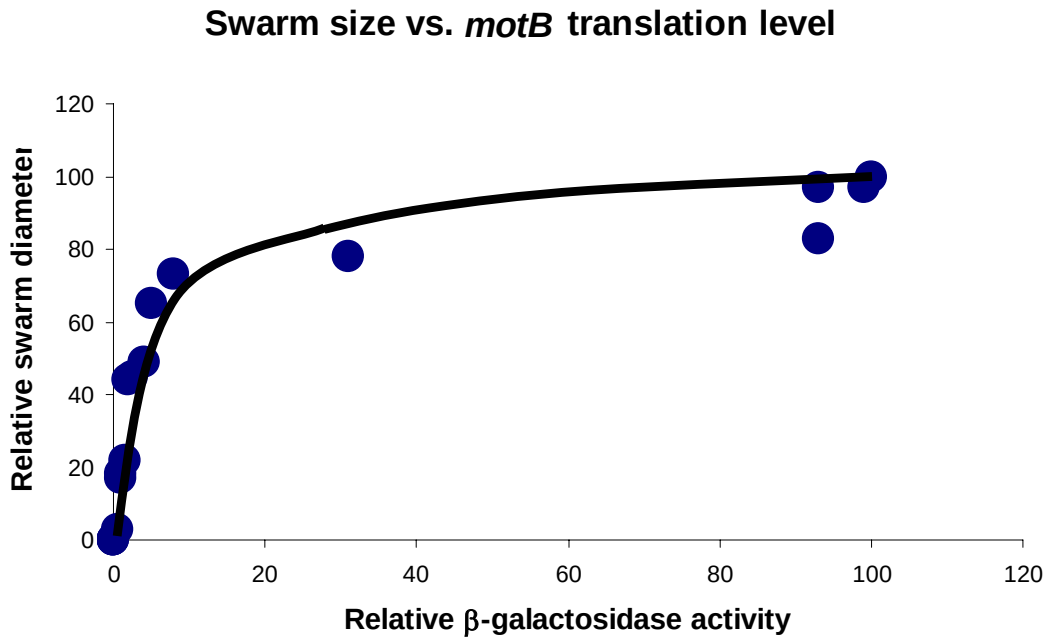

Figure 4.3. Graph of relative swarm diameters vs. relative β-galactosidase activities of mutants for which both measurements were obtained. Values used are from Tables 4.1 and 4.2.

The *motA* and *motB* genes are normally translated in a ratio of 1.5:1 (**Table 4.2**), and the MotA and MotB proteins are present in the cell in a ratio of 2:1[161,164] in a $MotA_4MotB_2$ complex.[164] Since MotB is relatively unstable in the absence of MotA,[173] it is perhaps advantageous that it is produced in slight excess to account for degradation that may occur before the final $MotA_4MotB_2$ complex forms. The situation is different with other well-known examples of translational coupling of bacterial genes, such as *nifLA* in *K. pneumoniae*[210] or *trpBA* in *E. coli*.[220,226-228] In the latter two cases, the two gene products occur in stoichiometrically equal complexes as NifLNifA dimers[229] and $TrpB_2TrpA_2$ tetramers,[230-232] respectively. For those systems, 100% efficient reinitiation is optimal. For MotAB, however, a more intricate system is required to establish a 1.5:1 ratio. We propose a mechanism by which a non-optimally placed *motB* SD sequence and *motA* mRNA secondary structure upstream of the *motB* translation start decrease the efficiency of translation initiation by the 30S subunits of ribosomes that have translated *motB*. Some features are revealed only under artificial conditions in which non-canonical start codons are introduced at the MotB translation start. However, the baroque scenario thus created illustrates how far natural selection may go to achieve the best outcome for each specific demand for regulation of gene expression.

Materials and Methods

Media. Routine media were prepared according to Miller[201]. Tryptone broth (TB) is 1 % (w/v) tryptone extract and 0.8 % (w/v) NaCl. Luria broth (LB) contains 1 % tryptone extract, 0.5 % (w/v) yeast extract. LB solid agar contains 1.5 % (w/v) Difco

agar and TB swarm plates contain 0.325% (w/v) Difco agar. Liquid cultures and agar plates were incubated at 37 °C for LB or 30°C for TB. Media were supplemented with chloramphenicol (Cm, 30 μg per ml) and 100 μg per ml 5-Bromo-4-Chloro-3-Indolyl-B-D-Galactopyranoside (X-Gal; Sigma) dissolved in dimethylformamide as needed. 1 mM Isopropyl β-D-1-thiogalactopyranoside (IPTG) was used for induction of the *tac* promoter of the p*HSG* vector.

Strains, plasmids, and enzymatic assays. Strain MM5000 (Δ*motAB*)[120] is a derivative of RP437[202] containing an internal, non-polar deletion within *motA* and *motB* (J. S. Parkinson, personal communication). Strain MM5003 (Δ*motB*) is a derivative of RP437 containing an internal, in-frame deletion in *motB*[160] that extends from base-pairs 359 to 781 (codons 119 to 260). MC4100 (*araD139* Δ(*argF-lac*)*U169 rpsL150 relA1 flbB5301 deoC1 ptsF25 rbsR*) (Laboratory Stock). Construction of pHSG575-*motAB* was previously described by Van Way[120].

The p*HSG*575-*motABlacZ* fusion plasmid was constructed by using primers to PCR amplify the entire *lacZ* from *pS105mycRϕlacZ*, except for the first three codons.[233] p*HSG575-motAB* was also amplified using two primers, one which annealed at the codon encoding residue 14 and another which annealed at the codon encoding residue 13 of *motB*. The products were gel purified and a 1.19 Kb fragment of *lacZ* and a 5.3 Kb p*HSG575-motAB* were extracted from the gel and ligated together by blunt end ligation and confirmed by sequencing. Primers were used to insert a TGA stop codon in-frame at

the end of *lacZ*. The product was also confirmed by testing for blue colonies on colorimetric plates.

The p*HSG575-motAlacZ* fusion plasmid was made by using p*HSG575-motABlacZ* as the template and two primers, one of which annealed to the first codon of *lacZ* (which encodes for residue four) and another which annealed at the codon coding for residue eight of *motA*. PCR amplification was then used to delete from residue six of MotA through residue 13 of MotB. The product was ligated and confirmed by sequencing and colorimetric plates.

The p*HSG575-motBlacZ* fusion plasmid was made by using primers and PCR amplification to delete *motA*, including its Shine-Dalgarno sequence, in p*HSG575-motAlacZ*.

Plasmids containing LacZ fusions were introduced into strain MC4100 and B-Galactosidase assays were performed according to the method of Miller[201].

Site directed mutagenesis. All mutations were introduced into pHSG575-*motAB*, pHSG575-*motB*, pHSG575-*motABlacZ*, and pHSG575-*motAlacZ* using the Quick-Change mutagenesis kit (Stratagene) according to the protocol supplied by the manufacturer. Mutagenized p*motAB* plasmids were transformed into MM5000, MM5003 and MC4100 strains. Transformants were selected on LB-Cm agar or LB-Cm+IPTG+X-Gal indicator plates to detect the *lacZ* fusions. Mutations were confirmed by dideoxynucleotide sequencing using the ABI Prism Dye-Terminator Cycle Sequencing Ready Kit with AmpliTaq DNA polymerase (PE Applied Biosystems).

Colorimetric detection of LacZ activity. MC4100 containing MotAB-LacZ, MotB-LacZ or MotA-LacZ fusions were plated onto LB plates + 1 mM IPTG + Cm + 100 μg per ml 5-Bromo-4-Chloro-3-Indolyl-B-D-Galactopyranoside (X-Gal; Sigma) dissolved in dimethylformamide, and screened for either blue or white colonies.

Motility assay. The motility of each strain was assessed by inoculating colonies into TB swarm plates. Plates were incubated at 32^{o}C for six to eight hours, and the diameter of each swarm was measured. Ten colonies of each strain were inoculated on one plate, and the swarming ability of a mutant was calculated as the ratio of the mean diameter of the ten swarms to the mean diameter of ten swarms formed by the appropriate control strain, either MM5003/p*motB*$^{+}$ or MM5000/p*motA*$^{+}$*B*$^{+}$.

SDS-PAGE and immunoblots. Whole cell extracts were taken at the completion of growth curves. A_{600} of .8 were collected by centrifugation, washed once in 1 ml TE and resuspended in 50 μl SDS loading buffer (2 % (w/v) SDS, 5 % (v/v) 2-mercaptoethanol, 8.5 % (v/v) glycerol, 60 mM Tris (pH .8), 0.0004 % (w/v) bromophenol blue). Freeze-thaw extracts were prepared from these resuspended cells by three alternating cycles of five minutes at −80 °C and five minutes of boiling prior to loading on gels for SDS-PAGE. Proteins were separated by 12 % acrylamide SDS-PAGE and transferred to polyvinylidene difluoride membranes (PVDF). Anti-MotB[149] was used to probe the immunoblots, and the cross-reacting protein was visualized with

alkaline phosphatase-conjugated, goat anti-rabbit antibody (BioRad). The blot was developed using SigmaFast (Sigma).

CHAPTER V

ASSOCIATION OF MotB WITH THE *E. coli* CELL WALL

Introduction

To accomplish the function of the MotAB complex as the stator of the flagellar motor, MotB is proposed to bind to the bacterial cell wall. MotB also shares a predicted amphipathic α-helix that shows homology with similar helices in OmpA and Pal, two proteins know to bind to peptidoglycan. However, there has been no compelling experimental evidence presented that MotB binds to the peptidoglycan layer of *E. coli* or any other bacterium.

Here, we report preliminary results from work that addresses this issue. Suppressors of amber (UAG) mutations introduced into *motB* identified two residues within the proposed peptidoglycan domain that may be crucial for binding to the cell wall. Attempts to cross-link MotB to the cell wall have so far yielded promising but inconclusive results.

Results

Mutational analysis. The program PredictProtein[234], available at http://cubic.bioc.Columbia.edu, identified five α-helices in the periplasmic domain of MotB. These helices cover residues 52-65, 109 – 135, 170 - 185, 210 - 227, and 267 – 289. Amber mutations introduced into the sequences encoding these helices resulted in a non-motile phenotype when the mutated genes were expressed together with wild-type

MotA from the pHSG575-*motAB* plasmid in the Δ*motAB* strain MM5000 (data not shown). The most N-terminal amber mutation was at position 9 and the most C-terminal was at position 264. Truncated MotB fragments, detected by immunoblotting with MotB antiserum, were observed in many of the mutants but not when the amber codon was inserted before position 107, at codon 165, or between codons 178 and 265 (data not shown). None of the cells expressing these truncated MotB proteins were motile.

To simulate the MotB proteins that would arise by *supF* suppression analysis (Van Way et al., 2000),[34] the UAC Tyr codon was inserted at the same position as the UAG amber codons in the mutants to gauge the effect of a Tyr residue inserted with 100% efficiency at each position. Most Tyr substitutions resulted in relative chemotactic swarm diameters at least 50% as large as swarms formed by MM5000/p*motA*$^{+}$*B*$^{+}$, and all of the mutants, except L183Y, L225Y, and V264Y, which were present at decreased levels, produced normal amounts of full-length MotB (data not shown). Most of the mutants had normal swarming ability, except that swarm diameters were < 30% of the wild-type value for S25Y, L183Y, and L225Y, whereas the T196Y, A215Y, and A218Y mutants were completely non-motile (**Fig. 5.1** and data not shown). Thus, four mutants with normal levels of MotB were seriously impaired for motility, and the V264Y mutant, with reduced levels of MotB, still showed reasonably good (60% of wild type) swarming.

Suppression analysis of amber mutants. The plasmids containing the *motB* amber mutations were introduced into the Δ*motAB supE* strain MM5000E, which inserts Gln at UAG codons with 35% efficiency. MM5000E/p*motAB* had a swarm diameter of

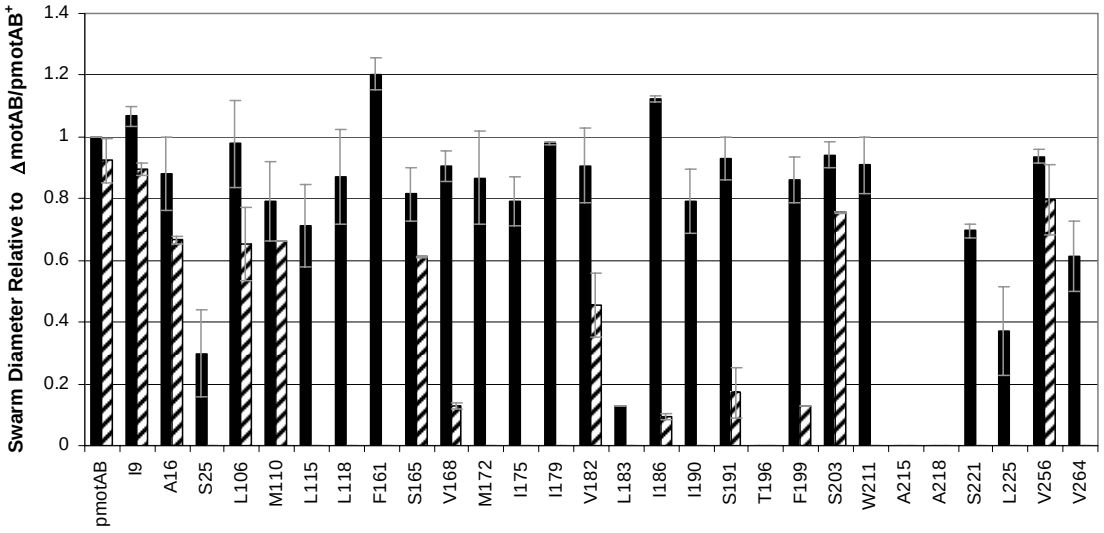

Figure 5.1. Motility of mutants in which selected residues within MotB were replaced with Tyr or amber mutations expressed in strain MM5000E (SupE). MotA and MotB mutant proteins were expressed in strain MM5000 (Δ*motAB*), and strains with amber mutations at the same positions were expressed in strain MM5000E (SupE). Swarm diameters are expressed relative to the diameter of swarms formed by the Δ*motAB* strain harboring wild-type p*motAB*. The swarm assay was carried out as described in Materials and Methods. Each bar in the histogram shows the mean diameter of ten swarms. Bars for Tyr mutants are black, and those for the amber mutations in the *supE* strain are hatched. Absence of a bar means that no swarming was observed.

92% relative to MM5000/p*motAB* and produced levels of MotB appropriate to its degree of motility (**Fig. 5.1** and data not shown). The $I9_{am}$, $A16_{am}$, $L106_{am}$, $M110_{am}$, $S165_{am}$, $S203_{am}$, and $V256_{am}$ plasmids supported good motility (over 50%) relative to MM5000/p*motAB* (**Fig. 5.1**) and produced levels of MotB appropriate to their motility (data not shown). The $V168_{am}$, $V182_{am}$, $I186_{am}$, $S191_{am}$, and $F199_{am}$ plasmids supported relative motilities below 50% of wild-type and produced levels of MotB proportional to their motility. The remaining amber mutations did not support any motility in the MM5000E strain (**Fig. 5.1**), and only $T196_{am}$, $W211_{am}$, $A215_{am}$, and $A218_{am}$ produced any full-length MotB, and even then at much reduced levels (data not shown).

Cross-linking of MotB to peptidoglycan. To obtain direct biochemical evidence for binding of MotB to the cell wall, a cross-linking approach with the reagents dithiobis(succinimidyl propionate) (DTSP) or dithiobis(sulfosuccinimidylpropionate) (DTSSP) was employed, using the procedure of Leduc[235] (see Materials and Methods). Briefly, DTSP or DTSSP, the latter of which is soluble in aqueous solution, was incubated with whole cells of strain MM5000 expressing p*motAB*. Murein sacculi were isolated by boiling the cells, followed by several rounds of centrifugation, and finally resuspension in SDS-marker dye, containing 2.8 M β-mercaptoethanol to reduce the cross-links. The samples were then run on SDS-PAGE gels. Immunoblots were probed with either MotB or OmpA antibody. This method had previously been used to demonstrate that OmpA cross-links to peptidoglycan.[153-157]

OmpA was visualized on immunoblots only when the cells had been incubated with DTSP or DTSSP. When MotAB was over-expressed in strain MM5000, a barely detectable band of MotB was seen in MM5000 when the cells were incubated with DTSSP. A smear of higher molecular-weight material stained with MotB antibody was also seen in lanes containing cross-linked samples, and both the band and smear were absent when the cross-linking reagent was not used.

Discussion

In a previous study (Van Way et al., 2000)[34], we found that an amber fragment containing the first 268 (of 308) residues of MotB still supported motility, whereas shorter fragments, including one ending at residue 261, did not. Here, we found that a MotB amber fragment of 264 residues also resulted in a non-motile phenotype. Thus, it appears that the predicted α-helix that extends from residues 267-289 of MotB does not play a crucial role in motility. However, the unstructured region immediately preceding it apparently is essential.

Another interesting helix is one extending from residues 109-135 as it is predicted to form a coiled-coil domain by the COILS prediction program available at http://www.ch.embnet.org/software/COILS_form.html.[236] Coiled-coil domains have been found to be sites of interaction between proteins[237,238] via hydrophobic residues from both domains interacting.[239] This domain may therefore serve as the point at which MotB dimers are formed and further mutational analysis is necessary if this is indeed the case.

The clearest results were obtained with mutagenesis of codons 210-227. The predicted α-helix formed by the residues encoded by this region is similar to known peptidoglycan-binding domains,[159] including the outer membrane proteins Pal[157,158] and OmpA.[153-157] (**Fig. 5.2**). Non-motile phenotypes were observed when Tyr was substituted for Ala-215 and Ala-218, and a large loss in motility was observed with the L225Y replacement (**Fig. 5.1**). A helical wheel diagram of this region shows that the conserved residues lie on one face of an α-helix (**Fig. 5.3**). We speculate that these residues may be on the peptidoglycan-binding face of the helix, and that introduction of the large Tyr residue within this region prevents proper binding. The residues that are conserved between MotB, Pal, and OmpA, fall on a different but overlapping face of the helix and include residues Ala-218 and Leu-225 (**Figs. 5.2 and 5.3**). The A215Y substitution, which alters a residue outside the conserved face of the helix, may disrupt another interaction, perhaps with the other peptidoglycan-binding domain of the MotB dimer.

We also attempted to determine biochemically whether MotB binds to peptidoglycan using cross-linking with the reagent DTSP or DTSSP. The results were inconclusive, for several possible reasons. One possibility is that very little MotB is actually bound to peptidoglycan when MotB is highly overexpressed. If MotB only binds to peptidoglycan when at a motor, then there would be only 80-168 MotB molecules bound to the cell wall per cell regardless of how much MotA and MotB is produced. For example, MotB might only recognize peptidoglycan that has been digested by the flagellum-specific peptidoglycan hydrolase, FlgJ, which is responsible for making a hole in peptidoglycan for the flagellar rod to pass through.[60,61]

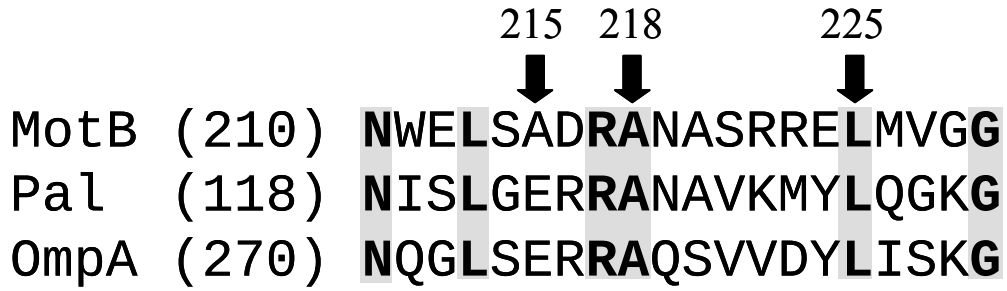

Figure 5.2. Sequence alignment of the predicted peptidoglycan-binding domains of MotB, Pal, and OmpA of *E. coli*. Pal and OmpA are known peptidoglycan-binding proteins. This region is the only one in which Pal, OmpA, and MotB show homology. The residues highlighted in gray are conserved among the three proteins. Residues Ala-215, Ala-218, and Leu-225 are labeled.

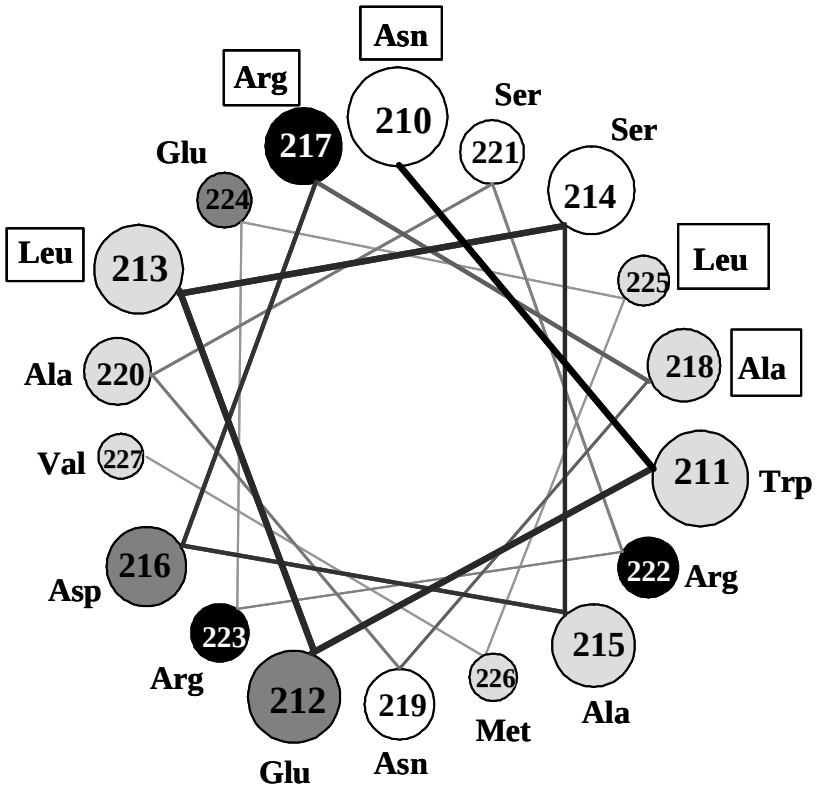

Figure 5.3. Helical-wheel projection of the predicted α-helix in the presumed peptidoglycan-binding domain extending from residues Asn-210 to Val-227 of MotB. Polar, uncharged residues are shown in white; nonpolar residues are shown in light gray; acidic residues are shown in dark gray; and basic residues are shown in black. Residues conserved in Pal, OmpA, and MotB are boxed.

A second possibility is that there is no primary amine (supplied only by the ε-amino group of a Lys residue) in the right position to be cross-linked to peptidoglycan by DTSP and DTSSP.[240] Both OmpA and Pal have a Lys residue in their peptidoglycan-binding domain at the position corresponding to Gly-228 of MotB. When the G228K replacement is made in MotB, motility remains normal. When we used this mutant form of MotB in the cross-linking experiment, in addition to a faint band at the normal position of MotB a high molecular weight smear that stained with MotB antibody was observed on the immunoblots in lanes loaded with samples treated with cross-linking reagent (data not shown). A large amount of residual peptidoglycan was observed in the sample wells during SDS-PAGE. It could be that this peptidoglycan impedes entry of MotB into the gel, so that instead of being confined to a tight band, MotB enters the gel matrix over an extended period of time, resulting in its migration as a smear. This problem might be avoided by treating the isolated peptidoglycan with an enzyme that digests the murein sacculus it into smaller pieces that will allow unrestricted migration of MotB into the gel.

Materials and Methods

Media. Routine media were prepared according to Miller[201]. Tryptone broth (TB) is 1 % (w/v) tryptone extract and 0.8 % (w/v) NaCl. Luria broth (LB) contains 1 % tryptone extract, 0.5 % (w/v) yeast extract. LB solid agar contains 1.5 % (w/v) Difco agar and TB swarm plates contain 0.325% (w/v) Difco agar. Liquid cultures and agar plates were incubated at 37 °C for LB or 30°C for TB. Media were supplemented with

chloramphenicol (Cm, 30 μg per ml) and 1 mM Isopropyl β-D-1-thiogalactopyranoside (IPTG) for induction of the *tac* promoter of p*HSG*, as needed.

Strains and plasmids. Strain MM5000 (Δ*motAB*)[120] is a derivative of RP437[202] containing an internal, non-polar deletion within *motA* and *motB* (J. S. Parkinson, personal communication). Strain RP3098 [*ΔflhA-flhD*] contains a deletion removing part of the *flhBAE* operon and all of the *meche, mocha*, and *flhDC* operons.[203] Construction of the supE (MM5000E) strain was described previously.[120] Construction of pHSG575-*motAB* was previously described by Van Way[120].

Site-directed mutagenesis. All mutations were introduced into pHSG575-*motAB* using the Quick-Change mutagenesis kit (Stratagene) according to the protocol supplied by the manufacturer. Mutagenized p*motAB* plasmids were transformed into MM5000. Transformants were selected on LB-Cm agar. Mutations were confirmed by dideoxynucleotide sequencing using the ABI Prism Dye-Terminator Cycle Sequencing Ready Kit with AmpliTaq DNA polymerase (PE Applied Biosystems).

Motility assay. The motility of each strain was assessed by inoculating colonies into TB swarm plates. Plates were incubated at 30°C for six to eight hours, and the diameter of each swarm was measured. Ten colonies of each strain were inoculated on one plate, and the swarming ability of a mutant was calculated as the ratio of the mean

diameter of the ten swarms to the diameter of the swarms formed by the appropriate control strain MM5000/p*motA*$^{+}$*B*$^{+}$.

Cross-linking of MotB. Cross-linking and isolation of peptidoglycan was performed according to the procedure of Leduc[235], with some modifications. Overnight cultures were grown in 5 ml TB+Cm, and then diluted 1:100 in 50 ml of TB+Cm. After 1 hour, 50 µl of 1 M IPTG was added and the cells were grown to an OD_{600} of .8. Whole cells were pelleted at 6000 rpm for 10 min. The pellet was resuspended in 1 ml of 50 mM sodium phosphate, pH 7.4, containing 20% sucrose. After 3 min. at room temperature, .125 ml of DTSP or DTSSP (80 mg/ml in DMSO) was added to the cells and incubated for 1 hr at room temperature. Cells were pelleted at 6000 rpm for 10 min. The cell pellet was suspended in 1 ml of 9% NaCl and mixed with 1 mL boiling 8% SDS for one hour at 100^{o}C. The cells were incubated overnight at 80^{o}C and then centrifuged for 30 min at 100,000 rpm in a Beckman TL100.4 rotor at 30^{o}C. The pelleted material was resuspended in 2 ml of water and washed by 4 cycles of resuspension and centrifugation. The final peptidoglycan pellet was resuspended in 40µl of SDS marker dye containing 2.8 M B-mercaptoethanol, boiled for 5 min. and run on SDS-PAGE gel.

SDS-PAGE and immunoblots. Whole cell extracts were taken at the completion of growth curves. A_{600} of .8 were collected by centrifugation, washed once in 1 ml TE and resuspended in 50 µl SDS loading buffer (2% (w/v) SDS, 5% (v/v) 2-mercaptoethanol, 8.5% (v/v) glycerol, 60 mM Tris (pH 6.8), 0.0004% (w/v) bromophenol

blue). Freeze-thaw extracts were prepared from these resuspended cells by three alternating cycles of five minutes at −80°C and five minutes of boiling prior to loading on gels for SDS-PAGE. Proteins were separated by 12% acrylamide SDS-PAGE and transferred to polyvinylidene difluoride membranes (PVDF). Anti-MotB[149] or anti-OmpA[157] was used to probe the immunoblots, and the cross-reacting protein was visualized with alkaline phosphatase-conjugated, goat anti-rabbit antibody (BioRad). The blot was developed using SigmaFast (Sigma).

CHAPTER VI

CONCLUSIONS

The flagellar motor of *E. coli* rotates both clockwise and counterclockwise to propel the bacterium in a three-dimensional random walk through its environment. The components and basic function of the motor are known. Central to function is the proton-conducting channel formed by the MotAB complex. The flow of protons down a transmembrane electrochemical gradient powers rotation of the flagellum.[98,140,241-244] An intact complex is made up of four MotA and two MotB subunits, and the actual proton channel is made up of the single transmembrane (TM) domain of MotB and TM3 and TM4 of MotA.[161,164]

The fact that MotB is stable only in a complex with MotA suggests that the $MotA_4B_2$ complex exists before incorporation into a motor. At high levels of MotAB expression, one would expect to see growth defects if these channels were always open and conducting protons. It has been speculated that the channel is originally occluded and opens only upon integration into the flagellar motor.[120] The same event could trigger the association of the peptidoglycan-binding domain of MotB with the cell wall. If this model holds, several conditions must be met: 1) MotA and MotB must assemble into a complex in the membrane before incorporation into a flagellar motor; 2) the channel must be blocked by some portion of MotA and/or MotB; 3) the block must be removed upon contact with the flagellar motor; 4) the MotAB complex must have a domain that

interacts with the motor to trigger opening of the channel; and 5) this event must be coupled with binding of the C-terminus of MotB to the cell wall.

The results reported in Chapter II describe the discovery and characterization of a region of MotB, formed by residues between Pro-52 and Pro-65, that serves as a plug for the proton channel. Deletion of this region results in the catastrophic growth defect one would expect if there is uncontrolled proton flow into the cell through overexpressed MotAB complexes. Expression, at wild-type levels, of MotB that contains a deletion of this region did not result in a growth defect or any disruption of motility in *Salmonella typhimurium*.[177] Overexpression of MotAB is thus required to see the phenotype. The effect is independent of the presence or absence of flagellar motors and is abolished by the D32N residue substitution in MotB, which eliminates proton flow through the channel.[166] It was concluded that the plug either blocks the channel or prevents its formation.

To confirm that the constitutively open proton channels resulted in uncontrolled proton flow into the cell, the internal pH of the cells was measured. There was a drop of 0.4 units in the internal pH of the cells when the plug was deleted, as well as a loss of intracellular K^+. The pH did not drop when the D32N mutation was introduced into the plugless mutant protein. It was striking that, under these conditions, the total proton motive force (pmf) was not compromised, because tethered cells expressing the MotB-deletion protein continued to spin at a normal speed long after growth had stopped. However, this may be due to the efflux of K^+. Although the ΔpH component of the pmf is apparently being depleted, due to the influx of H^+ into the cytoplasm, the efflux of K^+

may compensate for the depletion of ΔpH and increase ΔΨ to be able to maintain the pmf.

Based on further mutational analysis, it was proposed that, rather than interacting with MotA to block the channel, the predicted amphipathic helix of the plug lies parallel to the membrane at the hydrophobic/polar interface on the periplasmic side of the cell membrane. This interaction is exquisitely sensitive to the identity of certain hydrophobic residues, including Leu-58, Tyr-61, and, especially, Phe-62. Cysteine-crosslinking experiments show that, upon removal of the plug from the membrane, the hydrophobic faces of the two plug helices interact with one another to keep the channel open.

To further test this model, one may first need to confirm that this region exists as a helix. This could be accomplished by subjecting MotB to circular dichroism to characterize its secondary and tertiary structure. The major aspect of our model is that this predicted helix forms a “plug”, lies within the membrane, and not a “lid”, lies above the membrane, to block proton flow. To test this hypothesis, one could use labeling of the cysteine mutants that were created during this study, combining them each with the Y61F mutation. The Y61F mutation is believed to keep the helix buried in the membrane since it results in a non-motile phenotype. Utilizing this set of double mutants, and membrane-impermeable sulfhydryl reagents, the location of this region with respect to the membrane could be tested. This method is convenient as MotB does not contain any native Cys residues. Sulfhydryl reagents are available that contain either a biotin group, a fluorescent group or a radiolabel, allowing detection of labeled proteins by streptavidin binding, fluorescence, or autoradiography, respectively. Only those cysteines that are

accessible in the periplasm would be labeled. Another possibility is to pre-treat the cells with a membrane impermeable reagent and then with a membrane-permeable reagent and assay for the detectable groups of both reagents to determine which reagent labeled the cysteine to determine location in or out of the membrane. However, since this method would label all accessible cysteines present in the cell, it most likely would need to be performed in membrane vesicles or to use a reagent that would cause a size shift of MotB when run on SDS-PAGE and probed with MotB antibody.

It is not known what triggers the removal of the plug from the membrane. The interaction between the charged residues in the cytoplasmic loop of MotA with oppositely charged residues of FliG[109] suggested itself as a possibility. However, substitutions of these charged residues did not affect the flow of protons through the channel as would be expected if they served their hypothesized roles. Thus, the mechanism of what opens the proton channel remains a mystery.

The instability of MotB in the absence of MotA[173] suggested to us that the two proteins might interact very quickly after their translation and perhaps even co-assemble into the membrane. Translational coupling of the *motA* and *motB* genes might facilitate such a process. Sequence alignments of MotA and MotB from a number of bacteria identified a cluster of conserved positive charges at the N-terminus of MotB and clusters of negative charges at the C-terminus of MotA. We hypothesized that interaction of these charges, during or shortly after translation, stabilizes MotB due to its interaction with MotA. If these charge interactions are important, then removal of these charges should destabilize MotB. However, when mutations that remove these charges in MotA

and/or MotB were introduced, no difference in intercellular MotB levels was observed (Chapter III).

These results do not support the idea that MotA and MotB associate prior to insertion into the membrane, or at least not by electrostatic interactions between charged residues at the C-terminus of MotA and the N-terminus of MotB. However, removal of these charged residues did, in some cases, decrease or even eliminate motility. Suppressors that increase the motility of strains bearing the charge-change mutations were found (Chapter III), suggesting that charged residues may be involved in aligning MotA and MotB to form a functional complex. Nevertheless, the mode of MotB stabilization by MotA remains elusive.

The stop codon of *motA* and the start codon of *motB* form the sequence AUGA, the same overlap found in *nifL* and *nifA* of *Klebsiella pneumoniae*,[210] another pair of translationally coupled genes. In a coupled situation, translation of the upstream gene affects translation of the downstream gene in a predictable manner.[211,212] When MotB is expressed in *trans* with MotA, MotB levels are lower than when expression is in *cis*.[120] However, it remained unclear whether the decreased levels of MotB are due to relative contributions of decreased translation or faster turnover. The work described in Chapter IV shows that translation of MotA does influence the translation of MotB and that it is not degradation *per se* that leads to decreased MotB levels when it is expressed in *trans*.

Coupled translation of *motB* is not simply due to the opening of secondary structure around the *motB* translation start by ribosomes reading *motA*; it involves reinitiation by ribosomes that have just completed translating *motA*. The same

conclusion was drawn from the study of the translationally coupled *nifL* and *nifA*,[210] the coat and lysis genes of the phages MS2 and fr,[213,215] and the RNA phage GA coat and lysis genes.[216] A fair amount of MotB can be made *de novo* from the ribosome-binding site associated with *motB*, but this mode of translation is limited when *motB* is expressed in *cis*, perhaps due to competition with ribosomes translating *motA*. Thus, reinitiation is normally the major contributor to MotB production, with a minor contribution from *de novo* translation. This results in a translation ratio of 1.5:1 for MotA relative to MotB. To get to the final ratio of 2:1, some MotB, most likely not associated with MotA, must be degraded. As discussed above, it is still not known whether MotA and MotB associate prior to or after insertion into the membrane, nor is it known whether insertion is carried out autonomously, via the Sec pathway, or by some other mechanism.

At some point, MotB must bind to peptidoglycan, and MotB contains a sequence motif that has homology with known peptidoglycan binding proteins.[159] Since the MotAB proton channel provides the resistance against with which the spinning rotor must push, the association of MotB with the cell wall must be robust to allow for the development of high torque. An approach using a reversible cross-linker was utilized to attempt to demonstrate directly an interaction between MotB and the murein sacculus, the exoskeleton of the cell that remains after all of its less durable components have been solubilized (Chapter V). Sacculi were isolated, and the control protein OmpA, known to bind peptidoglycan, was identified in abundance by immunoblotting proteins released from the isolated cell wall. However, thus far results have been inconclusive with respect to MotB; a very faint band was seen after immunoblotting with MotB antibody, but it

was too marginal to be able to draw a conclusion either way. There was also a smear down the length of the lanes that were probed with MotB antibody that was absent in sacculi from cell that had not been treated with cross-linker.

These preliminary results are encouraging, but the procedure will need to be optimized. The smear is quite possibly MotB that is hindered from entering the SDS-PAGE gel because of the thick suspension of peptidoglycan in the samples. One possibility would be to degrade the peptidoglycan enzymatically after its isolation to reduce viscosity and allow MotB to enter the gel more efficiently. It is also possible that the band represents the amount of MotB that is actually present. If MotB only interacts with peptidoglycan when the complex is in contact with the motors, then there would be only about 100 or so MotB molecules (22 per motor) interacting with peptidoglycan per cell.[18,20,21] Assuming that cross-linking is not 100% efficient, the actual number per sacculus could be even lower. One remedy of this difficulty would be to use an N-terminal fusion of the periplasmic domain of MotB to a periplasmic protein, like PhoA. It may also be useful to repeat the experiment with the plugless version of MotB D32N. The notion here is that channel opening may be correlated with exposure of the peptidoglycan binding domain of MotB. The D32N substitution will allow the unplugged MotAB complex to be highly overexpressed, which should facilitate the detection of MotB.

Ultimately, it is also important to show when MotB binds to peptidoglycan. GFP-tagged MotB has been found to move within the membrane into position around the motor.[20] This result supports a model in which MotB is not always bound to

peptidoglycan. The central question is what connection exists between MotB binding to peptidoglycan and MotAB channel activation. Does binding of MotB to peptidoglycan "pull the plug" from the membrane, or does opening the channel expose the peptidoglycan-binding domain? Of course, a third possibility is that the two events are independent.

The work presented here provides a variety of new information about the function of the MotAB protein complex. However, much information is still needed. Research in other laboratories continues to address these questions, and I look forward to continuing to investigate how this proton channel functions. Aside from its intrinsic interest, discoveries made with this simple but elegant system may contribute to our understanding of many other channels and membrane-protein complexes, perhaps in ways too convoluted to imagine now. At least, that is my hope.

REFERENCES

1. Trachtenberg, S., & DeRosier, D. J. (1987). Three-dimensional structure of the frozen-hydrated flagellar filament: The left-handed filament of *Salmonella typhimurium*. *J. Mol. Biol*. **195**, 581-601.

2. Mimori, Y., Yamashita, I., Murata, K., Fujiyoshi, Y., Yonekura, K., Toyoshima, C., & Namba, K. (1995). The structure of the R-type straight flagellar filament of *Salmonella* at 9 A resolution by electron cryomicroscopy. *J. Mol. Biol*. **249**, 69-87.

3. Calladine, C. R. (1978). Change of waveform in bacterial flagella: The role of mechanics at the molecular level. *J. Mol. Biol*. **118**, 457-479.

4. Trachtenberg, S., & DeRosier, D. J. (1991). A molecular switch: Subunit rotations involved in the right-handed to left-handed transitions of *Salmonella typhimurium* flagellar filaments. *J. Mol. Biol*. **220**, 67-77.

5. Kamiya, R., & Asakura, S. (1977). Flagellar transformations at alkaline pH. *J. Mol. Biol*. **108**, 513-518.

6. Macnab, R. M. & Ornston, M. K. (1977). Normal-to-curly flagellar transitions and their role in bacterial tumbling: Stabilization of an alternative quaternary structure by mechanical force. *J. Mol. Biol*. **112**, 1-30.

7. Kanto, S., Okino, H., Aizawa, S.-I., & Yamaguchi, S. (1991). Amino acids responsible for flagellar shape are distributed in terminal regions of flagellin. *J. Mol. Biol*. **219**, 471-480.

8. Samatey, F. A., Imada, K., Nagashima, S., Vonderviszt, F., Kumasaka, T., Yamamoto, M., & Namba, K. (2001). Structure of the bacterial flagellar protofilament and implications for a switch for supercoiling. *Nature* **410**, 331-337.

9. DePamphilis, M. L. & Adler, J. (1971). Fine structure and isolation of the hook-basal body complex of flagella from *Escherichia coli* and *Bacillus subtilis*. *J. Bacteriol*. **105**, 384-395.

10. Berg, H. C. (1974). Dynamic properties of bacterial flagellar motors. *Nature* **249**, 77-79.

11. Stallmeyer, M. J. B., Aizawa, S.-I., Macnab, R. M., & DeRosier, D. J. (1989). Image reconstruction of the flagellar basal body of *Salmonella typhimurium*. *J. Mol. Biol*. **205**, 519-528.

12. Schoenhals, G. J. & Macnab, R. M. (1996). Physiological and biochemical analyses of FlgH, a lipoprotein forming the outer membrane L ring of the flagellar basal body of *Salmonella typhimurium*. *J. Bacteriol*. **178**, 4200-4207.

13. Khan, I. H., Reese, T. S., & Khan, S. (1992). The cytoplasmic component of the bacterial flagellar motor. *Proc. Natl. Acad. Sci.* USA **89**, 5956-5960.

14. Francis, N. R., Sosinsky, G. E. Thomas D., & DeRosier, D. J. (1994). Isolation, characterization and structure of bacterial flagellar motors containing the switch complex. *J. Mol. Biol*. **235**, 1261-1270.

15. Kojima, S. & Blair, D. F. (2004). The bacterial flagellar motor: Structure and function of a complex molecular machine. *Int. Rev. Cytol*. **233**, 93-134.

16. Thomas, D. R., Morgan, D. G., & DeRosier, D. J. (1999). Rotational symmetry of the C ring and mechanism for the flagellar rotary motor. *Proc. Natl. Acad. Sci.* USA **96**, 10134-10139.

17. Thomas, D., Morgan, D. G., & DeRosier, D. J. (2001). Structures of bacterial flagellar motors from two FliF-FliG gene fusion mutants. *J. Bacteriol*. **183**, 6404-6412.

18. Khan, S., Dapice, M., & Reese, T. (1988). Effects of *mot* gene expression on the structure of the flagellar motor. *J. Mol. Biol*. **202**, 575-584.

19. Coulton, J. W. & Murray, R. G. E. (1978). Cell envelope associations of *Aquaspirillum serpens* flagella. *J. Bacteriol*. **136**, 1037-1049.

20. Leake, M. C., Chandler, J. H., Wadhams, G. H., Bai, F., Berry, R. M., & Armitage, J. P. (2006). Stoichiometry and turnover in single, functioning membrane protein complexes. *Nature* **443**, 355-358.

21. Reid, S. W., Leake, M. C., Chandler, J. H., Lo, C-J., Armitage, J. P., & Berry, R. M. (2006). The maximum number of torque-generating units in the flagellar motor of *Escherichia coli* is at least 11. *Proc. Natl. Acad. Sci.* USA **103**, 8066-8071.

22. Komeda, Y. (1982). Fusions of flagellar operons to lactose genes on a Mu *lac* bacteriophage. *J. Bacteriol*. **150**, 16-26.

23. Kutsukake, K., Ohya, Y., & Iino, T. (1990). Transcriptional analysis of the flagellar regulon of *Salmonella typhimurium*. *J. Bacteriol*. **172**, 741-747.

24. Liu, X. & Matsumura, P. (1994). The FlhD/FlhC complex, a transcriptional activator of the *Escherichia coli* flagellar class II operons. *J. Bacteriol*. **176**, 7345-7351.

25. Nishimura, A. & Hirota, Y. (1989). A cell division regulatory mechanism controls the flagellar regulon in *Escherichia coli*. *Mol. Gen. Genet*. **216**, 340-346.

26. Pruss, B. M. & Matsumura, P. (1996). A regulator of the flagellar regulon of *Escherichia coli*, *flhD*, also affects cell division. *J. Bacteriol*. **178**, 668-674.

27. Pruss, B. M. & Matsumura, P. (1997). Cell cycle regulation of flagellar genes. *J. Bacteriol*. **179**, 5602-5604.

28. Qualding, C. & Stocker, B. A. D. (1962). An environmentally induced transition from the flagellated to the non-flagellated state in *Salmonella typhimurium*: The fate of parental flagella at cell division. *J. Gen. Microbiol*. **28**, 257-270.

29. Adler, J. & Templeton, B. (1967). The effect of environmental conditions on the motility of *Escherichia coli*. *J. Gen. Microbiol*. **46**, 175-184.

30. Silverman, M. & Simon, M. (1974). Characterization of *Escherichia coli* flagellar mutants that are insensitive to catabolite repression. *J. Bacteriol*. **120**, 1196-1203.

31. Pruss, B. M. & Wolfe, A. J. (1994). Regulation of acetyl phosphate synthesis and degradation, and the control of flagellar expression in *Escherichia coli*. *Mol. Microbiol*. **12**, 973-984.

32. Li, C., Louise, C. J., Shi, W., & Adler, J. (1993). Adverse conditions which cause lack of flagella in *Escherichia coli*. *J. Bacteriol*. **175**, 2229-2235.

33. Shi, W., Li, C., Louise, C. J., & Adler, J. (1993). Mechanism of adverse conditions causing lack of flagella in *Escherichia coli*. *J. Bacteriol*. **175**, 2236-2240.

34. Yokota, T. & Gots, J. S. (1970). Requirement of adenosine 3',5'-cyclic phosphate for flagellum formation in *Escherichia coli* and *Salmonella typhimurium*. *J. Bacteriol.* **103**, 513-516.

35. Kutsukake, K. (1997). Autogenous and global control of the flagellar master operon *flhD*, in *Salmonella typhimurium*. *Mol. Gen. Genet*. **254**, 440-448.

36. Ohnishi, K., Kutsukake, K., Suzuki, H., & Iino, T. (1990). Gene *fliA* encodes an alternative sigma factor specific for flagellar operons in *Salmonella typhimurium*. *Mol. Gen. Genet*. **221**, 139-147.

37. Hughes, K. T., Gillen, K. L., Semon, M. J., & Karlinsey, J. E. (1993). Sensing structural intermediates in bacterial flagellar assembly by export of a negative regulator. *Science* **262**, 1277-1280.

38. Kutsukake, K. (1994). Excretion of the anti-sigma factor through a flagellar structure couples flagellar gene expression with flagellar assembly in *Salmonella typhimurium*. *Mol. Gen. Genet*. **243**, 605-612.

39. Liu, X. & Matsumura, P. (1995). An alternative sigma factor controls transcription of flagellar class-III operons in *Escherichia coli*: Gene sequence, overproduction, purification and characterization. *Gene* **164**, 81-84.

40. Karlinsey, J. E., Shugo Tanaka, S., Bettenworth, V., Yamaguchi, S., Boos, W., Aizawa, S.-I., & Hughes, K. T. (2000). Completion of the hook-basal body of the *Salmonella typhimurium* flagellum is coupled to FlgM secretion and *fliC* transcription. *Mol. Microbiol*. **37**, 1220-1231.

41. Homma, M., Fujita, H., Yamaguchi, S., & Iino, T. (1984). Excretion of unassembled flagellin by *Salmonella typhimurium* mutants deficient in hook-associated proteins. *J. Bacteriol*. **159**, 1056-1059.

42. Suzuki, T., Iino, T., Horiguchi, T., & Yamaguchi, S. (1978). Incomplete flagellar structures in nonflagellate mutants of *Salmonella typhimurium*. *J. Bacteriol*. **133**, 904-915.

43. Suzuki, T. & Komeda, Y. (1981). Incomplete flagellar structures in *Escherichia coli* mutants. *J. Bacteriol*. **145**, 1036-1041.

44. Iino, T. (1985). Genetic control of flagellar morphogenesis in *Salmonella*. *In* "Sensing and Response in Microorganisms" (M. Eisenbach and M. Balaban, Eds.), pp. 83-92. Elsevier, New York.

45. Jones, C. J. & Macnab, R. M. (1990). Flagellar assembly in *Salmonella typhimurium*: Analysis with temperature-sensitive mutants. *J. Bacteriol*. **172**, 1327-1339.

46. Kubori, T., Shimamoto, N., Yamaguchi, S., Namba, K., & Aizawa, S.-I. (1992). Morphological pathway of flagellar assembly in *Salmonella typhimurium*. *J. Mol. Biol*. **226**, 433-446.

47. Macnab, R. M. (2003). How bacteria assemble flagella. *Annu. Rev. Microbiol*. **57**, 77-100.

48. Ueno, T., Oosawa, K., & Aizawa, S.-I. (1992). M ring, S ring, and proximal rod of the flagellar basal body of *Salmonella typhimurium* are composed of subunits of a single protein, FliF. *J. Mol. Biol*. **227**, 672-677.

49. Lux, R., Kar, N., & Khan, S. (2000). Overproduced *Salmonella typhimurium* flagellar motor switch complexes. *J. Mol. Biol*. **298**, 577-583.

50. Young, H. S., Dang, H., Lai, Y., DeRosier, D. J., & Khan, S. (2003). Variable symmetry in *Salmonella typhimurium* flagellar motors. *Biophys. J*. **84**, 571-577.

51. Morgan, D. G., Macnab, R. M., Francis, N. R., & DeRosier, D. J. (1993). Domain organization of the subunit of the *Salmonella typhimurium* flagellar hook. *J. Mol. Biol*. **229**, 79-84.

52. Morgan, D. G., Owen, C., Melanson, L. A., & DeRosier, D. J. (1995). Structure of bacterial flagellar filaments at 11 A resolution: Packing of the α-helices. *J. Mol. Biol*. **249**, 66-110.

53. Aizawa, S.-I. (2000). Flagella. In *Encyclopedia of Microbiology*, 2nd Ed. Academic Press, San Diego, CA, pp.380-389.

54. Kubori, T., Matsushima, Y., Nakamura, D., Uralil, J., Lara-Tejero, M., Sukhan, A., Galan, J. E., & Aizawa, S.-I. (1998). Supramolecular structure of the *Salmonella typhimurium* type III protein secretion system. *Science* **280**, 602-605.

55. Macnab, R. M. (1999). The bacterial flagellum: Reversible rotary propeller and type III export apparatus. *J. Bacteriol*. **181**, 7149-7153.

56. Bennett, J. C. Q. & Hughes, C. (2000). From flagellum assembly to virulence: The extended family of type III export chaperones. *Trends Microbiol*. **8**, 2020-204.

57. Yamaguchi, S., Aizawa, S.-I., Kihara, M., Isomura, M., Jones, C. J., & Macnab, R. M. (1986). Genetic evidence for a switching and energy-transducing complex in the flagellar motor of *Salmonella typhimurium*. *J. Bacteriol*. **168**, 1172-1179.

58. Homma, M., Kutsukake, K., Hasebe, M., Iino, T., & Macnab, R. M. (1990). FlgB, FlgC, FlgF and FlgG: A family of structurally related proteins in the flagellar basal body of *Salmonella typhimurium*. *J. Mol. Biol*. **211**, 465-477.

59. Minamino, T., Yamaguchi, S., & Macnab, R. M. (2000). Interaction between FliE and FlgB, a proximal rod component of the flagellar basal body of *Salmonella*. *J. Bacteriol*. **182**, 3029-3036.

60. Nambu, T., Minamino, T., Macnab, R. M., & Kutsukake, K. (1999). Peptidoglycan-hydrolyzing activity of the FlgJ protein, essential for flagellar rod formation in *Salmonella typhimurium*. *J. Bacteriol*. **181**, 1555-1561.

61. Hirano, T., Minamino, T. & Macnab, R. M. (2001). The role in flagellar rod assembly N-terminal domain of *Salmonella* FlgJ, a flagellum-specific muramidase. *J. Mol. Biol*. **312**, 359-369.

62. Jones, C. J., Homma, M. & Macnab, R. M. (1989). L-, P-, and M-ring proteins of the flagellar basal body of *Salmonella typhimurium*: Gene sequences and deduced protein sequences. *J. Bacteriol*. **171**, 3890-3900.

63. Homma, M., Komeda, Y., Iino, T. & Macnab, R. M. (1987). The *flaFIX* gene product *Salmonella typhimurium* is a flagellar basal body component with a signal peptide for export. *J. Bacteriol*. **169**, 1493-1498.

64. Jones, C. J., Macnab, R. M., Okino, H. & Aizawa, S.-I. (1990). Stoichiometric analysis of the flagellar hook-(basal body) complex of *Salmonella typhimurium*. *J. Mol. Biol*. **212**, 377-387.

65. Nambu, T. & Kutsukake, K. (2000). The *Salmonella* FlgA protein, a putative periplasmic chaperone essential for flagellar P ring formation. *Microbiology* **146**, 1171-1178.

66. Dailey, F. E. & Berg, H. C. (1993). Mutants in disulfide bond formation that disrupt flagellar assembly in *Escherichia coli*. *Proc. Natl. Acad. Sci.* USA **90**, 1043-1047.

67. Ohnishi, K. Ohto, Y. Aizawa, S.-I., Macnab, R. M. & Iino, T. (1994). FlgD is a scaffolding protein needed for flagellar hook assembly in *Salmonella typhimurium*. *J. Bacteriol*. **176**, 2272-2281.

68. Hirano, T., Yamaguchi, S., Oosawa, K., & Aizawa, S.-I. (1994). Roles of FliK and FlhB in determination of flagellar hook length in *Salmonella typhimurium*. *J. Bacteriol*. **176**, 5439-5449.

69. Ikeda, T., Homma, M. Iino, T., Asakura, S., & Kamiya, R. (1987). Localization and stoichiometry of hook-associated proteins within *Salmonella typhimurium* flagella. *J. Bacteriol*. **169**, 1168-1173.

70. Yoseki, T., Kutsukake, K., Ohnishi, K., & Iino, T. (1995). Functional analysis of the flagellar genes in the *fliD* operon of *Salmonella typhimurium*. *Microbiology* **141**, 1715-1722.

71. Fraser, G. M., Bennett, J. C. Q., & Hughes, C. (1999). Substrate-specific binding of hook-associated proteins by FlgN and FliT, putative chaperones for flagellum assembly. *Mol. Microbiol*. **32**, 569-580.

72. Bennett, J. C. Q. & Hughes, C. (2001). Substrate complexes and domain organization of the *Salmonella* flagellar export chaperones FlgN and FliT. *Mol. Microbiol*. **39**, 781-791.

73. Iino, T. (1969). Polarity of flagellar growth in *Salmonella*. *J. Gen. Microbiol*. **56**, 227-239.

74. Emerson, S. U., Tokuyasu, K., & Simon, M. I. (1970). Bacterial flagella: Polarity of elongation. *Science* **169**, 190-192.

75. Block, S. M. & Berg, H. C. (1984). Successive incorporation of force-generating units in the bacterial rotary motor. *Nature* **309**, 470-472.

76. Blair, D. F. & Berg, H. C. (1988). Restoration of torque in defective flagellar motors. *Science*, **242**, 1678-1681.

77. Minamino, T. & Macnab, R. M. (1999). Components of the *Salmonella* flagellar export apparatus and classification of export substrates. *J. Bacteriol*. **181**, 1388-1394.

78. Kihara, M., Minamino, T., Yamaguchi, S., & Macnab, R. M. (2001). Intergenic suppression between the flagellar MS ring protein FliF of *Salmonella* and FlhA, a membrane component of its export apparatus. *J. Bacteriol*. **183**, 1655-1662.

79. Nolling, J., Breton, G., Omelchenko, M. V., Makarova, K. S., Zeng, Q., Gibson, R., Lee, H. M., Dubois, J., Qiu, D., Hitti, J., Wolf, Y. I., Tatusov, R. L., Sabathe, F., Doucette-Stamm, L., Soucaille, P., Daly, M. J., Bennett, G. N., Koonin, E. V., & Smith, D. R. (2001). Genome sequence and comparative analysis of the solvent-producing bacterium *Clostridium acetobutylicum*. *J. Bacteriol*. **16**, 4823-4838.

80. Fan, F., & Macnab, R. M. (1996). Enzymatic characterization of FliI: An ATPase involved in flagellar assembly in *Salmonella typhimurium*. *J. Biol. Chem*. **271**, 31981-31988.

81. Vogler, A. P., Homma, M., Irikura, V. M., & Macnab, R. M. (1991). *Salmonella typhimurium* mutants defective in flagellar filament regrowth and sequence similarity of FliI to F_0F_1, vacuolar, and archaebacterial ATPase subunits. *J. Mol. Biol*. **173**, 3564-3572.

82. Minamino, T. & Macnab, R. M. (2000). FliH, a soluble component of the type III flagellar export apparatus of *Salmonella*, forms a complex with FliI and inhibits its ATPase activity. *Mol. Microbiol*. **37**, 1494-1503.

83. Auvray, F., Ozin, A. J., Claret, L., & Hughes, C. (2002). Intrinsic membrane targeting of the flagellar export ATPase FliI: Interaction with acidic phospholipids and FliH. *J. Mol. Biol*. **318**, 941-950.

84. Gonzalez-Pedrajo, B., Fraser, G. M., Minamino, T., & Macnab, R. M. (2002). Molecular dissection of *Salmonella* FliH, a regulator of the ATPase FliI and the type III flagellar protein export pathway. *Mol. Microbiol*. **45**, 967-982.

85. Minamino T., Chu, R., Yamaguchi, S., & Macnab, R. M. (2000). Role of FliJ in flagellar export in *Salmonella*. *J. Bacteriol*. **182**, 4207-4215.

86. Minamino, T., Doi, H., & Kutsukake, K. (1999). Substrate specificity switching of the flagellum-specific export apparatus during flagellar morphogenesis in *Salmonella typhimurium*. *Biosci. Biotechnol. Biochem*. **63**, 1301-1303.

87. Minamino, T. & Macnab, R. M. (2000). Domain structure of FlhB, a flagellar export component responsible for substrate-specificity switching. *J. Bacteriol*. **182**, 4906-4914.

88. Silverman, M. R. & Simon, M. I. (1972). Flagellar assembly mutants in *Escherichia coli*. *J. Bacteriol*. **112**, 986-993.

89. Patterson-Delafield, J., Martinez, R. J., Stocker, B. A. D., & Yamaguchi, S. (1973). A new *fla* gene in *Salmonella typhimurium-flaR*-and its mutant phenotype-superhooks. *Arch. Mikrobiol*. **90**, 107-120.

90. Muramoto, K., Makashima, S., Aizawa., S.-I., & Macnab, R. M. (1998). Effect of cellular level of FliK on flagellar hook and filament assembly in *Salmonella typhimurium. J. Mol. Biol*. **277**, 871-882.

91. Minamino, T., Gonzalez-Pedrajo, B., Yamaguchi, K., Aizawa, S.-I., & Macnab, R. M. (1999). FliK, the protein responsible for flagellar hook length control in *Salmonella*, is exported during hook assembly. *Mol. Microbiol*. **34**, 295-304.

92. Kutsukake, K., Minamino, T., & Yokoseki, T. (1994). Isolation and characterization of FliK-independent flagellation mutants from *Salmonella typhimurium*. *J. Bacteriol*. **176**, 7625-7629.

93. Williams, A. W., Yamaguchi, S., Togashi, F., Aizawa, S.-I., & Macnab, R. M. (1996). Mutations in *fliK* and *flhB* affecting flagellar hook and filament assembly in *Salmonella typhimurium*. *J. Bacteriol*. **178**, 2960-2970.

94. Macnab, R. M. (1992). Genetics and Biogenesis of bacterial flagella. *Annu. Rev. Genet*. **26**, 129-156.

95. Dean, G. E., Macnab, R. M., Stader, J., Matsumura, P., & Burke, C. (1984). Gene sequence and predicted amino acid sequence of the MotA protein, a membrane-associated protein required for flagellar rotation in *Escherichia coli*. *J. Bacteriol*. **159**, 991-999.

96. Stader, J., Matsumura, P., Vacante, D., Dean, G. E., & Macnab, R. M. (1986). Nucleotide sequence of the *Escherichia coli motB* gene and site-limited incorporation of its product into the cytoplasmic membrane. *J. Bacteriol*. **166**, 244-252.

97. Chun, S. Y. & Parkinson, J. S. (1988). Bacterial motility: Membrane topology of the *Escherichia coli* MotB protein. *Science* **239**, 276-278.

98. Blair, D. F. & Berg, H. C. (1990). The MotA protein of *E. coli* is a proton-conducting component of the flagellar motor. *Cell* **60**, 439-449.

99. Stolz, B. & Berg, H. C. (1991). Evidence for interactions between MotA and MotB, torque-generating elements of the flagellar motor of *Escherichia coli*. *J. Bacteriol*. **173**, 7033-7037.

100. Yamaguchi, S., Fujita, H., Ishihara, A., Aizawa, S.-I., & Macnab, R. M. (1986). Subdivision of flagellar genes of *Salmonella typhimurium* into regions responsible for assembly, rotation, and switching. *J. Bacteriol*. **166**, 187-193.

101. Zhao, R., Pathak, N., Jaffe, H., Reese, T. S., & Khan, S. (1996). FliN is a major structural protein of the C-ring in the *Salmonella typhimurium* flagellar basal body. *J. Mol. Biol*. **261**, 195-208.

102. Sockett, H., Yamaguchi, S., Kihara, M., Irikura, V. M., & Macnab, R. M. (1992). Molecular analysis of the flagellar switch protein FliM of *Salmonella typhimurium*. *J. Bacteriol*. **174**, 793-806.

103. Welch, M., Oosawa, K., Aizawa, S.-I., & Eisenbach, M. (1993). Phosphorylation-dependent binding of a signal molecule to the flagellar switch of bacteria. *Proc. Natl. Acad. Sci.* USA **90**, 8787-8791.

104. Toker, A. S. & Macnab, R. M. (1997). Distinct regions of bacterial flagellar switch protein FliM interact with FliG, FliN and CheY. *J. Mol. Biol*. **273**, 623-634.

105. Bren, A. & Eisenbach, M. (1998). The N terminus of the flagellar switch protein, FliM, is the binding domain for the chemotactic response regulator, CheY. *J. Mol. Biol*. **278**, 507-514.

106. Mathews, M. A. A., Tang, H. L., & Blair, D. F. (1998). Domain analysis of the FliM protein of *Escherichia coli*. *J. Bacteriol*. **180**, 5580-5590.

107. Irikura, V. M., Kihara, M., Yamaguchi, S., Sockett, H., & Macnab, R. M. (1993). *Salmonella typhimurium fliG* and *fliN* mutations causing defects in assembly, rotation, and switching of the flagellar motor. *J. Bacteriol*. **175**, 802-810.

108. Lloyd, S. A., Tang, H., Wang, X., Billings, S., & Blair, D. F. (1996). Torque generation in the flagellar motor of *Escherichia coli*: Evidence of a direct role for FliG but not for FliM or FliN. *J. Bacteriol*. **178**, 223-231.

109. Zhou, J., Lloyd, S. A., & Blair, D. F. (1998). Electrostatic interactions between rotor and stator in the bacterial flagellar motor. *Proc. Natl. Acad. Sci*. USA **95**, 6436-6441.

110. Oosawa, K., Ueno, T., & Aizawa, S.-I. (1994). Overproduction of the bacterial flagellar switch proteins and their interactions with the MS ring complex in vitro. *J. Bacteriol*. **176**, 3683-3691.

111. Brown, P. N., Mathews, M. A., Joss, L. A., Hill, C. P., & Blair, D. F. (2005). Crystal structure of the flagellar rotor protein FliN from *Thermotoga maritima*. *J. Bacteriol*. **187**, 2890-2902.

112. Brown, P. N., Hill, C. P., & Blair, D. F. (2002). Crystal structure of the middle and C-terminal domains of the flagellar rotor protein FliG. *EMBO J.* **13**, 3225-3234.

113. Sosinsky, G. E., Francis, N. R., DeRosier, D. J., Wall, J. S., Simon, M. N., & Hainfeld, J. (1992). Mass determination and estimation of subunit stoichiometry of the bacterial hook-basal body flagellar complex of *Salmonella typhimurium* by scanning transmission electron microscopy. *Proc. Natl. Acad. Sci.* USA **89**, 4801-4805.

114. Francis, N. R., Irikura, V. M., Yamaguchi, S., DeRosier, D.J., & Macnab, R. M. (1992). Localization of the *Salmonella typhimurium* flagellar switch protein fliG to the cytoplasmic M-ring face of the basal body. *Proc. Natl. Acad. Sci.* USA **89**, 6304-6308.

115. Marykwas, D. L. & Berg, H. C. (1996). A mutational analysis of the interaction between FliG and FliM, two components of the flagellar motor of *Escherichia coli*. *J. Bacteriol*. **178**, 1289-1294.

116. Tang, H., Braun, T. F., & Blair, D. F. (1996). Motility protein complexes in the bacterial flagellar motor. *J. Mol. Biol*. **261**, 209-221.

117. Thomas, D. R., Francis, N. R., Xu, C., & DeRosier, D. J. (2006). The three-dimensional structure of the flagellar rotor from a clockwise-locked mutant of *Salmonella enterica* serovar *Typhimurium*. *J. Bacteriol*. **188**, 7039-7048.

118. Brown, P. N., Terrazas, M., Paul, K., & Blair, D. F. (2007). Mutational analysis of the flagellar protein FliG: Sites of interaction with FliM and implications for organization of the switch complex. *J. Bacteriol*. 189, 305-312.

119. Garza, A. G., Biran, R., Wohlschlegel, J. A., & Manson, M. D. (1996). Mutations in *motB* suppressible by changes in stator or rotor components of the bacterial flagellar motor. *J. Mol. Biol*. **258**, 270-285.

120. Van Way, S. M., Hosking, E. R., Braun, T. F., & Manson, M. D. (2000). Mot protein assembly into the bacterial flagellum: a model based on mutational analysis of the *motB* gene. *J. Mol. Biol*. **297**, 7-24.

121. Cluzel, P, Surette, M., & Leibler, S. (2000). An ultrasensitive bacterial motor revealed by monitoring signaling proteins in single cells. *Science* **287**, 1652-1655.

122. Läuger, P. (1988). Torque and rotation rate of the bacterial flagellar motor. *Biophys. J*. **53**, 53-65.

123. Silverman, M. & Simon, M. (1974). Flagellar rotation and the mechanism of the bacterial motility. *Nature* **249**, 73-74.

124. Manson, M. D., Tedesco, P. M., & Berg, H. C. (1980). Energetics of flagellar rotation in bacteria. *J. Mol. Biol*. **138**, 541-561.

125. Khan, S. & Berg, H. C. (1983). Isotope and thermal effects in chemiosmotic coupling to the flagellar motor of *Streptococcus*. *Cell* **32**, 913-919.

126. Khan, S., Dapice, M., & Humayun, I. (1990). Energy transduction in the bacterial flagellar motor: Effects of load and pH. *Biophys. J*. **57**, 779-796.

127. Lowe, G., Meister, M., & Berg, H. C. (1987). Rapid rotation of flagellar bundles in swimming bacteria. *Nature* **325**, 637-640.

128. Chen, X. & Berg, H. C. (2000). Torque-speed relationship of the flagellar rotory motor of *Escherichia coli*. *Biophys. J*. **78**, 1036-1041.

129. Berg, H. C. & Turner, L. (1993). Torque generated by the flagellar motor of *Escherichia coli*. *Biophys. J*. **65**, 2201-2216.

130. Washizu, M., Kurahashi, Y., Iochi, H., Kurosawa, O., Aizawa, S.-I., Kudo, S., Magariyama, Y., & Hotani, H. (1993). Dielectrophoretic measurement of the bacterial motor characteristics. *IEEE Trans. Ind. Appl*. **29**, 286-294.

131. Berry, R. M. & Berg, H. C. (1999). Torque generated by the flagellar motor of *Escherichia coli* while driven backward. *Biophys. J*. **76**, 580-587.

132. Magariyama, Y., Sugiyama, S., Muramoto, K., Maekawa, Y., Kawagashi, I., Imae, Y., & Kudo, S. (1994). Very fast flagellar rotation. *Nature* **371**, 752.

133. Chen, X. & Berg, H. C. (2000). Solvent-isotope and pH effects on flagellar rotation in *Escherichia coli*. *Biophys. J*. **78**, 2280-2284.

134. Liu, J. Z., Dapice, M., & Khan, S. (1990). Ion selectivity of the *Vibrio alginolyticus* flagellar motor. *J. Bacteriol*. **172**, 5236-5244.

135. Slonczewski, J., Rosen B. P., Alger, J. R., & Macnab, R. M. (1981). pH homeostasis in *Escherichia coli*: Measurement by ^{31}P nuclear magnetic resonance of methylphosphonate and phosphate. *Proc. Natl. Acad. Sci* USA **78**, 6271-6275.

136. Shioi, J.-I., Matsuura, S., & Imae, Y. (1980). Quantitative measurements of protonmotive force and motility in *Bacillus subtilis*. *J. Bacteriol*. **144**, 891-897.

137. Ryu, W. S., Berry, R. M., & Berg, H. C. (2000). Torque-generating units of the flagellar motor of *Escherichia coli* have a high duty ratio. *Nature* **403**, 444-447.

138. Berry, R. M. & Berg, H. C. (1997). Absence of a barrier to backwards rotation of the bacterial flagellar motor demonstrated with optical tweezers. *Proc. Natl. Acad. Sci.* USA **94**, 14433-14437.

139. Silverman, M., Matsumura, P., & Simon, M. (1976). The identification of the *mot* gene product with Escherichia coli-lambda hybrids. *Proc. Natl. Acad. Sci*. USA **73**, 3126-3130.

140. Blair, D. F. & Berg, H. C. (1991). Mutations in the MotA protein of *Escherichia coli* reveal domains critical for proton conduction. *J. Mol. Biol*. **221**, 1433-1442.

141. Muramoto, K., Sugiyama, S., Cragoe, E. J. J., & Imae, Y. (1994). Successive inactivation of the force-generating units of sodium-driven bacterial flagellar motors by a photoreactive amiloride analog. *J. Biol. Chem*. **269**, 3374-3380.

142. Samuel, A. D. & Berg, H. C. (1995). Fluctuation analysis of rotational speeds of the bacterial flagellar motor. *Proc. Natl. Acad. Sci*. USA **92**, 3502-3506.

143. Samuel, A. D. & Berg, H. C. (1996). Torque-generating units of the bacterial flagellar motor step independently. *Biophys. J*. **71**, 918-923.

144. Sowa, Y., Rowe, A. D., Leake, M. C., Yakushi, T., Homma, M., Ishijima, A., & Berry, R. M. (2005). Direct observation of steps in rotation of the bacterial flagellar motor. *Nature* **437**, 916-919.

145. Zhou, J., Fazzio, R. T., & Blair, D. F. (1995). Membrane topology of the MotA protein of *Escherichia coli*. *J. Mol. Biol*. **251**, 237-242.

146. Lloyd, S. A. & Blair, D. F. (1997). Charged residues of the rotor protein FliG essential for torque generation in the flagellar motor of *Escherichia coli*. *J. Mol. Biol*. **266**, 733-744.

147. Zhou, J. & Blair, D. F. (1997). Residues of the cytoplasmic domain of MotA essential for torque generation in the bacterial flagellar motor. *J. Mol. Biol*. **273**, 428-439.

148. Yorimitsu. T., Sowa, Y., Ishijima, A., Yakushi, T., & Homma, T. (2002). The systematic substitutions around the conserved charged residues of the cytoplasmic loop of Na^+-driven flagellar motor component PomA. *J. Mol. Biol*. **320**, 403-413.

149. Braun, T. F., Poulson, S., Gully, J. F., Empey, J. C., Van Way, S. M., Putnam, A., & Blair, D. F. (1999). Function of proline residues of MotA in torque generation by the flagellar motor of *Escherichia coli*. *J. Bacteriol*. 181, 3542-3551.

150. Garza, A. G., Bronstein, P. A., Valdez, P. A., Harris-Haller, L. W., & Manson, M. D. (1996). Extragenic suppression of *motA* missense mutations of *Escherichia coli*. *J. Bacteriol*. **178**, 6116-6122.

151. Sharp, L. L., Zhou, J., & Blair, D. F. (1995). Tryptophan-scanning mutagenesis of MotB, an integral membrane protein essential for flagellar rotation in *Escherichia coli. Biochemistry* **34**, 9166-9171.

152. DeMot, R. & Vanderleyden, J. (1994). The C-terminal sequence conservation between OmpA-related outer membrane proteins MotB suggests a common function in both Gram-positive and Gram-negative bacteria, possibly in the interaction of these domains with peptidoglycan. *Mol. Microbiol*. **12**, 333-334.

153. Reithmeier, R. & Bragg, P. (1977). Cross-linking of the proteins in the outer membrane of *Escherichia coli*. *Biochim. Biophys. Acta* **466**, 245-256.

154. Endermann, R., Kramer, C., & Henning, U. (1978). Major outer membrane proteins of *Escherichia coli* K12: evidence for protein II* being a transmembrane protein. *FEBS Lett*. **86**, 21-24.

155. Endermann, R. & Henning, U. (1979). Nearest neighbors of major proteins in the outer membrane of *Escherichia coli* K12. *FEBS Lett*. **97**, 339-342.

156. Palva, T. (1979). Protein interactions in the outer membrane of *Escherichia coli*. *Eur. J. Biochem*. **93**, 495-503.

157. Leduc, M., Ishidate, K., Shakibai, N., & Rothfield, L. I. (1992). Interactions of *Escherichia coli* membrane lipoproteins with the murein sacculus. *J. Bacteriol*. **174**, 7982-7988.

158. Bouveret, E., Benedetti, H., Rigal, A., Loret, E., & Ladzunski, C. (1999). In vitro characterization of peptidoglycan-associated lipoprotein (Pal)-peptidoglycan and Pal-TolB interactions. *J. Bacteriol*. **181**, 6306-6311.

159. Koebnik, R. (1995). Proposal for a peptidoglycan-associating alpha-helical motif in the C-terminal regions of some bacterial cell-surface proteins. *Mol. Microbiol*. **16**, 1269-1270.

160. Garza, A. G., Harris-Haller, L. W., Stoebner, R. A., & Manson, M. D. (1995). Motility protein interactions in the bacterial flagellar motor. *Proc. Natl. Acad. Sci. USA*, **92**, 1970-1974.

161. Braun, T. F. & Blair, D. F. (2001). Targeted disulfide cross-linking of the MotB protein of *Escherichia coli*: Evidence for two H^+ channels in the stator complex. *Biochemistry* **40**, 13051-13059.

162. Sato, K. & Homma, M. (2000). Functional reconstitution of the Na^+-driven polar flagellar motor component of *Vibrio alginolyticus*. *J. Biol. Chem*. **275**, 5718-5722.

163. Sato, K. & Homma, M. (2000). Multimeric structure of PomA, a component of the Na^+-driven polar flagellar motor of *Vibrio alginolyticus*. *J. Biol. Chem*. **275**, 20223-20228.

164. Braun**,** T. F**,** Al-Mawsawi, L. Q., Kojima, S., & Blair, D. F. (2004). Arrangement of core membrane segments in the MotA/MotB proton-channel complex of *Escherichia coli*. *Biochemistry* **43**, 35-45.

165. Sharp, L. L., Zhou, J., & Blair, D. F. (1995). Features of MotA proton channel structure revealed by tryptophan-scanning mutagenesis. *Proc. Natl. Acad. Sci*. USA **92**, 7946-7950.

166. Zhou, J., Sharp, L. L., Tang, H. L., Lloyd, S. A., Billings, S., Braun, T. F., & Blair, D. M. (1998). Function of protonatable residues in the flagellar motor of *Escherichia coli*: A critical role for Asp 32 of MotB. *J. Bacteriol*. **180**, 2729-2735.

167. Kojima, S. & Blair, D. F. (2001). Conformational change in the stator of the bacterial flagellar motor. *Biochemistry* **40**, 13041-13050.

168. Walz, D. & Caplan, S. R. (2000). An electrostatic mechanism closely reproducing observed behavior in the bacterial flagellar motor. *Biophys. J*. **78**, 626-651.

169. Asai, Y, Kawagishi, I., Sockett, R. E., & Homma, M. (1999). Hybrid motor with H^+ and Na^+-driven components can rotate *Vibrio* polar flagella by using Na^+ ions. *J. Bacteriol*. **181**, 6332-6338.

170. Gosink, K. K. & Hase, C. C. (2000). Requirements for the conversion of the Na^+-driven flagellar motor of *Vibrio cholerae* to the H^+-driven motor of *Escherichia coli*. *J. Bacteriol*. **182**, 4234-4240.

171. Asai, Y., Kawagishi, I., Sockett, R. E., & Homma, M. (2000). Coupling ion specificity of chimeras between H^+- and Na^+-driven motor proteins, MotB and PomB, in *Vibrio* polar flagella. *EMBO J*. **19**, 3639-3648.

172. Asai, Y., Yakushi, T., Kawagishi, I., & Homma, M. (2003). Ion-coupling determinants of Na^+-driven and H^+-driven flagellar motors. *J. Mol. Biol*. **327**, 453-463.

173. Wilson, M. L. & Macnab, R. M. (1990). Co-overproduction and localization of the *Escherichia coli* motility proteins MotA and MotB. *J. Bacteriol*. **172**, 3932-3939.

174. Wilson. M. L. & Macnab, R. M. (1988). Overproduction of the MotA protein of *Escherichia coli* and estimation of its wild-type level. *J. Bacteriol*. **170**, 588-597.

175. Manoil, C. & Beckwith, J. (1986). A genetic approach to analyzing membrane protein topology. *Science* **233**, 1403-1408.

176. Manoil, C. & Beckwith, J. (1985). TnphoA: A transposon probe for protein export signals. *Proc. Natl. Acad. Sci*. USA **82**, 8129-8133.

177. Muramoto, K. & Macnab, R. M. (1998). Deletion analysis of MotA and MotB, components of the force-generating unit in the flagellar motor of *Salmonella*. *Mol. Microbiol*. **29**, 1191-1202.

178. Gardina, P. J., Bormans, A. F., Hawkins, M. A., Meeker, J. W., & Manson, M. D. (1997). Maltose-binding protein interacts simultaneously and asymmetrically with both subunits of the Tar chemoreceptor. *Mol. Microbiol*. **23**, 1181-1191.

179. Fung, D. C. & Berg, H. C. (1995). Powering the flagellar motor of *Escherichia coli* with an external voltage source. *Nature* **375**, 809-812.

180. Gruendling, A., Manson, M. D., & Young, R. (2001). Holins kill without warning. *Proc. Natl. Acad. Sci*. USA **98**, 9348-9352.

181. Berg, H. C. & Block, S. M. (1984). A miniature flow cell designed for rapid exchange of media under high-power microscope objectives. *J. Gen. Microbiol*. **130**, 2915-2920.

182. Roe, A. J., McLaggan, D., Davidson, I., O'Byrne, C., & Booth, I. R. (1998). Perturbation of anion balance during inhibition of growth of *Escherichia coli* by weak acids. *J. Bacteriol*. **180**, 767-772.

183. Kihara, M. & Macnab, R. M. (1981). Cytoplasmic pH mediates taxis and weak-acid repellent taxis of bacteria. *J. Bacteriol*. **145**, 1209-1221.

184. Repaske, D. R. & Adler, J. (1981). Change in intracellular pH of *Escherichia coli* mediates the chemotactic response to certain attractants and repellents. *J. Bacteriol*. **145**, 1196-1208.

185. Khan, S., Spudich, J. L., McCray, J. A., & Trentham, D. R. (1995). Chemotactic signal integration in bacteria. *Proc. Natl. Acad. Sci*. USA **92**, 9757-9761.

186. Arnold, C. N., McElhanon, J., Lee, A., Leonhart, R., & Siegele, D. A. (2001). Global analysis of *Escherichia coli* gene expression during the acetate-induced acid tolerance response. *J. Bacteriol*. **183**, 2178-2186.

187. Yau, W. M., Wimley, W. C., Gawrisch, K., & White, S. H. (1998). The preference of tryptophan for membrane interfaces. *Biochemistry* **37**, 14713-14718.

188. Braun, P. & Von Heijne, G. (1999). The aromatic residues Trp and Phe have different effects on the positioning of a transmembrane helix in the microsomal membrane. *Biochemistry* **38**, 9778-9782.

189. Deol, S. S., Bond, P. J., Domene, C., & Sansom, M. S. P. (2004). Lipid-protein interactions of integral membrane proteins: A comparative simulation study. *Biophys. J*. **87**, 3737-3749.

190. Draheim, R. R., Bormans, A. F., Lai, R.-Z., & Manson, M. D. (2005). Tryptophan residues flanking the second transmembrane helix (TM2) set the signaling state of the Tar chemoreceptor. *Biochemistry* **44**, 1268-1277.

191. Ramm, K. & Pluckthun, A. (2001). High enzymatic activity and chaperone function are mechanistically related features of the dimeric *E. coli* peptidyl-prolyl-isomerase FkpA. *J. Mol. Biol*. **310**, 485-498.

192. Webb, H. M., Ruddock, L. W., Marchant, R. J., Jonas, K., & Klappa, P. (2001). Interaction of the periplasmic peptidylprolyl *cis-trans* isomerase SurA with model peptides. *J. Biol. Chem*. **276**, 45622-45627.

193. Salmond, C. V., Kroll, R. V., & Booth, I. R. (1984). The effect of food preservatives on pH homeostasis in *Escherichia coli*. *J. Gen. Microbiol*. **130**, 2845-50.

194. Khan, S., & Macnab, R. M. (1980). The steady-state counterclockwise/clockwise ratio of bacterial flagellar motors is regulated by protonmotive force. *J. Mol. Biol*. **138**, 563-597.

195. Xing, J., Bai, F., Berry, R., & Oster, G. (2006). Torque-speed relationship of the bacterial flagellar motor. *Proc. Natl. Acad. Sci*. USA **103**, 1260-1265.

196. Brey, R. N., Rosen, B. P., & Sorensen, E. N. (1979). Cation/proton antiport systems in *Escherichia coli*. *J. Biol. Chem*. **255**, 39-44.

197. Kroll, R. G. & Booth, I. R. (1981). The role of potassium in the generation of a pH gradient in *Escherichia coli*. *Biochem J*. **198**, 691-698.

198. Bakker, E. P. & Mangerich, W. E. (1981). Interconversion of components of the bacterial proton motive force by electrogenic potassium transport. *J. Bacteriol*. **147**, 820-826.

199. Bakker, E. P. & Mangerich, W. E. (1982). N-ethylmaleimide induces K+ -H+ antiport activity in *Escherichia coli* K-12. *FEBS Lett*. **140**, 177-180.

200. Khan, S., Pierce, D., & Vale, R. D. (2000). Interactions of the chemotaxis signal protein CheY with bacterial flagellar motors visualized by evanescent wave microscopy. *Curr. Biol*. **10**, 927-930.

201. Miller, J. H. (1972). *Experiments in Molecular Genetics*, Cold Spring Harbor Laboratory Press, Cold Spring Harbor, NY.

202. Parkinson, J. S. & Houts, S. E. (1982). Isolation and behavior of *Escherichia coli* deletion mutants lacking chemotaxis functions. *J. Bacteriol*. **151**, 106-113.

203. Smith, R. A. & Parkinson, J. S. (1980). Overlapping genes at the *cheA* locus of *Escherichia coli*. *Proc. Natl. Acad. Sci*. USA **77**, 5370-5374.

204. Weerasuriya, S., Schneider, B. M., & Manson, M. D. (1998). Chimeric chemoreceptors in *Escherichia coli*: Signaling properties of Tar-Tap and Tap-Tar hybrids. *J. Bacteriol*. **180**, 914-920.

205. Guzman, L. M., Belin, D., Carson, M. J., & Beckwith, J. (1995). Tight regulation, modulation, and high-level expression by vectors containing the arabinose PBAD promoter. *J. Bacteriol*. **177**, 4121-4130.

206. Alexeyev, M. F. & Winkler, H. H. (1999). Membrane topology of the *Rickettsia prowazekii* ATP/ADP translocase revealed by novel dual *pho-lac* reporters. *J. Mol. Biol*. **285**, 1503-1513.

207. Dinnbier, U., Limpinsel, E., Schmid, R., & Bakker, E. P. (1988) Transient accumulation of potassium glutamate and its replacement by trehalose during adaptation of growing cells of *Escherichia coli* to elevated sodium chloride concentrations. *Arch. Microbiol.* **150,** 348-357.

208. Schleyer, M., Schmid, R., & Bakker, E. P. (1993) Transient, specific and extremely rapid release of osmolytes from growing cells of *Escherichia coli* K-12 exposed to hypoosmotic shock. *Arch. Microbiol.* **160,** 424-431.

209. Rottenberg, H. (1979) The measurement of membrane potential and ΔpH in cells, organelles and vesicles. *Methods Enzymol.* **55,** 547-569.

210. Govantes, F., Andujar, E., & Santero, E. (1998). Mechanism of translational coupling in the *nifLA* operon of *Klebsiella pneumoniae*. *EMBO* **17**, 2368-2377.

211. McCarthy, J. E. G. & Gualerzi, C. (1990). Translational control of prokaryotic gene expression. *Trends Genet*. **6**, 78-85.

212. Draper, D. (1996). Translational initiation. *In* Neidhart, F. C., Curtis, R., III, Ingraham, J. L., Lin, E. C. C., Low, K. B., Magasanik, B., Reznikoff, W. S., Riley, M., Schaechter, M., and Humbarger, H. E. (eds), *Escherichia coli* and *Salmonella*. *Cellular and Molecular Biology*. ASM Press, Washington DC, pp. 902-908.

213. Adhin, M. R. and van Duin, J. (1989). Translational regulation of the lysis gene in RNA bacteriophage fr requires a UUG initiation codon. *Mol. Gen. Genet*. **218**, 137-142.

214. Ivey-Hoyle, M. and Steege, D. A. (1992). Mutational analysis of an inherently defective translation initiation site. *J. Mol. Biol*. **224**, 1039-1054.

215. Adhin, M. R. and van Duin, J. (1990). Scanning model for translational reinitiation in eubacteria. *J. Mol. Biol*. **213**, 811-818.

216. Inokuchi, Y., Hirashima, A., Sekine, Y., Janosi, L., & Kaji, A. (2000). Role of ribosome recycling factor (RRF) in translational coupling. *EMBO* **19**, 3788-3798.

217. Baughman, G. & Nomura, M. (1983). Localization of the target site for translational regulation of the L11 operon and direct evidence for translational coupling in *Escherichia coli*. *Cell* **34**, 979-988.

218. Berkhout, B., Schmidt, B. F., van Strien, A., van Boom, J., van Westrenen, J., & van Duin, J. (1987). Lysis gene of bacteriophage MS2 is activated by translation termination at the overlapping coat gene. *J. Mol. Biol*. **195**, 517-524.

219. Schmidt, B. F., Berkhout, B., Overbeek, G. P., van Strien, A. & van Duin, J. (1987). Determination of the RNA secondary structure that regulates lysis gene expression in bacteriophage MS2. *J. Mol. Biol*. **195**, 505-516.

220. Das, A. & Yanofsky, C. (1989). Restoration of a translational stop-start overlap reinstates translational coupling in a mutant *trpB-rpA* gene pair of the *Escherichia coli* tryptophan operon. *Nucleic Acids Res*. **17**, 9333-9340.

221. de Smit, M. H. & van Duin, J. (1990). Control of prokaryotic translational initiation by mRNA secondary structure. *Prog. Nucleic Acid Res. Mol. Biol*. **38**, 1-35.

222. Balakin, A. G., Skripkin, E. A., Shatsky, I. N., & Bogdanov, A. A. (1992). Unusual ribosome binding properties of mRNA encoding bacteriophage λ repressor. *Nucleic Acids Res*. **20**, 563-571.

223. Jones, R. L., Jaskula, C. J., & Janssen, G. R. (1992). *In vivo* translational start site selection on leaderless mRNA transcribed from the *Steptomyces fradiae aph* gene. *J. Bacteriol*. **174**, 4753-4760.

224. Van Etten, W. J. & Janssen, (1998). An AUG initiation codon, not codon-anticodon complementarity, is required for the translation of unleadered mRNA in *Escherichia coli*. *Mol. Microbiol*. **27**, 987-1001.

225. Moll, I., Grill, S., Gualerzi, C. O., & Blasi, U. (2002). Leaderless mRNAs in bacteria: Surprises in ribosomal recruitment and translational control. *Mol. Microbiol*. **43**, 239-246.

226. Oppenheim, D. S. & Yanofsky, C. (1980). Translational coupling during expression of the tryptophan operon of *Escherichia coli*. *Genetics* **95**, 785-795.

227. Askoy, S., Squires, C. L., & Squires, C. (1984). Translational coupling of the *trpB* and *trpA* genes in the *Escherichia coli* tryptophan operon. *J. Bacteriol*. **157**, 363-367.

228. Das, A. & Yanofsky, C. (1984). A ribosome binding site sequence is necessary for efficient expression of the distal gene of a translationally-coupled gene pair. *Nucleic Acids Res*. **11**, 4757-4768.

229. Henderson, N., Austin, S., & Dixon, R. (1989). Role of metal ions in regulation of nitrogen fixation by the *nifL* gene product from *Klebsiella pneumoniae*. *Mol. Gen. Genet*. **216**, 484-491.

230. Wilson, D. A. & Crawford, I. P. (1965). Purification and properties of the B component of *Escherichia coli* tryptophan synthetase. *J. Biol. Chem*. **240**, 4801-4808.

231. Adachi, O., Kohn, L. D., & Miles, E. W. (1974). Cystalline $\alpha_2\beta_2$ complexes of tryptophan synthetase of *Escherichia coli*. *J. Biol. Chem*. **249**, 7756-7763.

232. Hyde, C. C., Ahmed, A., Padlan, E. A., Miles, E. W., & Davies, D. R. (1988). Three dimensional structure of the tryptophan synthase $\alpha_2\beta_2$ multienzyme complex from *Salmonella typhimurium*. *J. Biol. Chem*. **263**, 17857-17871.

233. Wang, I-N., Deaton, J., & Young, R. (2003). Sizing the holin lesion with an endolysin-ß-galactosidase fusion. *J. Bacteriol*. **185**, 779-787.

234. Rost, B., Yachdav, G., & Liu, J. (2003). The PredictProtein Server. Nucleic Acids Research 32(Web Server issue):W321-W326.

235. Leduc, M., Joseleau-Petit, D., & Rothfield, L. I. (1989). Interactions of membrane lipoproteins with the murein sacculus of *Escherichia coli* as shown by chemical crosslinking studies of intact cells. *FEMS Microbiol. Lett*. **60**, 11-14.

236. Lupas, A., Van Dyke, M., & Stock, J. (1991). Predicting coiled coils from protein sequences. *Science* **252**:1162-1164.

237. Cohen, C., & Parry, D. A. D. (1990). α-helical coiled-coils and bundles: How to design an α-helical protein. *Proteins* **7**, 1-15.

238. Lupas, A. (1996). Coiled coils: New structures and new functions. *Trends Biochem Sci*. **31**, 375-382.

239. Harbury, P. B., Zhang, T., Kim, P. S., & Alber, T. (1993). A switch between two-, three-, and four-stranded coiled-coils in GCN4 leucine zipper mutants. *Science* **262**, 1401-1407.

240. Lomant, A. J. & Fairbanks, G. (1976). Chemical probes of extended biological structures: Synthesis and properties of the cleavable protein cross-linking reagent [^{32}S]dithiobis(succinimidyl propionate). *J. Mol. Biol*. **104**, 243-261.

241. Larsen, S. H., Adler, J., Gargus, J. J., & Hogg, R. W. (1974). Chemomechanical coupling without ATP: The source of energy for motility and chemotaxis in bacteria. *Proc. Natl. Acad. Sci*. USA **89**, 5959-5960.

242. Manson, M. D., Tedesco, P., Berg, H. C., Harold, F. M., & van der Drift, C. (1977). A protonmotive force drives bacterial flagella. *Proc. Natl. Acad. Sci*. USA **74**, 3060-3064.

243. Matsuura, S., Shioi, J.-I., & Imae, Y. (1977). Motility in *Bacillus subtilis* driven by an artificial protonmotive force. *FEBS Lett*. **82**, 197-190.

244. Glagolev, A. N. & Skulachev, V. P. (1978). The proton pump is a molecular engine of motile bacteria. *Nature* **272**, 280-282.

VITA

Name: Edan Robert Hosking

Address: 1885 Oakland Dr.
Mount Pleasant, MI 48858

Email: hosking@umich.edu

Education: B.S., Biology, Central Michigan University, 1997